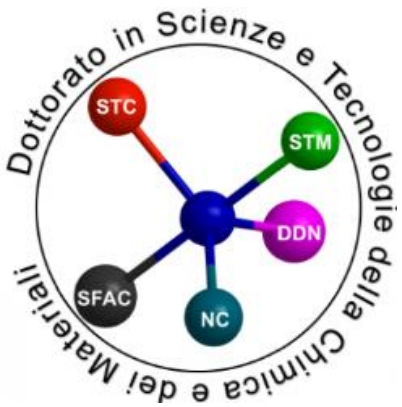

UNIVERSITA' DEGLI STUDI DI GENOVA

Scuola di Dottorato in Scienze e Tecnologie della Chimica e dei Materiali

Corso di Dottorato in Scienze e Tecnologie Chimiche

XXX CICLO

Polymer nanoparticles and nanofibers: Drug delivery and environmental applications

Mahdi Forouharshad

Tutor: Prof. Orietta Monticelli

Index of Contents

Introduction

Since "nanotechnology" was presented by Nobel laureate Richard P. Feynman during his well famous 1959 lecture "There's Plenty of Room at the Bottom", there have been made various revolutionary developments in the field of nanotechnology. However, nanotechnology has emerged in the last decade as an exciting new research field. Nanotechnology represents the design, production, and application of materials at atomic, molecular and macromolecular scales, in order to produce new nanosized structures where at least one dimension is of roughly 1 to 100 nm, i.e., less than 0.1 μm. However, materials below or next to 1 μm (1000 nm) can be also commonly referred as nanomaterials or, more correctly, ultrathin materials. According to this, specifically within fiber science related literature, fibers with diameters below 1 μm are broadly accepted as nanofibers.

Nanotechnology and nanoscience studies have emerged rapidly during the past years in a broad range of product domains. Today, nanoscience represents one of the rapidly growing scientific disciplines due to its enormous potential and impact in many different technological and engineering applications, which includes the development of new materials with novel and advanced performances.

Recently, the nano-scaled materials have attracted extensive research interests due to their high anisotropy and huge specific surface area. Furthermore, the continuously increasing interest in the nanostructure materials results from their numerous potential applications in various areas, particularly in biomedical sciences. Today, nanofibers and nanoparticles are at the forefront of nanotechnology because of their unique properties such as low density, extremely high surface area to volume ratio, flexibility in surface functionalities, superior mechanical performance (e.g. stiffness and tensile strength), and high pore volume and controllable pore size that cannot be found in other structures.

In this context, our researches have been concentrated on the production and modification of polymeric nanofibers and nanoparticles as drug delivery and environment applications.

To this purpose, selected materials for the nanofibers development (polyhedral oligomeric silsesquioxanes, modified poly(amido-amine) dendrimers, and modified hyperbranched polyglycerol) were combined with biopolymers, namely (poly(L-lactide) (PLLA) and poly(ε-caprolactone) (PCL) which enable us to overcome typical shortcomings of the above polymer matrices. As well, poly(styrene-co-maleic anhydride) (PSMA) amphiphilic copolymer was used for production of nanoparticles.

In the following paragraph, a quick overview of the whole thesis structure is provided.

Outline of the thesis

Chapter 1 is dedicated to the polymer and composite nanofibers. Fabrication methods, influence of parameters, drawbacks and applications of polymer and composite nanofibers are described.

Chapter 2 is focused on polymer and composite nanoparticles. Preparation methods from dispersion of preformed polymer and application as carriers for therapeutic agents are presented. Particular emphasize is given to electrospray and nanoprecipitation method along with organic-organic composite nanoparticles.

Chapter 3 is the review of various polymers that are used in this thesis. Their structures, synthesis, properties and drawbacks are described.

Chapter 4 describes the application of *ad-hoc*-synthesized star polymers as novel additives for tuning poly(L-lactide) and poly(ε-caprolactone) electrospun fiber properties. Indeed, a novel drug delivery system consisting of poly(ε-caprolactone) electrospun fibers containing an *ad-hoc*-

synthesized star polymer made up of a poly(amido-amine) (PAMAM) core and PCL branches (PAMAM-PCL) was developed. The preparation of electrospun fibers starting from solutions containing the neat PCL as well as the mixture PCL/PAMAM-PCL and applying optimized electrospinning conditions to obtain defect free fibers is described. The drug delivery system was built up by directly introducing doxorubicin (DOXO) into the electrospinning solutions. In vitro cytotoxicity tests were carried out by putting in contact DOXO-loaded and DOXO-free PCL and PCL/PAMAM-PCL electrospun fibers with different kind of cancer cell lines.

In Chapter 5 a new strategy for the functionalization of sc-PLA nanofibers (prepared by electrospinning of equimolar solutions of high-molecular-weight PLLA and PDLA) is presented. This nanofibers modification consisted in the introduction of functionalized amino polyhedral oligomeric silsesquioxanes (POSS-NH_2) directly into the electrospinning solutions. This was possible by employing as a solvent system a 2:1 mixture of chloroform ($CHCl_3$) and 1,1,1,3,3,3-hexafluoro-2-propanol (HFIP) which proved suitable for both polymer-pair and POSS molecules solubilization, while simultaneously enabling to obtain homogeneous and bead-free fibers once the electrospinning conditions are properly optimized. Indeed, the specific effect of the single components of the solvent mixture, $CHCl_3$ and HFIP, on fiber structuration and morphology was evaluated. The sc-PLA/POSS-NH_2 fibers, characterized by a submicrometric dispersion of the silsesquioxanes underwent a grafting reaction with β-cyclodextrin molecules, activated to nucleophilic substitution via monotosylation (CD-O-Ts). The reaction was first investigated on neat POSS-NH_2 and optimized conditions were then applied for sc-PLA/POSS-NH_2 fibers. IR and XPS measurements demonstrated the formation of a novel hybrid molecule, characterized by the linkage of the cyclodextrin to the silsesquioxane siliceous cage (POSS-NH-CD). Concerning the fibers, SEM measurements was used for studying the modification of fibers morphology, while by applying TGA analysis it was possible to evaluate the amount of the grafted cyclodextrin. Finally, UV measurements demonstrated the capacity of the novel synthesized hybrid molecule, based on POSS and cyclodextrin, to absorb water pollutants, by having chosen, as model compounds, alizarin red and 2-chlorophenol.

Lastly, *Chapter* 6 describes the application of poly(styrene-co-maleic anhydride)(PSMA) nanoparticles as protein carrier. To this purpose, PSMA nanoparticles were produced by combining precipitation and electrospray technique. Different experimental conditions were tested in order to optimize the nanoparticle dimensions and production yield. The nanoparticles were characterized by IR, FE-SEM, and DLS. Then obtained nanoparticles were used for the conjugation of a functional protein to their surface. The proteolytic enzyme papain was chosen as model protein. The successful papain-nanoparticle conjugation was demonstrated by zeta potential, IR and FE-SEM measurements. The residual catalytic activity of the conjugated enzyme molecules was studied and found to be around 79% respect to the same amount of free enzyme.

CHAPTER 1. Polymer and composite nanofibers: preparation and application

1.1 Polymer Nanofibers

With the rapid growth of nanoscience in recent years, nanofibers technology has been greatly accelerated to create nanoscale fibers from a broad range of polymeric materials.

As previuosly underlined, nanofibes are fibers with a diameter of less than one micron. Nanofibers possess unique properties that distinguish them from other structures, like extraordinary high surface area per unit mass, high porosity, layer thinness, high permeability, low basis weight, cost effectiveness, superior directional strength, etc.[1] The unique properties of nanofibers make them promising materials for a variety of applications from medical to consumer products and industrial to high-tech applications. They can be used in several fields such as high-performance filtration, aerospace, capacitors, transistors, drug delivery systems, battery separators, energy storage, fuel cells, information technology, wound dressing, vascular grafts, enzyme immobilization, electrochemical sensing, composite materials, reinforcements, blood vessel engineering and tissue engineering.[2–4] The existing fibers spinning technologies cannot produce robust fibers with a diameter smaller than 2 μm due to limitations in the process. The process widely used for the fabrication of nanofibers is electrospinning, because of its simplicity and suitability for a variety of polymers, ceramics, and metals. Other processes include melt blowing,[5,6] template synthesize,[7,8] flash-spinning,[9] phase-separation,[10] drawing,[11] and self-assembly.[12,13] In most of these processes, the fibers are collected as nonwoven random fibers mats known as nanoweb, consisting of fibers having diameters from several nanometers to hundreds of nanometers.

1.1.1 Meltblowing

Melt blowing is a conventional fabrication method of micro- and nanofibers where a polymer melt is extruded through small nozzles surrounded by high speed blowing gas (Figure 1.1). The technology of melt blowing was first developed in the 1950s at the Naval Research Laboratory of United States. In the melt blowing process, a molten polymer is extruded through the orifice of a die. The fibers are formed by the elongation of the polymer streams coming out of the orifice by air-drag and are collected on the surface of a suitable collector in the form of a web. The average fibers diameter mainly depends on the throughput rate, melt viscosity, melt temperature, air temperature, and air velocity. The substantial benefits of melt blowing are simplicity, high specific productivity, and solvent-free operation. The difficulty in fabricating nanofibers in melt blowing is due to the inability to design sufficiently small orifice in the die and the high viscosity of the polymeric melt. Recently, nanofibres have been fabricated by special die designs with a small orifice, reducing the viscosity of the polymeric melt and suitable modification of the melt blowing setup.[5] Polymers with thermoplastic behavior are applicable for melt blowing. The process was suitable for many melt-spinnable commercial polymers, copolymers and their blends such as polyesters, polyolefins (PE and PP), PA, nylons, PU, PVC, PVA and ethylene vinyl acetate.[14]

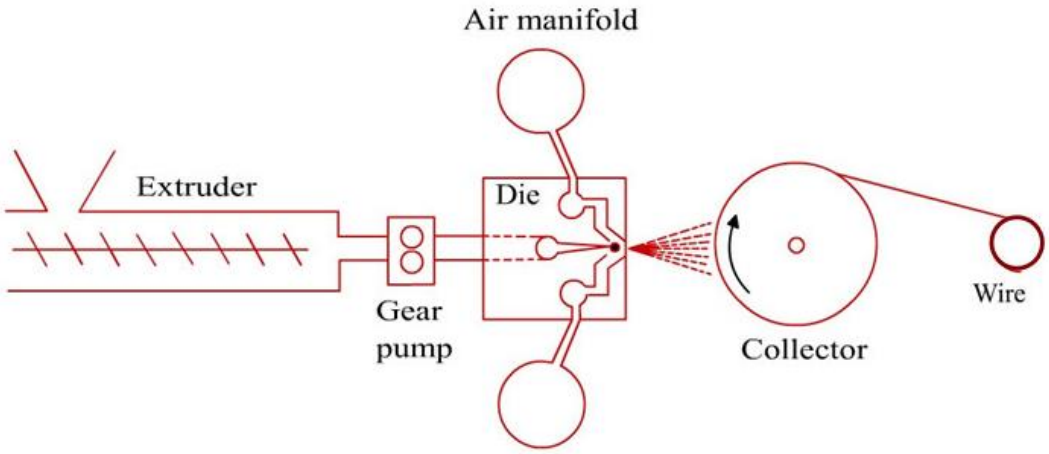

Figure 1.1. Meltblowing setup.

1.1.2 Template synthesize

This method entails synthesizing the desired material within the pores of a nanoporous membrane. The membranes employed have cylindrical pores of uniform diameter. They view each of these pores as a beaker in which a particle of the desired material is synthesized. Because of the cylindrical shape of these pores, a nanocylinder of the desired material is obtained in each pore. Depending on the material and the chemistry of the pore wall, this nanocylinder may be solid (a fibril) or hollow (a tubule) (Figure 1.2).

The template method has a number of interesting and useful features. First, it is very general; we have used this method to prepare tubules and fibrils composed of electronically conductive polymers, metals, semiconductors, carbons, and other materials. Furthermore, nanostructures with extraordinarily small diameters can be prepared.[15]

Li et al. combined the extrusion technology with the template method for the production of polymeric nanofibres of thermoplastic polymers. In this process, the molten polymer was forced through the pores of an anodic aluminum oxide membrane (AAOM) and then subsequently cooled down to room temperature. A special stainless steel appliance was designed to support the thin AAOM, to bear the pressure and to restrict the molten polymer movement along the direction of the pores. The appliance containing the polymer was placed on the hot plate of a compressor (with temperature controlled functions) followed by the forcing of the polymeric melt (indicated by the arrow). The hot plate was stopped after two hours of heating and the pressure was maintained until the system cooled to room temperature. Isolated nanofibres of PE were obtained by the removal of the AAOM with sodium hydroxide/ethanol (20 wt%). Finally, the nanofibres were broken down from the bulk feeding film by ultrasound (in ethanol for 5 min.) to form isolated fibres. The diameter of the PE fibres ranges from 150 to 400nm (diameter of AAOM pores ¼ 200 nm) and the length of fibres correspond to the length of the pores in AAOM (i.e. 60 μm).[16]

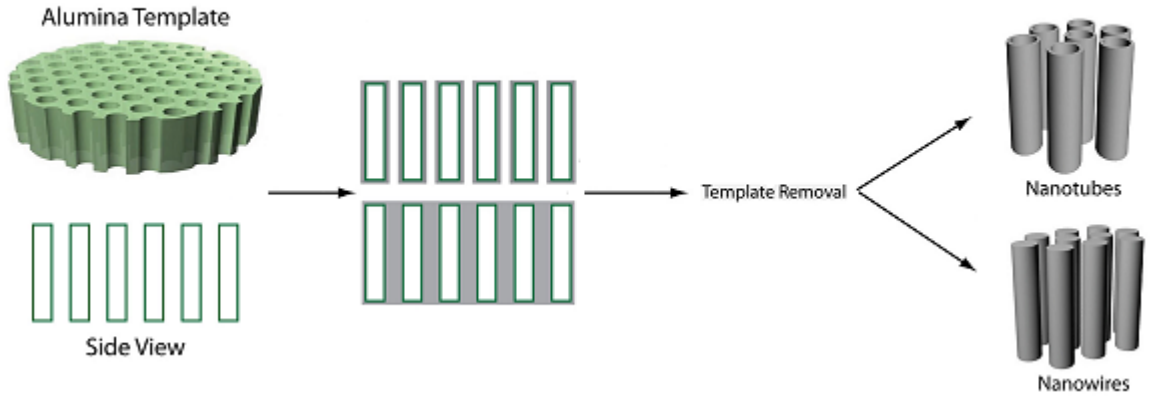

Figure 1.2. Template synthesis scheme.

1.1.3 Flash-spinning

In the flash-spinning process, a solution of fibers forming a polymer in a liquid spin agent is spun into a zone of lower temperature and substantially lower pressure to generate Plexi-filamentary film-fibril strands (Figure 1.3). A spin agent is required for flash-spinning which: (1) should be a non-solvent to the polymer below its normal boiling point, (2) can form a solution with the polymer at high pressure, (3) can form a desired two-phase dispersion with the polymer when the solution pressure is reduced slightly, and (4) should vaporize when the flash is released into a substantially low-pressure zone. The flash-spinning process was described by Blades and White of DuPont in 1963 and since then several patents have been filed. Weinberg et al. produced nanofibres of polyolefins with fibers length of 3–10 mm and at a production rate which is at least two orders of magnitude higher than the conventional electrospinning using flash-spinning.[9] The nonwoven fibrous webs produced had significantly different morphology (i.e. complex interconnecting networks or webs of large and small polyolefin filaments or fibers similar to spider webs) than those produced by other technologies. Flash-spinning is more suitable for difficult-to-dissolve polymers such as polyolefins and high molecular weight polymers. The spinning temperature should be higher than the melting point of the polymer and the boiling point of the solvent in order to effect solvent evaporation prior to the collection of the polymer. The flash-spinning process does not produce fibrous webs consisting completely of nanofibres.

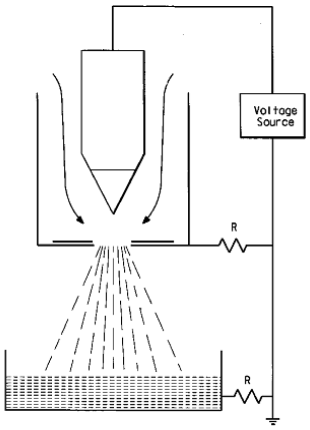

Figure 1.3. Flash-spinning setup.[9]

1.1.4 Phase Separation

The phase separation consists of dissolution, gelation, extraction using a different solvent, freezing, and drying resulting in nanoscale porous foam (Figure 1.4). The process takes a relatively long period of time to transfer the solid polymer into the nano-porous foam. In phase-separation, the gel of a polymer is prepared by storing the homogeneous solution of the polymer at the required concentration in a refrigerator set at the gelation temperature. The gel is then immersed in distilled water for solvent exchange, followed by the removal from the distilled water, blotting with filter paper and finally transferring to a freeze-drying vessel leading to a nanofiber matrix.[10] The phase-separation process was used for the fabrication of nanofibers matrices of poly-L-lactic acid and blends of poly-L-lactic acid and polycaprolactone.[17,18] Although the phase-separation process is very simple, it is only limited to the laboratory scale.

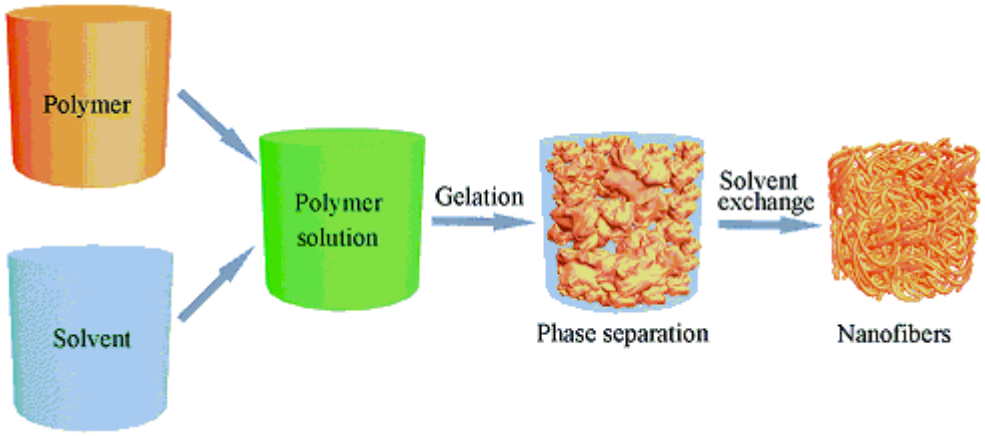

Figure 1.4. Schematic diagram of the phase separation process.[18]

1.1.5 Self-assembly

The self-assembly is a process in which individual, pre-existing components organize themselves into desired patterns and functions (Figure 1.5). However, similarly to the phase separation, the self-assembly is time-consuming in processing continuous polymer nanofibers. In general, self-assembly of nanofibers refers to the build-up of nanoscale fibers using smaller molecules as basic building blocks.[19] The small molecules are arranged in a concentric manner which upon extension in a normal plane produces the longitudinal axes of the nanofibres. In self-assembly, the final (desired) structure is 'encoded' in the shape of the small blocks, as compared to traditional techniques (such as lithography) where the desired structure must be carved out from a large block of matter. Self-assembly is thus referred to as a 'bottom-up' manufacturing technique, whereas lithography is a 'top-down' technique. The synthesis of molecules for self-assembly often involves a chemical process called convergent synthesis. This process requires standard laboratory equipment and is limited to specific polymers. In self-assembly, the shape and properties of nanofibres depend on the molecules and the intermolecular forces that bring the molecules together. Nanofibres of various polymeric configurations such as diblock copolymers; triblock copolymers; triblock polymers (of peptide amphiphilic and dendrimers); and bold form (of glucosamide and its deacetylated derivatives) can be assembled by this process. Nanofibres from diblock copolymers and triblock polymers were prepared by Liu et al. and Yan et al. respectively by self-assembly.[20,21]

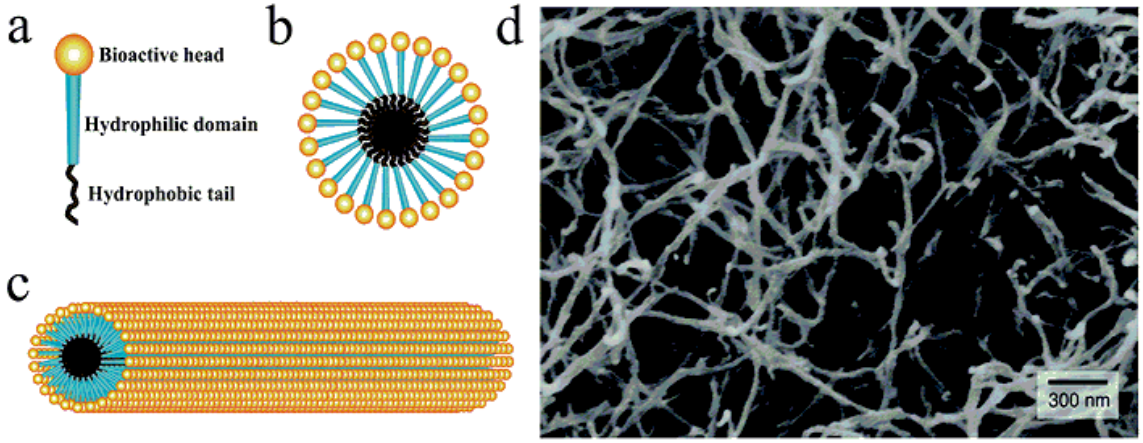

Figure 1.5. Schematic illustration of the molecular self-assembly process. (a) The molecular structure of a typical peptide amphiphilic molecule. (b) Formation of a micelle at the initial phase of the self-assembly process. (c) A cylindrical micelle formed by the self-assembly of peptide amphiphilic molecules. (d) SEM image of the peptide amphiphilic nanofibers by self-assembly.[22]

1.1.6 Drawing

The drawing is a process similar to dry spinning in fiber industry, which can make one-by-one very long single nanofibers. However, only a viscoelastic material that can undergo strong deformations while being cohesive enough to support the stresses developed during pulling can be made into nanofibers through drawing. In the drawing process, a millimetric droplet of a solution is allowed to evaporate after it is deposited on a silicon dioxide (SiO_2) surface. The droplet becomes more concentrated at the edge because of evaporation due to capillary flow. A micropipette is dipped into the droplet near the contact line with the surface and then withdrawn at a speed of 100 mm/s, resulting in a nanofiber being pulled out. The pulled fiber is then deposited on another surface by touching it with the end of the micropipette (Figure 1.6). From each droplet, nanofibres can be drawn for several times. Nanofibres of sodium citrate were formed by dissolving it in chloroauric acid through the drawing process.[11] This process is simple but limited to laboratory scale as nanofibers are formed one by one.[23,24]

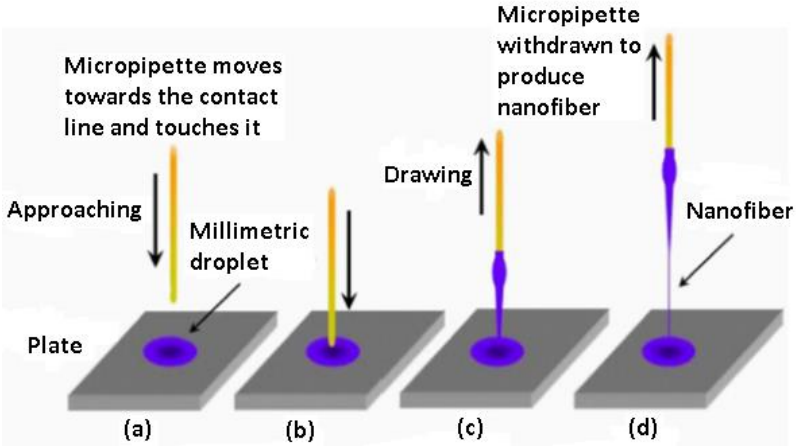

Figure 1.6. Schematic illustration of nanofibers fabrication by direct drawing process from molten or solution droplet. (a) An iron or silica rod is approaching the droplet. (b) The rod end is immersed into the droplet. (c) The rod conglutinated polymer is being drawn out. (d) A polymer nanofiber is formed.[23]

1.1.7 Electrospinning

Unlike several different processing techniques that can be used for fabrication of nanofibers, an additional unique synthetic method, electrostatic spinning (electrospinning), has received much attention in recent years. The process of electrospinning has been known for almost 80 years and the first patent was issued to Formhals in 1934.[25] Reneker and Chun, who revived interest in this technology in the early 1990s, has shown the possibility to electrospin a wide range of polymer solutions in 1996.[26] Electrospinning is a novel process for forming superfine fibers with diameters ranging from 10 μm down to 5 nm by forcing a polymer melt or solution through a spinneret with an electric field.[27,28] It is currently the most widely used method for the production of polymeric nanofibers, due to its simplicity, cost effective, and suitability to yield very long fibers from various polymers. The apparatus that is used for electrospinning, is made up of a syringe pump to control the flow rate of the polymer solution, high voltage power to supply positive or negative polarity and a conducting flat plate or rotating drum which acting as a ground collector (Figure 1.7). In electrospinning, a high voltage is applied to a polymer fluid such that charges are induced within the fluid. When charges within the fluid reached a critical amount, a fluid jet will erupt from the droplet at the tip of the needle resulting in the formation of a Taylor cone. The electrospinning jet will travel towards the region of lower potential, which in most cases, is a grounded collector. There are many parameters that can influence on the morphology, average fibers diameter, porosity, uniformity and mechanical properties of the resultant electrospun fibers. These parameters include (1) the solution parameters such as viscosity, concentration, conductivity, dielectric constant and surface tension, (2) systemic parameters such as polymer type, molecular weight, and solvent used, (3) process parameters such as voltage, flow rate, distance, and collection plate, and (4) ambient parameters such as temperature, humidity, and air velocity in the electrospinning chamber.[29] With the understanding of these parameters, it is possible to come out with setups to yield fibrous structures of various forms and arrangements. It is also possible to create nanofiber with different morphology and properties by varying the parameters.

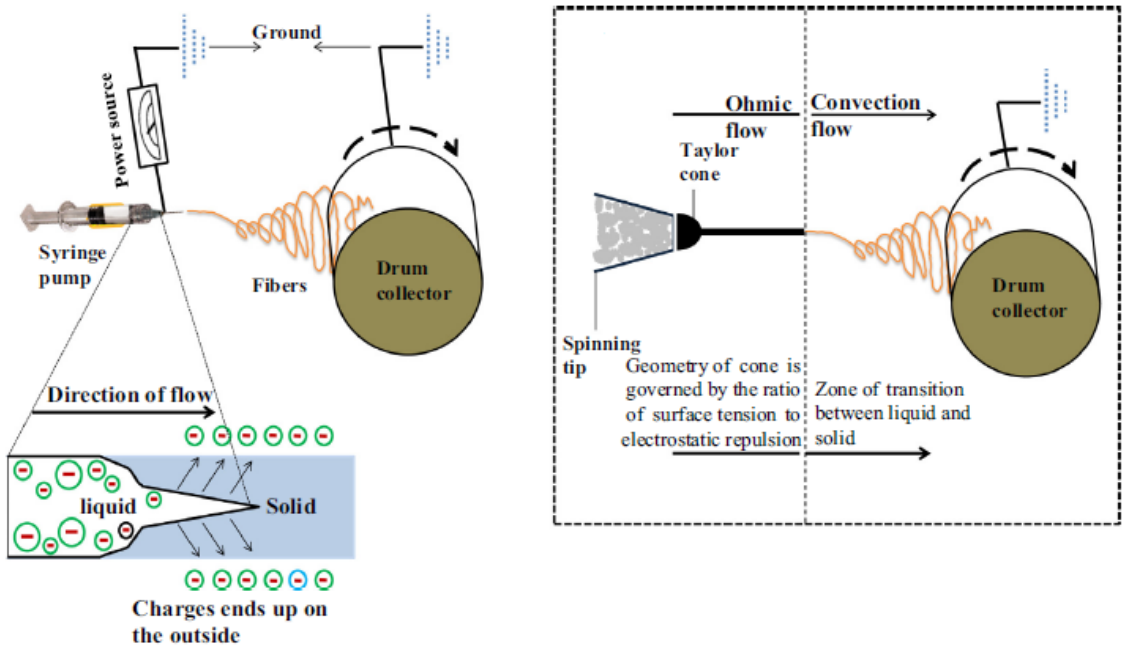

Figure 1.7. Schematic depicting electrospinning setup and phenomenon of electrospinning.[27]

1.1.7.1 Solution parameters

Some solution parameters play an important role in fiber formation and structure. In relative order of their impact on the electrospinning process, these include polymer concentration, solvent volatility, and solvent conductivity.

1.1.7.1.1 Concentration

The concentration of the polymer solution has the most significant influence in the electrospinning process and the resultant fiber morphology. The solution must have a high enough polymer concentration for chain entanglements to occur; however, the solution cannot be either too dilute or too concentrated.[28] At very low concentration, polymer fiber will break up into droplets before reaching the collector due to the effects of surface tension and polymeric micro or nanoparticles will be obtained and electrospray occurs instead of electrospinning due to the low viscosity and high surface tensions of the solution. With increasing concentration, a mixture of beads and fibers will be obtained. As the concentration increases, the shape of the bead changes from spherical to spindle-like. Finally, when the solution concentration to be optimum, uniform and smooth nanofibers can be produced (Figure 1.8). However, if polymer solution is too concentrated not only nanofibers cannot be formed but also helix-shaped microribbons will be observed.[30–33]

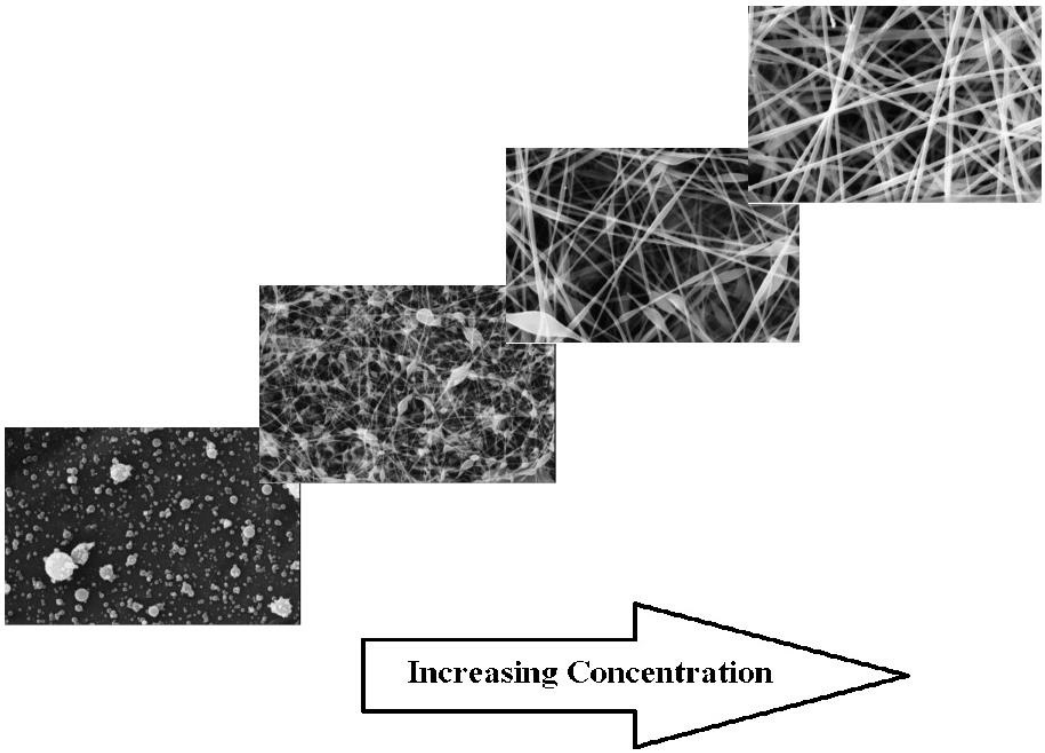

Figure 1.8. Concentration effect on the morphology of the electrospun nanofibers.[33]

1.1.7.1.2 Molecular weight and solution viscosity

One of the factors that affect the viscosity of the solution is the molecular weight of the polymer. In principle, molecular weight reflects the entanglement of polymer chains in solutions, namely the solution viscosity. Generally, when a polymer of higher molecular weight is dissolved in a solvent, its viscosity will be higher than the solution of the same polymer but of a lower molecular

weight.[30] One of the conditions necessary for electrospinning to occur where fibers are formed is that the solution must consist of a polymer of sufficient molecular weight and the solution must be of sufficient viscosity. As the jet leaves the needle tip during electrospinning, the polymer solution is stretched as it travels towards the collection plate. During the stretching of the polymer solution, it is the entanglement of the molecule chains that prevents the electrically driven jet from breaking up thus maintaining a continuous solution jet. As a result, monomeric polymer solution does not form fibers when electrospun. Keeping the concentration fixed, using a polymer with too low molecular weight leads to the formation of beads rather than fibers, increasing the molecular weight will give smooth fibers, whereas a very high molecular weight results in electrospun fibers having very large diameters.[34,35]

1.1.7.1.3 Viscosity

Solution viscosity is the critical key in determining the fiber morphology. It has been proven that continuous and smooth fibers cannot be obtained in very low viscosity, whereas very high viscosity results in the hard ejection of jets from solution, namely there is a requirement of suitable viscosity for electrospinning. Generally, the solution viscosity can be tuned by adjusting the polymer concentration of the solution; thus, different products can be obtained. The viscosity range of a different polymer or oligomer solution at which electrospinning is done is different. It is important to note that viscosity, polymer concentration, and polymeric molecular weight are related to each other. For the solution of low viscosity, surface tension is the dominant factor and just beads or beaded fiber formed. If the solution is of suitable viscosity, continuous fibers can be obtained (Figure 1.9).[33,36]

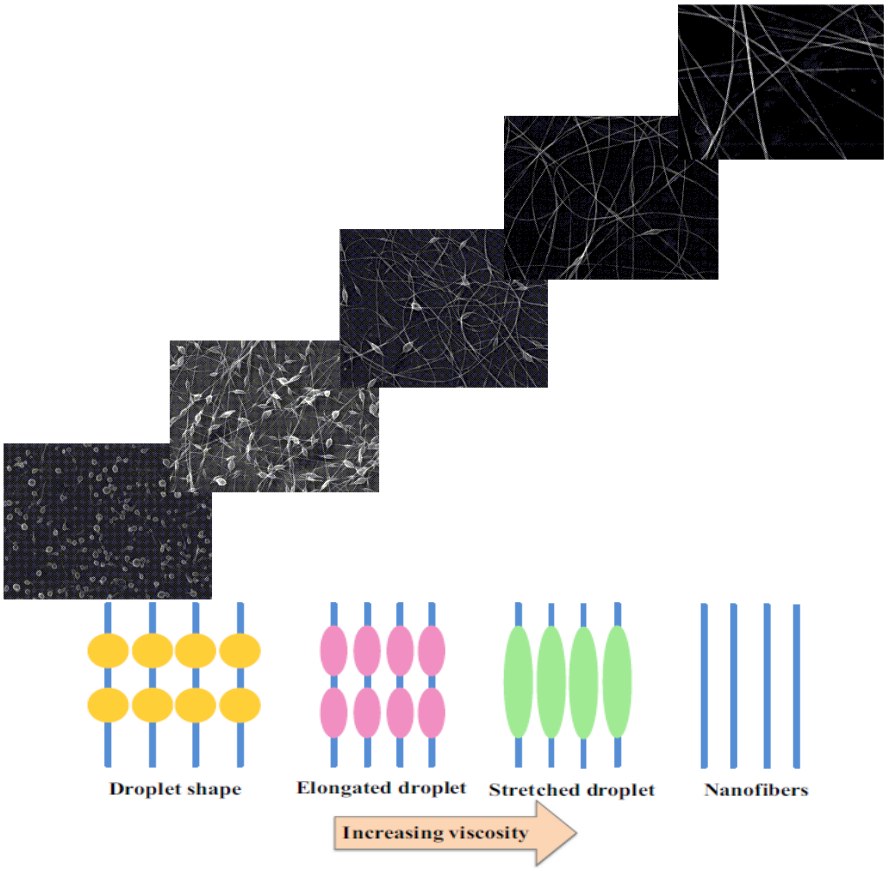

Figure 1.9. Viscosity effect on the morphology of the electrospun nanofibers.[36]

1.1.7.1.4 Surface tension

Surface tension, more likely to be a function of solvent compositions of the solution, plays a critical role in the electrospinning process and by reducing the surface tension of a nanofiber solution, fibers can be obtained without beads. The initiation of electrospinning requires the charged solution to overcome its surface tension. However, as the jet travels towards the collection plate, the surface tension may cause the formation of beads along with the jet. Surface tension has the effect of decreasing the surface area per unit mass of a fluid. In this case, when there is a high concentration of free solvent molecules, there is a greater tendency for the solvent molecules to congregate and adopt a spherical shape due to surface tension. A higher viscosity will mean that there is greater interaction between the solvent and polymer molecules thus when the solution is stretched under the influence of the charges, the solvent molecules will tend to spread over the entangled polymer molecules thus reducing the tendency for the solvent molecules to come together under the influence of surface tension.[37,38]

1.1.7.1.5 Solution conductivity

Electrospinning involves stretching of the solution caused by repulsion of the charges at its surface. Therefore if the conductivity of the solution is increased, more charges can be carried by the electrospinning jet. Solutions with high conductivity will have a greater charge carrying capacity than solutions with low conductivity. Thus, the fiber jet of highly conductive solutions will be subjected to a greater tensile force in the presence of an electric field than a fiber jet from a solution with a low conductivity. As a result, smooth fibers are formed which may otherwise yield beaded fibers. The increased in the stretching of the solution also will tend to yield fibers of smaller. However, there is a limit to the reduction in the fiber diameter.[30,39,40]

1.1.7.1.6 Dielectric effect of solvent

The dielectric constant of a solvent has a significant influence on electrospinning. Generally, a solution with a greater dielectric property reduces the beads formation and the diameter of the resultant electrospun fiber.[32] Solvents such as N, N-Dimethylformamide (DMF) may add to a solution to increase its dielectric property to improve the fiber morphology.[41] The bending instability of the electrospinning jet also increases with higher dielectric constant. This is shown by increased deposition area of the fibers.[42]

1.1.7.1.7 Solvent volatility

Choice of solvent is also critical as to whether fibers are capable of forming, as well as influencing fiber porosity. In order for sufficient solvent evaporation to occur between the capillary tip and the collector, a volatile solvent must be used. As the fiber jet travels through the atmosphere toward the collector a phase separation occurs before the solid polymer fibers are deposited, a process that is greatly influenced by the volatility of the solvent.[42]

1.1.7.2 Processing parameters

In addition to the solution parameters, a number of processing parameters (external factors) play an important role in fiber formation and morphology. This includes the voltage supplied, the feed rate, temperature of the solution, type of collector, and distance between the needle tip and

collector. These parameters have a certain influence in the fiber morphology although they are less significant than the solution parameters.

1.1.7.2.1 Voltage

Within the electrospinning process, applied voltage is the crucial factor. The high voltage will induce the necessary charges on the solution and together with the external electric field, will initiate the electrospinning process when the electrostatic force in the solution overcomes the surface tension of the solution. Generally, both high negative or positive voltage of more than 6kV is able to cause the solution drop at the tip of the needle to distort into the shape of a Taylor Cone during jet initiation (Figure 1.10). Depending on the feed rate of the solution, a higher voltage may be required so that the Taylor Cone is stable. The columbic repulsive force in the jet will then stretch the viscoelastic solution. If the applied voltage is higher, the greater amount of charges will cause the jet to accelerate faster and more volume of solution will be drawn from the tip of the needle. This may result in a smaller and less stable Taylor Cone. When the drawing of the solution to the collection plate is faster than the supply from the source, the Taylor Cone may recede into the needle. As both the voltage supplied and the resultant electric field have an influence in the stretching and the acceleration of the jet, they will have an influence on the morphology of the fibers obtained. In most cases, a higher voltage will lead to greater stretching of the solution due to the greater columbic forces in the jet as well as the stronger electric field. These have the effect of reducing the diameter of the fibers and also encourage faster solvent evaporation to yield drier fibers.[43,44]

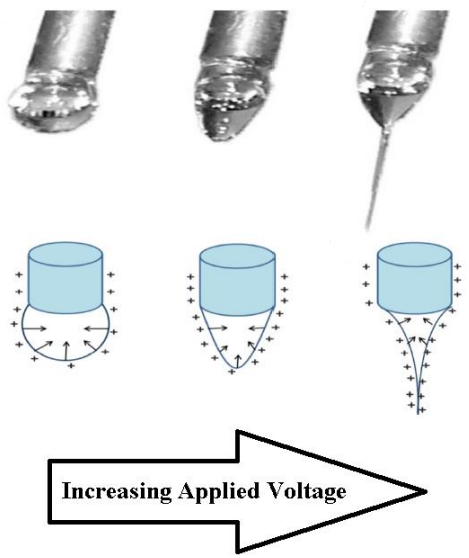

Figure 1.10. Digital images showing the three stage deformation of the polyvinylpyrrolidone droplet under the influence of increasing electric field. The cartoon shows the mechanism of the effect of charges on the polymeric droplets.[27]

1.1.7.2.2 Flow rate

The flow rate of the polymer solution within the syringe is another important process parameter. Generally, the lower flow rate is more recommended as the polymer solution will get enough time for polarization. If the flow rate is very high, bead fibers with thick diameter are formed rather than the smooth fibers with thin diameter owing to the short drying time prior to reaching the collector and low stretching forces. Polymer flow rate also has an impact on fibers size and additionally can influence fiber porosity as well as fiber shape.[45] Increasing the flow rate above the critical value could lead to the formation of beads. For example, in case of polystyrene, when the flow rate was increased to 0.10 μL/min, bead formation was observed. However, when the flow rate was reduced to 0.07 μL/min, bead-free nanofibers were formed. Increasing the flow rate beyond a critical value not only leads to increase in the pore size and fiber diameter but also to bead formation (due to incomplete drying of the nanofiber jet during the flight between the needle tip and metallic collector).[45] Because increases and decreases in the flow rate affect the nanofiber formation and diameter, a minimum flow rate is preferred to maintain a balance between the leaving polymeric solution and replacement of that solution with a new one during jet formation.[45,46]

1.1.7.2.3 Temperature

The temperature of the solution has both the effect of increasing its evaporation rate and reducing the viscosity of the polymer solution. The increase in the evaporation of the solvent and the decrease in the viscosity of the solution work by two apposite mechanisms, however, both lead to decrease in the mean fiber diameter. When polyurethane is electrospun at a higher temperature, the fibers produced have a more uniform diameter. This may be due to the lower viscosity of the solution and greater solubility of the polymer in the solvent which allows more even stretching of the solution. With a lower viscosity, the Columbic forces are able to exert a greater stretching force on the solution thus resulting in fibers of smaller diameter. Increased polymer molecules mobility due to increased temperature also allows the Columbic force to stretch the solution further. However, in cases where biological substances such as enzymes and proteins are added to the solution for electrospinning, the use of high temperature may cause the substance to lose its functionality.[47]

1.1.7.2.4 Distance between tip and collector

In several cases, the flight time, as well as the electric field strength, will affect the electrospinning process and the resultant fibers. Varying the distance between the tip and the collector will have a direct influence in both the flight time and the electric field strength. To form independent fibers, sufficient time must be given to the electrospinning jet to allow most of the solvents to be evaporated. When the distance between the tip and the collector is reduced, the jet will have a shorter distance to travel before it reaches the collector plate. Moreover, the electric field strength will also increase at the same time and this will increase the acceleration of the jet to the collector. As a result, there may not have enough time for the solvents to evaporate when it hits the collector. When the distance is too low, excess solvent may cause the fibers to merge where they contact to form junctions resulting in inter and intra-layer bonding.[48,49]

1.1.7.3 Ambient parameters

The effect of the electrospinning jet surrounding is one area which is still poorly investigated. Any interaction between the surrounding and the polymer solution may have an effect on the electrospun fiber morphology. High humidity, for example, was found to cause the formation of pores on the surface of the fibers. Since electrospinning is influenced by external electric field, any changes in the electrospinning environment will also affect the electrospinning process.

1.1.7.3.1 Humidity

The humidity of the electrospinning environment may have an influence in the polymer solution during electrospinning. At high humidity, it is likely that water condenses on the surface of the fiber when electrospinning is carried out under normal atmosphere. As a result, this may have an influence on the fiber morphology especially polymer dissolved in volatile solvents. Experiments using polysulfone (PS) dissolved in Dichloromethane (DMF) shows that at a humidity of less than 50%, the fiber surfaces are smooth. However, an increased in the humidity during electrospinning will cause circular pores to form on the fiber surfaces.[50]

As for the humidity, low humidity may dry the solvent totally and increase the velocity of the solvent evaporation. On the contrary, high humidity will lead to the thick fiber diameter owing to the charges on the jet can be neutralized and the stretching forces become small.[51]

1.2 Composite nanofibers

At the nanoscale, these nanomaterials provide abundant opportunities to create unique material combinations by accessing new properties through the exploitation of the unique synergy between these materials. Nanocomposites are considered as one of the most highly researched areas in nanomaterials by the virtue of their improved mechanical properties, dimensional stability, thermal/chemical stability, and electrical conductivity. Polymer nanocomposites are the result of combination between polymers and organic or inorganic fillers at the nanometer scale. The filler can be one-dimensional (e.g., nanotubes and fibres), two-dimensional (e.g., clay), or three-dimensional (e.g., spherical particles). These nanocomposites, due to their improved physical/chemical properties, establish applications ranging from energy, sensors, biotechnology, smart materials, filtration, and regenerative medicine. These nanocomposites contribute to producing light/efficient batteries,[52–55] fuel cells,[56–58] fabricating structural components with high strength-to-weight ratio,[59,60] lightweight sensors,[61] as well as magnetic and fluorescent nanocomposites for efficient viewing/removing of the tumors.[62,63]

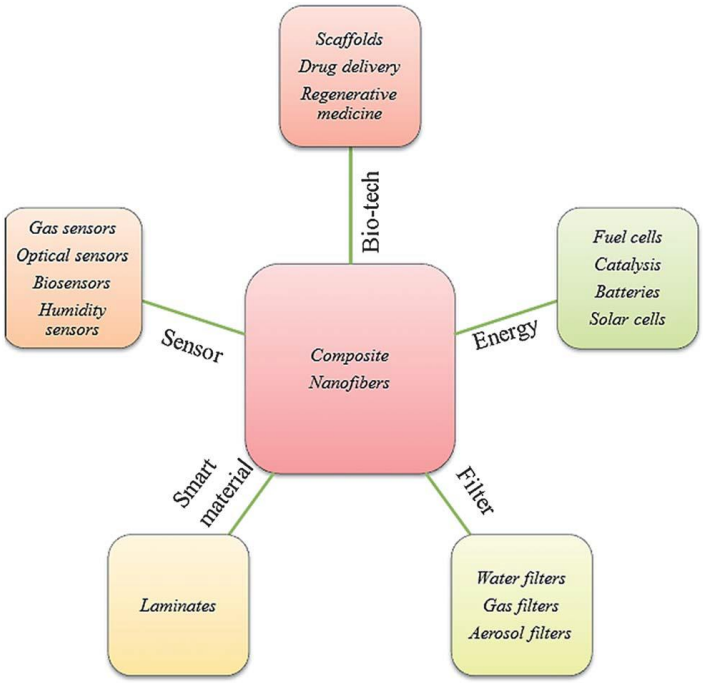

Figure 1.11. Fabrication and characterization of electrospun nanocomposites on the basis of their applications.[64]

The categorization in figure 1.11 is designed to cover future/ongoing research/industrial trends pertaining to nanofiber based nanocomposites. Comprehensive study of properties in nanoscale dimensions relating to their respective large scale counterparts were performed to achieve a clear understanding of the synergistic advantage of nanoscale dimensions. It is well-known that understanding the change in properties as the fiber dimensions decrease to the nanoscale is important to optimize the resultant properties of nanocomposites. As one/both of the components of the composites are electrospun nanofibers, emphasis is given to compare/summarize the enhancement or shortcomings of the nanofiber based nanocomposites with respect to the nanoparticle based nanocomposites. Nanofibrous scaffolds are ideal for the purpose of tissue regeneration because their dimensions are similar to the components of the extra cellular matrix (ECM) and mimic its fibrillar structure, providing essential signals for cellular assembly and proliferation. There are several scaffold fabrication techniques namely, electrospinning (random, aligned, core shell and vertical nanofibers), self-assembly, phase separation, melt-blown and template synthesis. Electrospinning is one of the most promising techniques for designing natural/polymer nanofibrous scaffolds for tissue engineering applications.

ECM is a complex arrangement of proteins and polysaccharides such as collagen, gelatin, chitosan, hyaluronic acid, proteoglycans, glycosaminoglycans and elastin, fabricated nanocomposites are also possess such adhesion factors, chemical functionalities and mechanical properties. Though drug molecules have significant potency against the disease for their release or the delivery of drugs at the desired site, without loss of their activity makes the difference. Thus drug delivery finds its importance and the use of biodegradable polymers for this purpose is inevitable.[64]

Recently, the synthesis and design of composite materials by blending nano-sized inorganic/organic and organic materials have generated great interests in the fields of material sciences due to their improved and enhanced properties and applicability.[64]

Simple technique used for the production of these composites, due to their distinction from the conventional polymer nanocomposites (film or bulky fiber) in the physical size of host polymer matrix and embedded particles of these hybrid materials and details of electrospinning/electrospraying set-up presented before. The electrospun composite nanofibers are found to possess both the advantages of organic polymers such as lightweight, flexibility and molding capability, and special functionality of inorganic/organic species such as high strength and thermal stability. Through electrospinning, the nanocomposite can be fabricated by any of the below methodologies:

1) Employing two or more precursor solution for the electrospinning to achieve multi-component nanofibers such as bi-component and core/shell nanofibers.[65,66]

2) Electrospinning of polymer solutions with dispersed inorganic/organic nanoparticles.[67,68]

3) Surface treatment of the electrospun nanofibers to achieve composite nanofibers.[69,70]

1.2.1 Composite nanofibers with inorganic additives

Organic–inorganic hybrid nanofibers can be easily obtained by electrospinning polymer solutions containing inorganic fillers, such as metal salts or metal and metalloid oxide nanoparticles, minerals etc., on condition that the inorganic phase is soluble or well dispersed in the initial polymer solution. Therefore, the preparation of the starting dispersion to be electrospun requires great attention and is a relevant issue in the production of hybrid fibers. A homogeneous inorganic filler dispersion, the absence of nanoparticle aggregation, and a narrow particle size distribution represent key challenges since these conditions are required to achieve optimal interaction between the nanofiller and the polymer phase.[71] Several metal (such as silver, gold or cobalt NPs), metal oxide (such as silicon, titanium, magnesium, aluminum, iron, zinc, and other mixed metal oxides), and metal chloride (such as cobalt chloride) nanoparticles were successfully incorporated into polymer fibers via direct dispersion electrospinning to obtain organic–inorganic nanofibers.[72–77]

Silver is typically incorporated within polymer fibers to confer antibacterial properties to the final fabric, for filtering applications or wound healing in the biomedical sector. In an interesting paper by He et al., Ag NPs were directly dispersed in a poly(vinyl alcohol) (PVA) solution, and assembled in an ordered linear chain-like structure along the fiber axis during the fiber stretching and thinning that occurs in the electrospinning process.[78]

Silica nanoparticles were electrospun with synthetic polymers such as polyacrylonitrile (PAN),[79] poly(vinylidene difluoride) (PVDF),[80] poly(methyl methacylate) (PMMA),[81] and PVA.[82] SiO_2 NPs were often embedded within electrospun polymer fibers to improve the mechanical properties of the obtained membranes, enhancing the tensile strength and Young's modulus and thus causing a reinforcing effect.[80]

Titanium oxide nanoparticles are typically used as inorganic fillers capable of improving mechanical and thermal properties of the polymer, as bactericide additives, and as nanocomponents with photocatalytic activity. Depending on the type of crystalline phase (anatase, rutile, or brookite), TiO_2 can be used as photocatalyst (anatase), or as white pigment (rutile) in industry. TiO_2 NPs were electrospun in combination with both hydrophobic (such as polysulfone (PSU),[83] PVDF,[84] and poly(ε-caprolactone) (PCL)[85]) and hydrophilic (PVA)[75] polymers. In particular, TiO_2 NPs incorporation increased the tensile strength of PSU membranes and their air permeability through the formation of micro- and nanoscale roughness on the fiber surface.[80]

Among metal chloride nanoparticles, $CoCl_2$ is used for applications in humidity sensing, as well as catalysis, e.g., for hydrogen production. $CoCl_2$ was successfully electrospun by direct dispersion into nanofibers of PVDF and PEO.[86,87]

The most straightforward methodology for incorporating inorganic nanoparticles into polymer fibers is to directly disperse them in the polymer solution before electrospinning. The simplest approach involves the addition of the inorganic nanoparticles to the polymer solution, followed by stirring or sonication to obtain a homogeneous suspension/mixture that is directly electrospun. Alternatively, the suspension containing the inorganic nanoparticles is prepared by ultrasonication or vigorous stirring and the polymer solution is subsequently added dropwise to obtain a hybrid organic–inorganic suspension that is then electrospun. The simple direct dispersion strategy is, however, quite problematic when a high loading of nanoparticles is desired, due to the high viscosity of the resulting dispersion that eventually prevents fiber formation and to the tendency of the nanoparticles to agglomerate. Particle aggregation might cause formation of bead defects along the fiber axis, heterogeneity in the final composite fiber and, therefore, poor quality of the obtained nanofibrous mat, with adverse effects on its properties. In order to facilitate uniform dispersion of the inorganic nanoparticles in polymer nanofibers, a modified nanoparticles is sometimes used.[73] Surface modification of inorganic nanoparticles has attracted a great deal of attention because it produces excellent integration and an improved interface between nanoparticles and polymer matrices.[88] To improve the dispersion stability of nanoparticles in aqueous media or polymer matrices, it is essential that the particle surface modification, involving polymer surfactant molecules or other modifiers, generates a strong repulsion between nanoparticles and increases compatibility of nanoparticles with matrices.

In the recent report by Hashem et al. surface of titanium oxide nanoparticles were modified with biodegradable nanocellolose and the surface modified TiO_2 were easily embedded in the polyimide matrix to fabricate membrane. Consequently, uniformly dispersion of surface modified TiO_2 with average diameter of around 50nm and a narrow size distribution was successfully achieved in polyimide matrix.[89]

1.2.2 Composite nanofibers with organic additives

Polymer blends are physical mixtures of at least two structurally different polymers, which adhere together with no covalent bonding between them. Each constituent can be a polymer or a copolymer, with a linear, branched or crosslinked structure. When one of the mixed polymers is the minor component, it can be considered simply as an additive. In the search for new polymeric materials, the composite with organic additives is a promising method for obtaining desirable properties using already known polymers. Organic additives same as polymer nanoparticles dendritic hyperbranched polymers (HBP) and dendrimers, have a high potential as additives and modifiers in engineering materials. The chemical and physical structure of star polymers induce unique properties that can solve the problems related to processability, property compromises, and compatibility, which are found with commercial additives and modifiers. As far as the addition of inorganic additives is concerned, various types of nanofillers were used such as metal NPs, metal oxide NPs, carbon nanotubes, and graphene, they are capable to modify properties of polymer nanofibers. Nevertheless, some issues have to be considered, which are mainly related to the dispersion of the inorganic phase into the polymer matrix, the material final properties depending on the quality of the dispersion, and the filler biocompatibility. The simple direct dispersion strategy is quite problematic when a high loading of nanoparticles is desired, due to the high viscosity of the resulting dispersion that eventually prevents fiber formation and to the tendency of the nanoparticles to agglomerate. Particle aggregation might cause formation of bead defects along the

fiber axis, heterogeneity in the final composite fiber and, therefore, poor quality of the obtained nanofibrous mat, with adverse effects on its properties.[71] An additional problem found in organic-inorganic nanocomposites is lower impact strength than that found in the organic precursor alone due to the stiffness of the inorganic material, leading to the use of elastomeric additives to increase the toughness of the composites.[88] On the other hand, even though organic additives, usually characterized by a better compatibility with organic matrix and capable of modifying the polymer properties, but are often found to decrease its mechanical properties. In general, among the organic additives that can be used to change linear polymer features, star polymers represent ideal fillers because of their compact shape and elevated concentration of functional end groups.[90,91] The specific advantages of the star polymer molecules are that (a) their chemistry can readily be tailored to have suitable mechanical properties, (b) they are reactive, and (c) they can readily be made compatible with the surrounding matrix material. However, as the above macromolecules are characterized by a higher solubility than their linear homologous, their leaching from the polymer matrix can limit the application of the related composite material.

Donald et al. reported for the first time the fabrication of electrospun nanocomposite fibers composed of dendrimer derivatives, namely PEGylated PAMAM dendrimers, blended with a small amount of high-molecular-weight polyethylene oxide (PEO). The dendrimer fibrous mats show weak mechanical properties that can be improved by adding more stable copolymers such as PLGA without compromising the functionality of dendrimers. In addition, dendrimer surface groups may be chemically functionalized to form a cross-linked network following electrospinning to further enhance structural stability and mechanical properties of dendrimer fibrous mats. Further improvements in the mat's mechanical properties can make it a potential platform for drug delivery and tissue engineering applications.[92]

1.3 Composite nanofibers application

As demonstrated in previous sections, electrospinning is a remarkably simple and powerful technique for generating composite nanomaterials. Because of the multifunctional properties of the composite materials, they are expected to be applied in many fields, such as energy, filters, sensors, and biomedical fields.

1.3.1 Energy applications

Energy is one of the most important global problems facing society in the 21st century. At present, fossil fuels including coal, oil, and natural gas supply most of the energy we purchase and makes what we do possible. However, fossil fuels pose a dilemma for human society. Fossil fuels are not renewable; once they are gone they are gone. Furthermore, pollutants emitted during the burning of fossil fuels degrade the environment and greenhouse gases lead to the global-warming problem. Therefore, developing technology and devices for highly efficient and clean energy is a meaningful challenge. Efficient use of energy is often connected with energy-conservation devices, such as solar cells, fuel cells, and energy-storage devices such as supercapacitors.[93]

1.3.1.1 Catalysis

The degradation of organic pollutants such as dyes and pesticides in aqueous solution by photocatalysis, using semiconductor metal oxides such as titanium oxide, zinc oxide, tin oxide and copper oxide (TiO_2, ZnO, SnO_2, CuO) has been the subject of great research due to their size-tunable physicochemical properties, high activities, durability and low cost. However, the fast

recombination rate of photo-generated electron/hole pairs in the bulk semiconductor materials lowers their photo-catalytic efficiency. To overcome these drawbacks, composite materials are being fabricated in order to extend the light absorption spectrum as well as suppressing the recombination of photo-generated electrons by virtue of the different Fermi levels of the ingredients in the composite materials. Due to their very large aspect ratios, photo-catalyst materials with fibrous morphology are superior to particles as far as the recycling and aggregation are concerned.[64] In principle, composite catalysts based on the electrospun polymeric or ceramic nanofibers mats can be synthesized in two ways. The first method is to electrospin the mixed solution of polymer or ceramic precursors with the metal salt to yield mats of composite fibers. Subsequently, the metal salts in the composite nanofibers need to be reduced, either by heating at high temperature or in the presence of a reducing agent, yielding polymer/metal or ceramic/metal composite nanofibers. The other method is posttreatment of the electrospun nanofibers mats to deposit metal nanoparticles on the surface of the fibers.[94]

1.3.1.2 Batteries

Among various energy storage devices available, rechargeable lithium-ion batteries with their high-energy density, long cycle lives, and flexible design, are considered as the effective solution to the ever- increasing demand for high-energy density electrochemical power sources. This demand has promoted research efforts towards the developing high-capacity alternative electrode materials with long life cycle, improved safety, reduced carbon-footprint, and low cost. In this regard, Ji et al. fabricated a variety of composite materials through electrospinning and observed improved performance with regard to their pure counterparts. The composite material included nickel particles dispersed in carbon nanofibers, copper/carbon composite and polyacrylonitrile/polypyrrole composite nanofibers. They observed that the anode performance improved from the incorporation of a Li-inactive nickel.[95] Recently, Chen and co-workers have synthesized carbon/cobalt composite nanofibers via electrospinning and a subsequent heating treatment. The asprepared carbon/cobalt composite nanofibers have a high conductivity, a large reversible capacity of more than 800mAh g^{-1}, and good cycling performance.[96]

1.3.1.3 Fuel cells

The fuel cells work on the same principle as batteries for converting chemical energy into electricity with the difference that the batteries are standalone devices whereas chemicals are constantly supplied into the fuel cell. The majority of fuel cells used hydrogen and oxygen as the main fuel source for producing electricity. Fuel cells are usually classified based on the operating temperature or the type of electrolyte used. On the basis of operating temperatures, the fuel cells can be classified as polymer exchange membrane fuel cell (low temperature 60 to 80°C i.e. low warm-up time), solid oxide fuel cell (high temperature 700 to 1000°C , low reliability with high stability in continuous use) and molten-carbonate fuel cell (600°C). The proton exchange membrane fuel cell converts chemical energy into electrical energy with high efficiency and low pollutants and thus making it one of the most promising power sources for portable and automotive applications. The focus is on developing membranes that are able to achieve appreciably high proton conductivity, low gas permeability into the fuel and oxidant, high thermal stability, and durability.[64] Among different kinds of fuel cell, the direct methanol fuel cells (DMFCs) have been widely studied recently for their room-temperature operation and potential high energy density. In DMFCs, supporting materials are necessary to load catalysts of platinum nanoparticles or its alloy. It has been proved that the supporting materials have a great effect on the catalytic activity of platinum

nanoparticles. To improve the anode catalyst performance, the supporting materials should be stable, a good electron conductor, and have a large surface area. Therefore, various carbon materials such as mesocarbon, carbon fibers, and carbon nanotubes have been widely used as catalyst supports for DMFCs. Through the electrospinning technique, continuous nanoscale carbon fibers and nanoporous carbon fibers have been synthesized, which are good candidates for catalyst supports.[94] Han and co-workers have synthesized Pt-cluster-supported carbon fibrous mats (CFMs/Pt) by the electrospinning and electrodepositing methods for DMFCs. In contrast to the commercial catalyst, the catalytic peak current on optimum CFMs/Pt electrode has increased.[97]

1.3.1.4 Solar cells

Gratzel was the first person to fabricate dye-sensitized solar cells (DSSCs) in 1991.[98] Within the past decade, DSSCs have gained considerable attention as a potential technique for harnessing sunlight, a largely abundant renewable-energy source. For dye-sensitized solar cells, it is believed that metal oxide nanostructures with one-dimension morphology have a better charge conduction for increasing energy conversion efficiency. Electrospun TiO_2 nanofibers or nanorods are most widely studied as an electrode for DSSCs for their high surface area and large pores for the increased adsorption of dye sensitizers. In order to improve the adhesion between one-dimension TiO_2 nanomaterials and the conductive substrates, many methods have been investigated, such as hot press pretreatment, solvent vapor, mechanical grinding, use of an ultrathin surface treatment layer on conductive substrates, and so on.[94] After the anchoring of ruthenium dyes onto the electrospun TiO_2 nanomaterials to form composites for DSSCs, the best-performing DSSC gives a current density of 13.6mA cm^{-2}, an open-circuit voltage of 0.8 V, a fill factor of 51%, and an energy-conversion efficiency of 5.8%.[99]

1.3.2 Filters

Air filtration technologies have traditionally found numerous applications such as in semiconductor and the health-care industry. One of the key elements for effective air filtration is the filter media, usually made of nonwoven fabrics, such as glass fibers, electrospun fibers, etc. The usual criteria for high performance air filters are high filtration efficiency with low pressure drop. Kim et al. fabricated poly(acrylonitrile) nano-web on a commercial melt-blown poly(propylene) (PP) filter medium to generate composite filter media.[162] Structural characterization performed on the composite filter showed that a thin layer of electrospun nano-web can improve the overall performance by increasing filtration efficiency without significantly increasing the pressure drop of the composite membrane.[64]

1.3.3 Sensors

In recent years, the development of composite based gas sensor technology has received considerable attention in many areas such as agriculture, medicine, meteorology, aerospace application on board space vehicles and other industrial facilities. Polymer and metal oxide composites have been extensively investigated as sensitive materials, which exhibited better sensing properties, such as shorter response time, smaller hysteresis, higher sensitivity and improved stability. Many strategies have been developed to fabricate composite sensors with high sensitivity and excellent reproducibility. Enhancement of sensor performance can be achieve through (1) an accurate control of the morphology in the nanometre range of composition and of the surface state of the sensing materials, (2) the integration of the sensor components (3) the optimization of the

working temperature of sensitive layer, the operating mode, and the signal processing, and (4) the use of filters exhibiting selective gas retention or conversion properties. All these rely on new, highly sensitive materials and good fabrication technology.

Many researchers expect to obtain composite nanofiber sensors with high sensitivity, rapid response, reversibility at room temperature and convenient operation. Among all methods, electrospinning is one of the simplest and most cost effective techniques to produce organic/inorganic nanofibers for sensor applicaton.[64]

1.3.4 Biomedical applications

From a biological viewpoint, electrospun nanofibers are the most promising material that can be applicable in medicine and pharmacy because almost all human tissues and organs, including bone, dentin, collagen, cartilage, and skin, have dimensions on this order. During the past few years, the field of application for electrospun polymeric nanofibers has developed very quickly; a series of natural polymers, such as proteins, polysaccharides, DNAs and lipids and synthetic polymers such as polyurethane, polyvinyl alcohol, polyethylene oxide, polycaprolactone, polylactic acid, polyglycolide, polydioxanone, polyphosphazene derivatives, and synthetic copolymers have been electrospun into nanofibers. Such electrospun materials can be applied for tissue engineering, immobilized enzymes, wound healing, artificial blood vessels, drug delivery, and so on.[94] However, the limited properties of electrospun polymer nanofibers with only one component restrict their application in biomedical engineering. Therefore, electrospun composite nanofibrous scaffolds are an appealing option. In the following, there are a few examples of applications of one-dimension electrospun composite nanomaterials for drug delivery, tissue engineering, and wound dressing.

1.3.4.1 Tissue engineering

Electrospun nanofiber scaffolds have high surface area and high porosity, which is a good candidate for use in tissue engineering. Various biocompatible and biodegradable polymers have been electrospun to form fiber scaffolds.[94] However, there are not many reports on the fabrication of electrospun scaffolds based on polymer/polymer and polymer/inorganic composites, which can enhance both the physical properties and biological functionality.

Zhang and co-workers demonstrated that PCL/gelatin composite fibers could be prepared by electrospinning their mixed solutions in 2,2,2-trifluoroehtanol solvent. Compared to either PCL or gelatin fibers alone, the mechanical properties and wettability were both improved. Moreover, as a promising scaffolds for bone-marrow stromal cell (BMSC) culture, the PCL/gelatin composite fibers were more favorable for BMSC growth and migration than PCL scaffold alone. This was due to the good hydrophilicity, cellular affinity, and dissolution of PCL/gelatin composite nanofibers during cell culture, as well as the elongation and deformation properties of the composite scaffold.[100]

Kohand co-workers successfully prepared PLLA/laminin composite nanofibers through three different methods: covalent binding, physical adsorption, and blended electrospinning. The results showed that blended electrospinning affords a useful and easy method to modify polymer nanofibers to produce composite biomimetic scaffolds for enhancing neurite outgrowth compared to the other two methods, which have potential applications in neural tissue repair.[101]

Composite nanofibers with a core/sheath structure can also be used for tissue-engineering applications. Zhang and coworkers prepared collagen-coated PCL nanofibers by a coaxial electrospinning technique. The authors used the synthetic polymer (PCL) with better mechanical

performance as the core and natural polymer (collagen) for functional purposes. The results showed that coatings of collagen on electrospun PCL nanofibers favored cell proliferation.[102]

In addition to polymer/polymer or polymer/biological composite nanofibers, inorganic nanocomponents were also incorporated into polymer nanofibers for the application of tissue engineering. For example, the incorporation of calcium carbonate, calcium phosphate, and hydroxyl-apatite (HA), with similar crystallographic structure to inorganic materials found in natural bones, into the electrospun polymer scaffold made of a synthetic biodegradable or natural polymer was able to assist the bone cell regeneration. Fujihara and co-workers demonstrated the incorporation of calcium carbonate in the electrospun PCL scaffold by electrospinning the mixture of PCL and calcium carbonate at different compositions on the surface of electrospun PCL nanofibrous mats. Therefore, the mats consist of both functional layer (PCL/calcium carbonate) and mechanical support layer (PCL). The results showed that both composite mats with different PCL/calcium carbonate compositions exhibit good cell attachment and proliferation.[103] Similar results have also been observed for betatertiary calcium phosphate incorporated into electrospun PLA scaffolds.[104]

1.3.4.2 Drug delivery

A drug-delivery system consists of a formulation or a device that enables introduction of a therapeutic agent in the body and enhances its efficacy and safety by controlling the rate, time, and site of release within the body. This system is aimed at delivering and retaining a sufficient amount of drug for an adequate period of time, and it is also expected to avoid degradation of non-released drugs within the body.[105]

Electrospun nanofibers for drug delivery have many advantages, such as easy implementation, little influence on the drug activity, well-controlled release rate, and so on.[94] In most cases, the release of water-soluble drugs incorporated into a water-soluble polymer will exhibit an early stage burst. Therefore, the emulsion electrospinning method and composite nanofibers was proposed. Emulsion electrospinning of polymer/drug system encapsulates drugs inside the polymer nanofibers.[106] Hsiao and co-workers demonstrated that using electrospun composite nanofibers (PLGA/PLA/PEG-b-PLA) showed a sustained release profile after the initial burst compared to PLGA scaffold. This was because the drug could be trapped in electrospun nanofibers as a complex with the hydrophilic block of PEG-b-PLA, resulting in the sustained release behavior. However, such a method could not avoid the initial burst.[107] Similar to emulsion electrospinning, coaxial electrospinning could also encapsulate drugs in the PCL fibers, forming a core/sheath structure. The degradation and drug release rates of the composite nanofibers were related to the hydrophilicity of the drugs. The drug release was smooth and no burst release occurred.[108]

Another promising way to control the release profile of drugs is by coating a thin layer of polymer on the surface of drug encapsulated electrospun nanofibers. Greiner and co-workers prepared bovine serum albumin (BSA)-loaded PVA nanofibers by electrospinning. By modifying a layer of Poly(p-xylylene) (PPX) using a CVD method, they obtained BSA-loaded PPX/PVA composite fibers. In contrast with PVA fibers, no burst release for PPX/PVA composite fibers was observed.[109]

1.3.4.3 Wound dressing

Effective wound dressings are highly desired in various areas, such as promoting wound healing, hemostasis, skin regeneration, diabetic ulcers, and tissue engineering. A good wound dressing can maintain a moist environment at the interface, provide mechanical protection, prevent

bacterial penetration, and allow gas-fluid exchange. In addition, it is non-adhesive to the wound and easily removed without trauma. However, the dressings used in specific fields may have their unique properties and requirements.

A variety of nanofibers prepared with renewable materials including chitosan, fibrinogen, silk fibrin, bacterial cellulose, gelatin, and collagen and composites of these materials can promote wound healing and show antibacterial activity, good adhesion, good absorption, and nontoxicity and sufficient gas-exchange properties.[110] The mats prepared with the nanofibers have unique porous structures and high surface areas, which are beneficial to cell regeneration and the wetness of the wound. In addition, the mats can protect the wound from the harmful external environments.[110] The bioactive molecules or drugs can be easily incorporated in the fibers by electrospinning to provide additional functions such as anti-inflammatory activity and tissue growth-promoting activity.[111,112]

As well, polymer/Ag composite nanofibers have been widely studied for the application of wound dressing because elemental Ag and Ag salts have been used as antimicrobial agents for decades. Hong and co-workers demonstrated that PVA/Ag composite nanofibers could be prepared by electrospinning PVA/$AgNO_3$ aqueous solution, followed by heat treatment or UV radiation. TEM images of the obtained PVA/Ag composite nanofibers showed that Ag nanoparticles were generated and well dispersed in the near surface of the electrospun nanofibers, indicating Ag ions have been reduced to Ag nanoparticles either by heat treatment or UV radiation. Electrospun PVA/Ag composite nanofibers showed excellent antibacterial activity; however, the disadvantage was the gray–blue discoloration on the skin.[113] In order to reduce the discoloration, silver-loaded zirconium phosphate nanoparticles have also been investigated as wound-dressing materials. The results showed that the composite fibers maintained the strong killing abilities against the tested bacteria strains, although Ag existed in the zirconium phosphate nanoparticles. Moreover, discoloration has not been observed in the nanofibers.[114] Recently, Youngs and co-workers demonstrated that the encapsulation of silver-imidazole cyclophane gem-diol complex into hydrophilic Tecophilic nanofibers also showed excellent bactericidal activity. The composite fibers released silver nanoparticles in a sustained profile over a long time. Therefore, the rate of bactericidal activity of the silver complex was significantly improved, and the amount of silver used was much reduced. The composite fibers as scaffold were found to be effective against E. coli, P. aeruginosa, S. aureus, C. albicans, A. niger,and S. cerevisiae.[115]

1.4 References

1. Huang ZM, Zhang YZ, Kotaki M, Ramakrishna S. A review on polymer nanofibers by electrospinning and their applications in nanocomposites. *Compos Sci Technol*. 2003;63(15):2223-2253. doi:10.1016/S0266-3538(03)00178-7.

2. Khan I, Saeed K, Khan I. Nanoparticles: Properties, applications and toxicities. *Arab J Chem*. 2017. doi:10.1016/j.arabjc.2017.05.011.

3. Bhattarai SR, Bhattarai N, Yi HK, Hwang PH, Cha D Il, Kim HY. Novel biodegradable electrospun membrane: Scaffold for tissue engineering. *Biomaterials*. 2004;25(13):2595-2602. doi:10.1016/j.biomaterials.2003.09.043.

4. Xu CY, Inai R, Kotaki M, Ramakrishna S. Aligned biodegradable nanofibrous structure: A potential scaffold for blood vessel engineering. *Biomaterials*. 2004;25(5):877-886. doi:10.1016/S0142-9612(03)00593-3.

5. Ellison CJ, Phatak A, Giles DW, Macosko CW, Bates FS. Melt blown nanofibers: Fiber diameter distributions and onset of fiber breakup. *Polymer (Guildf)*. 2007;48(11):3306-3316. doi:10.1016/j.polymer.2007.04.005.

6. Zuo F, Tan DH, Wang Z, Jeung S, MacOsko CW, Bates FS. Nanofibers from melt blown fiber-in-fiber polymer blends. *ACS Macro Lett*. 2013;2(4):301-305. doi:10.1021/mz400053n.
7. Martin CR. Membrane-Based Synthesis of Nanomaterials. *Chem Mater*. 1996;8(8):1739-1746. doi:10.1021/cm960166s.
8. Feng L, Li S, Li H, et al. Super-hydrophobic surface of aligned polyacrylonitrile nanofibers. *Angew Chemie - Int Ed*. 2002;41(7):1221-1223. doi:10.1002/1521-3773(20020402)41:7<1221::AID-ANIE1221>3.0.CO;2-G.
9. Weinberg M, Dee G, Harding T. Flash spun web containing sub-micron filaments and process for forming same. 2006:1-15. US20060135020A1
10. Ma PX, Zhang R. Synthetic nano-scale fibrous extracellular matrix. *J Biomed Mater Res*. 1999;46(1):60-72. doi:10.1002/(SICI)1097-4636(199907)46:1<60::AID-JBM7>3.0.CO;2-H.
11. Ondarcuhu T, Joachim C. Drawing a single nanofibre over handreds of microns. *Europhys Lett*. 1998;42(2):215-220.
12. Whitesides GM. Self-Assembly at All Scales. *Science (80-)*. 2002;295(5564):2418-2421. doi:10.1126/science.1070821.
13. Liu G, Ding J, Qiao L, et al. Polystyrene - block - poly (2 - cinnamoylethyl methacrylate) Nanofibers - Preparation , Characterization , and Liquid Crystalline Properties. *Chem - A Eur J*. 1999;5(9):2740-2749. doi:http://dx.doi.org/10.1002/(SICI)1521-3765(19990903)5:9<2740::AID-CHEM2740>3.0.CO;2-V.
14. Dutton KC. Overview and analysis of the meltblown process and parameters. *J Text Apparel, Technol Manag*. 2008;6(1):25. http://ojs.cnr.ncsu.edu/index.php/JTATM/article/view/342.
15. Huczko A. Template-based synthesis of nanomaterials. *Appl Phys A Mater Sci Process*. 2000;70(4):365-376. doi:10.1007/s003390051050.
16. Li H, Ke Y, Hu Y. Polymer nanofibers prepared by template melt extrusion. *J Appl Polym Sci*. 2006;99(3):1018-1023. doi:10.1002/app.22597.
17. Meredith JC, Amis EJ. LCST phase separation in biodegradable polymer blends: poly(D,L-lactide) and poly(epsilon-caprolactone). *Macromol Chem Phys*. 2000;201(6):733-739. doi:10.1002/(sici)1521-3935(20000301)201:6<733::aid-macp733>3.3.co;2-x.
18. He C, Nie W, Feng W. Engineering of biomimetic nanofibrous matrices for drug delivery and tissue engineering. *J Mater Chem B*. 2014;2(45):7828-7848. doi:10.1039/C4TB01464B.
19. Hartgerink JD, Beniash E, Stupp SI. Self-assembly and mineralization of peptide-amphiphile nanofibers. *Science*. 2001;294(5547):1684-1688. doi:10.1126/science.1063187.
20. Liu G, Qiao L, Guo A. Diblock Copolymer Nanofibers. *Macromolecules*. 1996;29(16):5508-5510. doi:10.1021/ma9604653.
21. Yan X, Liu G, Liu F, et al. Superparamagnetic Triblock Copolymer/Fe2O3 Hybrid Nanofibers NSERC of Canada is acknowledged for sponsoring this research. Dr. R. Yamdagni and Ms. Q. Wu are thanked for help with the use of their NMR magnet. Dr. Zhao Li is thanked for performing the TGA a. *Angew Chemie Int Ed*. 2001;40(19):3593. doi:10.1002/1521-3773(20011001)40:19<3593::AID-ANIE3593>3.0.CO;2-U.
22. Silva GA. Selective Differentiation of Neural Progenitor Cells by High-Epitope Density Nanofibers. *Science (80-)*. 2004;303(5662):1352-1355. doi:10.1126/science.1093783.
23. Xing X, Wang Y, Li B. Nanofibers drawing and nanodevices assembly in poly(trimethylene terephthalate). *Opt Express*. 2008;16(14):10815-10822. doi:10.1364/OE.16.010815.
24. Tong L, Mazur E. Glass nanofibers for micro- and nano-scale photonic devices. *J Non Cryst Solids*. 2008;354(12-13):1240-1244. doi:10.1016/j.jnoncrysol.2006.10.090.
25. Formhals A. Oct. 2, 1934- A," FORMHALS-. 1934. US1975504A
26. Reneker DH, Chun I. Nanometre diameter fibres of polymer, produced by electrospinning. *Nanotechnology*. 1996;7(3):216-223. doi:10.1088/0957-4484/7/3/009.

27. Haider A, Haider S, Kang IK. A comprehensive review summarizing the effect of electrospinning parameters and potential applications of nanofibers in biomedical and biotechnology. *Arab J Chem*. 2015. doi:10.1016/j.arabjc.2015.11.015.
28. Deitzel J., Kleinmeyer J, Harris D, Beck Tan N. The effect of processing variables on the morphology of electrospun nanofibers and textiles. *Polymer (Guildf)*. 2001;42(1):261-272. doi:10.1016/S0032-3861(00)00250-0.
29. Zafar M, Najeeb S, Khurshid Z, et al. Potential of electrospun nanofibers for biomedical and dental applications. *Materials (Basel)*. 2016;9(2):1-21. doi:10.3390/ma9020073.
30. Bhardwaj N, Kundu SC. Electrospinning: A fascinating fiber fabrication technique. *Biotechnol Adv*. 2010;28(3):325-347. doi:10.1016/j.biotechadv.2010.01.004.
31. Kim B, Park H, Lee S-H, Sigmund WM. Poly(acrylic acid) nanofibers by electrospinning. *Mater Lett*. 2005;59(7):829-832. doi:10.1016/j.matlet.2004.11.032.
32. Son WK, Youk JH, Lee TS, Park WH. The effects of solution properties and polyelectrolyte on electrospinning of ultrafine poly(ethylene oxide) fibers. *Polymer (Guildf)*. 2004;45(9):2959-2966. doi:10.1016/j.polymer.2004.03.006.
33. Zong X, Kim K, Fang D, Ran S, Hsiao BS, Chu B. Structure and process relationship of electrospun bioabsorbable nanofiber membranes. *Polymer (Guildf)*. 2002;43(16):4403-4412. doi:10.1016/S0032-3861(02)00275-6.
34. Gupta P, Elkins C, Long TE, Wilkes GL. Electrospinning of linear homopolymers of poly(methyl methacrylate): Exploring relationships between fiber formation, viscosity, molecular weight and concentration in a good solvent. *Polymer (Guildf)*. 2005;46(13):4799-4810. doi:10.1016/j.polymer.2005.04.021.
35. Tan S-H, Inai R, Kotaki M, Ramakrishna S. Systematic parameter study for ultra-fine fiber fabrication via electrospinning process. *Polymer (Guildf)*. 2005;46(16):6128-6134. doi:10.1016/j.polymer.2005.05.068.
36. Fong H, Chun I, Reneker DH. Beaded nanofibers formed during electrospinning. *Polymer (Guildf)*. 1999;40(16):4585-4592. doi:10.1016/S0032-3861(99)00068-3.
37. Nasouri K, Shoushtari AM, Mojtahedi MRM. Effects of polymer/solvent systems on electrospun polyvinylpyrrolidone nanofiber morphology and diameter. *Polym Sci Ser A*. 2015;57(6):747-755. doi:10.1134/S0965545X15060164.
38. Casasola R, Thomas NL, Trybala A, Georgiadou S. Electrospun poly lactic acid (PLA) fibres: Effect of different solvent systems on fibre morphology and diameter. *Polym (United Kingdom)*. 2014;55(18):4728-4737. doi:10.1016/j.polymer.2014.06.032.
39. Jun Z, Hou H, Schaper A, Wendorff JH, Greiner A. Poly-L-lactide nanofibers by electrospinning - Influence of solution viscosity and electrical conductivity on fiber diameter and fiber morphology. *E-Polymers*. 2003;3(1):1-9. doi:10.1515/epoly.2003.3.1.102.
40. Jiang H, Fang D, Hsiao BS, Chu B, Chen W. Optimization and characterization of dextran membranes prepared by electrospinning. *Biomacromolecules*. 2004;5(2):326-333. doi:10.1021/bm034345w.
41. Du L, Xu H, Zhang Y, Zou F. Electrospinning of polycaprolatone nanofibers with DMF additive: The effect of solution proprieties on jet perturbation and fiber morphologies. *Fibers Polym*. 2016;17(5):751-759. doi:10.1007/s12221-016-6045-3.
42. Hsu CM, Shivkumar S. N,N-dimethylformamide additions to the solution for the electrospinning of poly(ε-caprolactone) nanofibers. *Macromol Mater Eng*. 2004;289(4):334-340. doi:10.1002/mame.200300224.
43. Sill TJ, von Recum HA. Electrospinning: Applications in drug delivery and tissue engineering. *Biomaterials*. 2008;29(13):1989-2006. doi:10.1016/j.biomaterials.2008.01.011.
44. Demir MM, Yilgor I, Yilgor E, Erman B. Electrospinning of polyurethane fibers. *Polymer*

(Guildf). 2002;43(11):3303-3309. doi:10.1016/S0032-3861(02)00136-2.
45. Megelski S, Stephens JS, Bruce Chase D, Rabolt JF. Micro- and nanostructured surface morphology on electrospun polymer fibers. *Macromolecules*. 2002;35(22):8456-8466. doi:10.1021/ma020444a.
46. Zeleny J. The role of surface instability in electrical discharges from drops of alcohol and water in air at atmospheric pressure. *J Franklin Inst*. 1935;219(6). doi:http://dx.doi.org/10.1016/S0016-0032(35)91985-8.
47. Nangrejo M, Bragman F, Ahmad Z, Stride E, Edirisinghe M. Hot electrospinning of polyurethane fibres. *Mater Lett*. 2012;68:482-485. doi:10.1016/j.matlet.2011.11.019.
48. Matabola KP, Moutloali RM. The influence of electrospinning parameters on the morphology and diameter of poly(vinyledene fluoride) nanofibers- Effect of sodium chloride. *J Mater Sci*. 2013;48(16):5475-5482. doi:10.1007/s10853-013-7341-6.
49. Wang T, Kumar S. Electrospinning of polyacrylonitrile nanofibers. *J Appl Polym Sci*. 2006;102(2):1023-1029. doi:10.1002/app.24123.
50. Huang L, Bui NN, Manickam SS, McCutcheon JR. Controlling electrospun nanofiber morphology and mechanical properties using humidity. *J Polym Sci Part B Polym Phys*. 2011;49(24):1734-1744. doi:10.1002/polb.22371.
51. Pelipenko J, Kristl J, Janković B, Baumgartner S, Kocbek P. The impact of relative humidity during electrospinning on the morphology and mechanical properties of nanofibers. *Int J Pharm*. 2013;456:125-134. doi:10.1016/j.ijpharm.2013.07.078.
52. Cui L, Yang Y, Hsu C, Cui Y. Carbon - Silicon Core - Shell Nanowires as High Capacity Electrode for Lithium Ion Batteries 2009. *Nano Lett*. 2009;9 No.9(Cvd):1-5. doi:10.1021/nl901670t.
53. Lu H-W, Li D, Sun K, Li Y-S, Fu Z-W. Carbon nanotube reinforced NiO fibers for rechargeable lithium batteries. *Solid State Sci*. 2009;11(5):982-987. doi:10.1016/j.solidstatesciences.2009.02.014.
54. Ji L, Zhang X. Electrospun carbon nanofibers containing silicon particles as an energy-storage medium. *Carbon N Y*. 2009;47(14):3219-3226. doi:10.1016/j.carbon.2009.07.039.
55. Goyal A, Reddy ALM, Ajayan PM. Flexible carbon nanotube-Cu2O hybrid electrodes for Li-ion batteries. *Small*. 2011;7(12):1709-1713. doi:10.1002/smll.201002051.
56. Lee JJ, Park EW, Hyun SH. Performance and evaluation of Cu-based nano-composite anodes for direct utilisation of hydrocarbon fuels in SOFCs. *Fuel Cells*. 2010;10(1):145-155. doi:10.1002/fuce.200800186.
57. Mollá S, Compañ V. Polyvinyl alcohol nanofiber reinforced Nafion membranes for fuel cell applications. *J Memb Sci*. 2011;372(1-2):191-200. doi:10.1016/j.memsci.2011.02.001.
58. Choi BG, Hong J, Park YC, et al. Innovative polymer nanocomposite electrolytes: Nanoscale manipulation of ion channels by functionalized graphenes. *ACS Nano*. 2011;5(6):5167-5174. doi:10.1021/nn2013113.
59. Liu L, Huang ZM, He CL, Han XJ. Mechanical performance of laminated composites incorporated with nanofibrous membranes. *Mater Sci Eng A*. 2006;435-436:309-317. doi:10.1016/j.msea.2006.07.064.
60. Sihn S, Kim RY, Huh W, Lee KH, Roy AK. Improvement of damage resistance in laminated composites with electrospun nano-interlayers. *Compos Sci Technol*. 2008;68(3-4):673-683. doi:10.1016/j.compscitech.2007.09.015.
61. Dong S, Chen X, Gu L, et al. A biocompatible titanium nitride nanorods derived nanostructured electrode for biosensing and bioelectrochemical energy conversion. *Biosens Bioelectron*. 2011;26(10):4088-4094. doi:10.1016/j.bios.2011.03.040.
62. Khlebtsov B, Panfilova E, Khanadeev V, et al. Nanocomposites containing silica-coated gold-

silver nanocages and Yb-2,4-dimethoxyhematoporphyrin: Multifunctional capability of IR-luminescence detection, photosensitization, and photothermolysis. *ACS Nano*. 2011;5(9):7077-7089. doi:10.1021/nn2017974.
63. Balogh L, Nigavekar SS, Nair BM, et al. Significant effect of size on the in vivo biodistribution of gold composite nanodevices in mouse tumor models. *Nanomedicine Nanotechnology, Biol Med*. 2007;3(4):281-296. doi:10.1016/j.nano.2007.09.001.
64. Sahay R, Kumar PS, Sridhar R, et al. Electrospun composite nanofibers and their multifaceted applications. *J Mater Chem*. 2012;22(26):12953. doi:10.1039/c2jm30966a.
65. Bellan LM, Craighead HG. Nanomanufacturing Using Electrospinning. *J Manuf Sci Eng*. 2009;131(3):34001. doi:10.1115/1.3123342.
66. Wang N, Chen H, Lin L, et al. Multicomponent phase change microfibers prepared by temperature control multifluidic electrospinning. *Macromol Rapid Commun*. 2010;31(18):1622-1627. doi:10.1002/marc.201000185.
67. Ayutsede J, Gandhi M, Sukigara S, et al. Carbon nanotube reinforced Bombyx mori silk nanofibers by the electrospinning process. *Biomacromolecules*. 2006;7(1):208-214. doi:10.1021/bm0505888.
68. Aryal S, Kim CK, Kim KW, Khil MS, Kim HY. Multi-walled carbon nanotubes/TiO2 composite nanofiber by electrospinning. *Mater Sci Eng C*. 2008;28(1):75-79. doi:10.1016/j.msec.2007.10.002.
69. Ayodeji O, Graham E, Kniss D, Lannutti J, Tomasko D. Carbon dioxide impregnation of electrospun polycaprolactone fibers. *J Supercrit Fluids*. 2007;41(1):173-178. doi:10.1016/j.supflu.2006.09.011.
70. Bianco A, Iardino G, Bertarelli C, Miozzo L, Papagni A, Zerbi G. Modification of surface properties of electrospun polyamide nanofibers by means of a perfluorinated acridine. *Appl Surf Sci*. 2007;253(20):8360-8364. doi:10.1016/j.apsusc.2007.04.003.
71. Hoffmann F, Fröba M. *Organic –Inorganic Hybrid Nanomaterials*.; 2011. doi:10.1007/978-3-319-13593-9.
72. Xu X, Yang Q, Wang Y, Yu H, Chen X, Jing X. Biodegradable electrospun poly(l-lactide) fibers containing antibacterial silver nanoparticles. *Eur Polym J*. 2006;42(9):2081-2087. doi:10.1016/j.eurpolymj.2006.03.032.
73. Kim GM, Wutzier A, Radusch HJ, et al. One-dimensional arrangement of gold nanoparticles by electrospinning. *Chem Mater*. 2005;17(20):4949-4957. doi:10.1021/cm0508120.
74. Mortimer CJ, Wright CJ. The fabrication of iron oxide nanoparticle-nanofiber composites by electrospinning and their applications in tissue engineering. *Biotechnol J*. 2017;12(7):1-10. doi:10.1002/biot.201600693.
75. Hamadanian M, Akbari A, Jabbari V. Electrospun titanium dioxide nanofibers: Fabrication, properties and its application in photo-oxidative degradation of methyl orange (MO). *Fibers Polym*. 2011;12(7):880-885. doi:10.1007/s12221-011-0880-z.
76. Jamnongkan T, Shirota R, Sukumaran SK, Sugimoto M, Koyama K. Effect of ZnO nanoparticles on the electrospinning of poly(vinyl alcohol) from aqueous solution: Influence of particle size. *Polym Eng Sci*. 2014;54(9):1969-1975. doi:10.1002/pen.23730.
77. Wu H, Zhang R, Liu X, Lin D, Pan W. Electrospinning of Fe, Co, and Ni nanofibers: Synthesis, assembly, and magnetic properties. *Chem Mater*. 2007;19(14):3506-3511. doi:10.1021/cm070280i.
78. Zhang CL, Lv KP, Cong HP, Yu SH. Controlled assemblies of gold nanorods in PVA nanofiber matrix as flexible free-standing SERS substrates by electrospinning. *Small*. 2012;8(5):647-653. doi:10.1002/smll.201290030.
79. Wang N, Si Y, Wang N, et al. Multilevel structured polyacrylonitrile/silica nanofibrous membranes for high-performance air filtration. *Sep Purif Technol*. 2014;126:44-51.

doi:10.1016/j.seppur.2014.02.017.
80. Kim YJ, Ahn CH, Lee MB, Choi MS. Characteristics of electrospun PVDF/SiO2 composite nanofiber membranes as polymer electrolyte. *Mater Chem Phys*. 2011;127(1-2):137-142. doi:10.1016/j.matchemphys.2011.01.046.
81. Hsu CY, Liu YL. Rhodamine B-anchored silica nanoparticles displaying white-light photoluminescence and their uses in preparations of photoluminescent polymeric films and nanofibers. *J Colloid Interface Sci*. 2010;350(1):75-82. doi:10.1016/j.jcis.2010.06.011.
82. Jin Y, Yang D, Kang D, Xiang X. Fabrication of necklace-like structures via electrospinning. *Langmuir*. 2010;26(2):1186-1190. doi:10.1021/la902313t.
83. Wan H, Wang N, Yang J, et al. Hierarchically structured polysulfone/titania fibrous membranes with enhanced air filtration performance. *J Colloid Interface Sci*. 2014;417:18-26. doi:10.1016/j.jcis.2013.11.009.
84. Cui WW, Tang DY, Gong ZL. Electrospun poly(vinylidene fluoride)/poly(methyl methacrylate) grafted TiO 2 composite nanofibrous membrane as polymer electrolyte for lithium-ion batteries. *J Power Sources*. 2013;223:206-213. doi:10.1016/j.jpowsour.2012.09.049.
85. Gupta KK, Kundan A, Mishra PK, et al. Polycaprolactone composites with TiO2 for potential nanobiomaterials: tunable properties using different phases. *Phys Chem Chem Phys*. 2012;14(37):12844. doi:10.1039/c2cp41789h.
86. Chinnappan A, Kang HC, Kim H. Preparation of PVDF nanofiber composites for hydrogen generation from sodium borohydride. *Energy*. 2011;36(2):755-759. doi:10.1016/j.energy.2010.12.048.
87. Abiona AA, Ajao JA, Chigome S, Kana JBK, Osinkolu GA, Maaza M. Synthesis and characterization of cobalt chloride/poly(ethylene oxide) electrospun hybrid nanofibers. *J Sol-Gel Sci Technol*. 2010;55(2):235-241. doi:10.1007/s10971-010-2239-0.
88. Kango S, Kalia S, Celli A, Njuguna J, Habibi Y, Kumar R. Surface modification of inorganic nanoparticles for development of organic-inorganic nanocomposites - A review. *Prog Polym Sci*. 2013;38(8):1232-1261. doi:10.1016/j.progpolymsci.2013.02.003.
89. Ahmadizadegan H. Surface modification of TiO2 nanoparticles with biodegradable nanocellolose and synthesis of novel polyimide/cellulose/TiO2 membrane. *J Colloid Interface Sci*. 2017;491:390-400. doi:10.1016/j.jcis.2016.11.043.
90. Inoue K. Functional dendrimers, hyperbranched and star polymers. *Prog Polym Sci*. 2000;25(4):453-571. doi:10.1016/S0079-6700(00)00011-3.
91. Cameron DJA, Shaver MP. Aliphatic polyester polymer stars: synthesis, properties and applications in biomedicine and nanotechnology. *Chem Soc Rev*. 2011;40(3):1761-1776. doi:10.1039/C0CS00091D.
92. Aduba DC, Overlin JW, Frierson CD, Bowlin GL, Yang H. Electrospinning of PEGylated polyamidoamine dendrimer fibers. *Mater Sci Eng C*. 2015;56:189-194. doi:10.1016/j.msec.2015.06.025.
93. Thavasi V, Singh G, Ramakrishna S. Electrospun nanofibers in energy and environmental applications. *Energy Environ Sci*. 2008;1(2):205. doi:10.1039/b809074m.
94. Lu X, Wang C, Wei Y. One-dimensional composite nanomaterials: Synthesis by electrospinning and their applications. *Small*. 2009;5(21):2349-2370. doi:10.1002/smll.200900445.
95. Ji L, Lin Z, Medford AJ, Zhang X. In-situ encapsulation of nickel particles in electrospun carbon nanofibers and the resultant electrochemical performance. *Chem - A Eur J*. 2009;15(41):10718-10722. doi:10.1002/chem.200902012.
96. Wang L, Yu Y, Chen PC, Chen CH. Electrospun carbon-cobalt composite nanofiber as an anode material for lithium ion batteries. *Scr Mater*. 2008;58(5):405-408. doi:10.1016/j.scriptamat.2007.10.024.

97. Li M, Han G, Yang B. Fabrication of the catalytic electrodes for methanol oxidation on electrospinning-derived carbon fibrous mats. *Electrochem commun*. 2008;10(6):880-883. doi:10.1016/j.elecom.2008.04.002.
98. O'Regan B, Grätzel M. A low-cost, high-efficiency solar cell based on dye-sensitized colloidal TiO2 films. *Nature*. 1991;353(6346):737-740. doi:10.1038/353737a0.
99. Fujihara K, Kumar A, Jose R, Ramakrishna S, Uchida S. Spray deposition of electrospun TiO_2 nanorods for dye-sensitized solar cell. *Nanotechnology*. 2007;18(36):365709. doi:10.1088/0957-4484/18/36/365709.
100. Zhang Y, Ouyang H, Chwee TL, Ramakrishna S, Huang ZM. Electrospinning of gelatin fibers and gelatin/PCL composite fibrous scaffolds. *J Biomed Mater Res - Part B Appl Biomater*. 2005;72(1):156-165. doi:10.1002/jbm.b.30128.
101. Koh HS, Yong T, Chan CK, Ramakrishna S. Enhancement of neurite outgrowth using nano-structured scaffolds coupled with laminin. *Biomaterials*. 2008;29(26):3574-3582. doi:10.1016/j.biomaterials.2008.05.014.
102. Zhang YZ, Venugopal J, Huang ZM, Lim CT, Ramakrishna S. Characterization of the surface biocompatibility of the electrospun PCL-Collagen nanofibers using fibroblasts. *Biomacromolecules*. 2005;6(5):2583-2589. doi:10.1021/bm050314k.
103. Fujihara K, Kotaki M, Ramakrishna S. Guided bone regeneration membrane made of polycaprolactone/calcium carbonate composite nano-fibers. *Biomaterials*. 2005;26(19):4139-4147. doi:10.1016/j.biomaterials.2004.09.014.
104. Fan HS, Wen XT, Tan YF, Wang R, Cao HD, Zhang XD. Compare of Electrospinning PLA and PLA/β-TCP Scaffold in Vitro. *Mater Sci Forum*. 2005;475-479:2379-2382. doi:10.4028/www.scientific.net/MSF.475-479.2379.
105. Zamani M, Prabhakaran MP, Ramakrishna S. Advances in drug delivery via electrospun and electrosprayed nanomaterials. *Int J Nanomedicine*. 2013;8:2997-3017. doi:10.2147/IJN.S43575.
106. Xu X, Yang L, Xu X, et al. Ultrafine medicated fibers electrospun from W/O emulsions. *J Control Release*. 2005;108(1):33-42. doi:10.1016/j.jconrel.2005.07.021.
107. Kim K, Luu YK, Chang C, et al. Incorporation and controlled release of a hydrophilic antibiotic using poly(lactide-co-glycolide)-based electrospun nanofibrous scaffolds. *J Control Release*. 2004;98(1):47-56. doi:10.1016/j.jconrel.2004.04.009.
108. Huang ZM, He CL, Yang A, et al. Encapsulating drugs in biodegradable ultrafine fibers through co-axial electrospinning. *J Biomed Mater Res - Part A*. 2006;77(1):169-179. doi:10.1002/jbm.a.30564.
109. Zeng J, Aigner A, Czubayko F, Kissel T, Wendorff JH, Greiner A. Poly(vinyl alcohol) nanofibers by electrospinning as a protein delivery system and the retardation of enzyme release by additional polymer coatings. *Biomacromolecules*. 2005;6(3):1484-1488. doi:10.1021/bm0492576.
110. Zhao Y, Qiu Y, Wang H, Chen Y, Jin S, Chen S. Preparation of Nanofibers with Renewable Polymers and Their Application in Wound Dressing. *Int J Polym Sci*. 2016;2016. doi:10.1155/2016/4672839.
111. Nguyen TTT, Ghosh C, Hwang SG, Tran LD, Park JS. Characteristics of curcumin-loaded poly (lactic acid) nanofibers for wound healing. *J Mater Sci*. 2013;48(20):7125-7133. doi:10.1007/s10853-013-7527-y.
112. Goh YF, Shakir I, Hussain R. Electrospun fibers for tissue engineering, drug delivery, and wound dressing. *J Mater Sci*. 2013;48(8):3027-3054. doi:10.1007/s10853-013-7145-8.
113. Hong KH. Preparation and properties of electrospun poly(vinyl alcohol)/silver fiber web as wound dressings. *Polym Eng Sci*. 2007;47(1):43-49. doi:10.1002/pen.20660.
114. Duan Y, Jia J, Wang S, Yan W, Jin L, Wang Z. Preparation of antimicrobial poly(ε-caprolactone) electrospun nanofibers containing silver-loaded zirconium phosphate nanoparticles. *J*

Appl Polym Sci. 2007;106(2):1208-1214. doi:10.1002/app.26786.
115. Melaiye A, Sun Z, Hindi K, et al. Silver(I)-imidazole cyclophane gem-diol complexes encapsulated by electrospun tecophilic nanofibers: Formation of nanosilver particles and antimicrobial activity. *J Am Chem Soc*. 2005;127(7):2285-2291. doi:10.1021/ja040226s.

CHAPTER 2. Polymer and composite nanoparticles: preparation and application

2.1 Polymer nanoparticles

Nanosized particles have attractive characteristics, which have received considerable attention in the last decade. Nanoparticles are solid particles or particulate dispersions (colloids) with size in the range of 10–1000 nm that are produced by mechanical or chemical means.[1] Nanoparticles are assemblies of atoms or molecules at nanometer scale with unique and useful technical properties, different from those of the bulk material, attributable to their small size. With the size reduction, the surface/volume ratio is enlarged providing a larger reactive area of the interface, which is expected to have extensive applications in various fields such as drug delivery systems, biotechnology, biosensors, electronics, photonics, conducting materials, catalysts, nanocomposites, agriculture and environment.[2–5]

Polymer-based NP (PNP) is a collective term which is given to any kind of polymer NP but specifically, is applied for nanospheres and nanocapsules. The difference between these two forms lies in their morphology and body architecture. Nanospheres are formed by a dense polymeric matrix, whereas nanocapsules are composed of a hollow or oil core surrounded by a polymeric membrane.[6]

The historical development of PNPs was created by Paul Ehrlich with the first experimental efforts by Ursula Scheffel. Extensive works were conducted by the group of Peter Speiser at ETH Zurich in the late 1960s and early 1970s.[7]

The field of PNPs is quickly growing and playing a key role in the extensive fields ranging from photonics, electronics, sensors, medicine, pollution control and environmental technology. PNPs have long been used as main components in established everyday coatings, paints and adhesives products. More recently, they have found applications in biomedical fields such as bio-imaging, drug delivery, and diagnostics. PNP-based materials with unique physical and chemical characteristics might become future commands for the progress of new nanomaterials.[4,5]

2.1.1 Methods for preparation of nanoparticles from dispersion of preformed polymer

2.1.1.1 Solvent evaporation

Solvent evaporation was the first method developed to prepare PNPs from preformed polymers. These methods include the elimination of the organic solvents, where the polymer is dissolved, which can be achieved by evaporation or by extraction. Methods consist of oil-in-water (o/w), water-in-oil-in-water (w/o/w), solid-in-oil-in-water (s/o/w), oil-in-oil-in-water (o/o/w), and oil in oil (o/o), etc. emulsion solvent evaporation method.

In single emulsion method, initially, the polymeric supporting material is dissolved in a volatile organic solvent. In the next stage, the organic phase should be emulsified under high-energy source such as ultrasonicator or homogenizer into an external aqueous or oil phase consisting of a nonsolvent of the polymers which is immiscible with the organic solvent that contains an appropriate amount of surface active agent (stabilizer) (Figure 2.1). Exposing to a high-energy source, the emulsion is worn out into nanodroplets since it is the key point in attaining nanoparticles. Once the emulsion is stabilized, continuous magnetic stirring at room temperature or

under reduced pressure should be continued to evaporate the organic solvent. Afterward, the solidified nanoparticles can be collected by ultracentrifugation and washed with distilled water to remove additives such as surfactants. Finally, the product is lyophilized.[4,8]

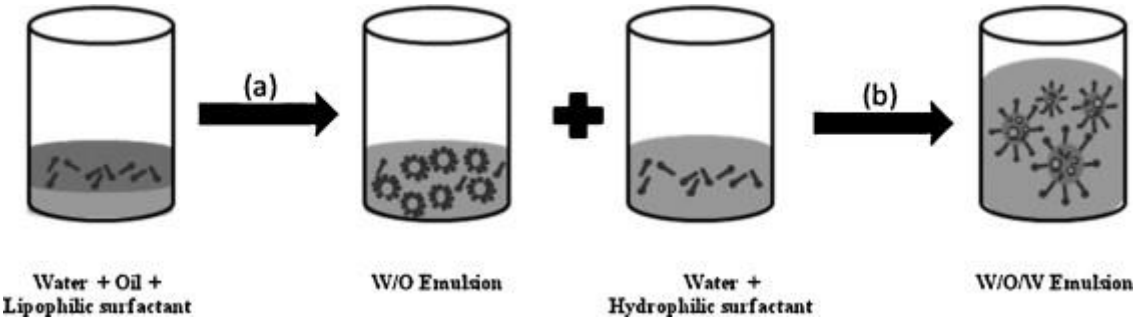

Figure 2.1. Preparation of w/o/w double emulsion: (a) high-shear emulsification and (b) low-shear emulsification.[8]

2.1.1.2 Nanoprecipitation

Nanoprecipitation is the spontaneous precipitation of the polymer in non-solvent phase by solvent displacement. The nanoprecipitation method was first introduced by Fessi and co-workers in 1989.[9] This one-step preparation method immediately attracted wide attention due to its simplicity, speed, and economic feasibility. It involves the precipitation of a preformed polymer from an organic solution and the diffusion of the organic solvent in the aqueous medium in the presence or absence of surfactant.[10–13] Nanoprecipitation systems encompass three parts: polymer, polymer solvent, and non-solvent of the polymer. The polymer is initially dissolved in the intermediate polarity water-miscible organic solvent, and then the organic solution is added into the non-solvent with magnetic stirring under ambient conditions (Figure 2.2). Nanoparticles are formed by precipitation simultaneously with the polymer diffused into the non-solvent and particle size can be regulated by the concentration of polymer, speed of stirring, rate of injection of two phases and solvent/non-solvent solubility and proportion.

In the nanoprecipitation process, the selection of solvent and non-solvent has a crucial impact on nanoparticle formation. The solvent should have a high solubility of the polymer of interest; be miscible in the non-solvent, and be facile to removable from the product following precipitation. Acetone and ethanol are two frequently used organic solvents in the nanoprecipitation process. If the polymer is not very soluble in organic solvents, multiple solvent blends could be used to improve the polymer solubility. Some of the advantages associated with this method are: (1) large amounts of toxic solvents are the avoided and (2) submicron particle sizes with narrow size distribution are the obtained (3) without the use of external energy sources. In spite of this, the principal limitation is related to the drug solubility. Since nanoprecipitation was proven to be inappropriate for the entrapment of water-soluble molecules, most of the drug incorporation studies focused on poorly water-soluble and amphiphilic compounds highly soluble in water-miscible organic solvents.[8,14,15]

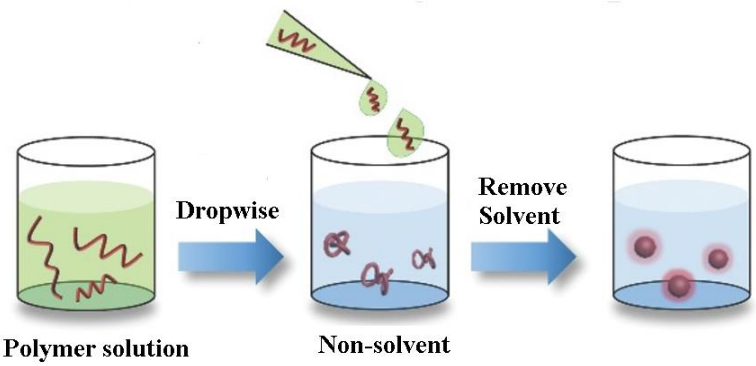

Figure 2.2. Scheme for the fabrication of PNPs by nanoprecipitation method.

2.1.1.3 Emulsification/solvent diffusion (ESD)

Emulsion solvent diffusion (ESD) is a modified version of solvent evaporation method that is among the most continually employed methods for the fabrication of PNPs from polymers. The origin of the process lies in the efforts of Quintanar-Guerrero et al.[16] This technique is the combination of two steps, i.e., emulsification and diffusion process. Polymer waterlogged solvent system is emulsified into an aqueous phase under homogenization. The solvent diffuses from the globules to the extramural phase. Then, it is allowed to diffuse into the non-solvent by adding an excess amount of non-solvent phase. The diffusion of the solvent takes molecules in the external phase and forms regions of supersaturation, from which polymer chain aggregates or globules are formed. Consequently, nanoparticles are formulated due to the physicochemical imbalance caused by solvent transfer. Particle size was found affected by water-logging and polymer concentration. This technique presents several advantages, such as high encapsulation efficiencies, no need for homogenization, high batch-to-batch reproducibility, ease of scale-up, simplicity, and narrow size distribution. Disadvantages are the high volumes of water to be eliminated from the suspension and the leakage of the water-soluble drug into the saturated-aqueous external phase during emulsification, reducing encapsulation efficiency.[6,16]

2.1.1.4 Salting out

One alternative to the widely applied emulsion and nanoprecipitation procedures is the salting-out method. Salting out is based on the separation of a water miscible solvent from aqueous solution via a salting out effect. The solution is emulsified under vigorous stirring in an aqueous gel containing the salting-out agent and, if required, a stabilizer. The addition of a high amount of water to the o/w emulsion allows the formation of nanospheres that can be purified and recovered by cross-flow filtration (Figure 2.3). The compounds commonly employed as salting-out agents are electrolytes such as magnesium chloride, sodium chloride or magnesium acetate and non-electrolytes such as sucrose. This method is especially suitable when high quantities of polymer and drug are required. The need of intensive purification of the resulted nanospheres, as well as the incompatibility of most of the salts employed with the bioactive compounds, are the principal limitations associated with this technique.[4,14]

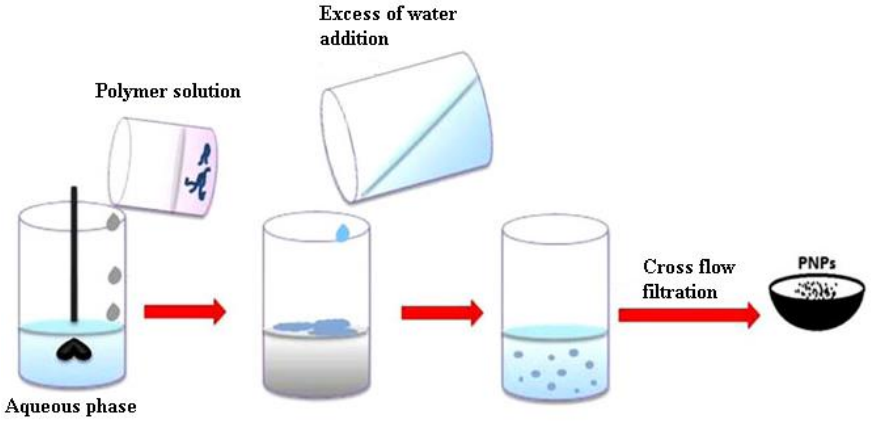

Figure 2.3. Scheme for the fabrication of PNPs by salting-out method.[4]

2.1.1.5 Dialysis

Dialysis offers a simple and effective method for the preparation of small, narrow-distributed polymer nanoparticles.[17,18] The polymer is dissolved in an organic solvent and placed inside a dialysis tube with the proper molecular weight cut off. Dialysis is performed against a non-solvent miscible with the former miscible. The displacement of the solvent inside the membrane is followed by the progressive aggregation of the polymer due to a loss of solubility and the formation of homogeneous suspensions of nanoparticles (Figure 2.4). The mechanism of PNP formation by dialysis method is not fully understood at present. It is thought that it may be based on a mechanism similar to that of nanoprecipitation proposed by the Fessi et al.[9] A number of polymer and copolymer nanoparticles were obtained by this technique. Poly(benzyl-l-glutamate)-b-poly(ethylene oxide), poly(lactide)-b-poly(ethylene oxide) nanoparticles were prepared using DMF as the solvent.[19,20] The solvent used in the preparation of the polymer solution affects the morphology and particle size distribution of the nanoparticles.

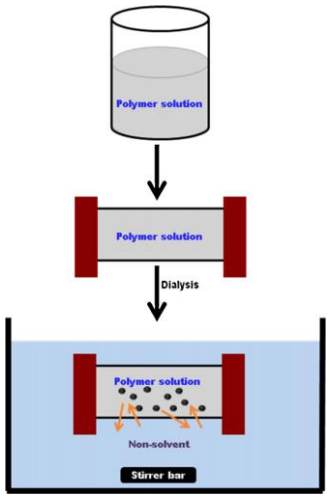

Figure 2.4. Schematic representation of osmosis based method for preparation of polymer nanoparticles.[15]

2.1.1.6 Spray drying

Spray-drying is a rapid, continuous, cost-effective, reproducible and scalable process for producing a dry powder from a liquid phase. This is done by removing the solvent from the solution containing solvent and polymer as a solute. The spray-drying process consists of four fundamental steps: (1) atomization of the liquid feed, (2) drying of spray into drying gas, (3) formation of dry particles and (4) separation and collection of the dry product from the drying gas.[21] First, the fluid is fed into the drying chamber by a peristaltic pump through an atomizer or nozzle that can be a rotary atomizer, a pressure nozzle or a two-fluid nozzle and the atomization occurs by centrifugal, pressure or kinetic energy, respectively. The small droplets generated by the solution come in contact with the hot air, the solvent content of each droplet is instantaneously evaporated and dried nano and microparticles are finally formed that are separated from the drying gas by means of a cyclone that deposes them in a glass collector situated in the bottom of the device (Figure 2.5). The particle sizes obtained are at submicron-to-micron scale and could be administered by different routes. One particle is usually formed from one droplet. The polymer precipitation on the surface of droplets leads to the formation of particles if the solute concentration at the center of the droplet is lesser than the equilibrium saturation.

The variables that affect the characteristics of the product and that can be tuned are (1) process parameters, (2) properties of the liquid feed and (3) equipment design. Spray drying was explored a favorable and fairly reproducible method, having improved therapeutic efficacy.[22,23]

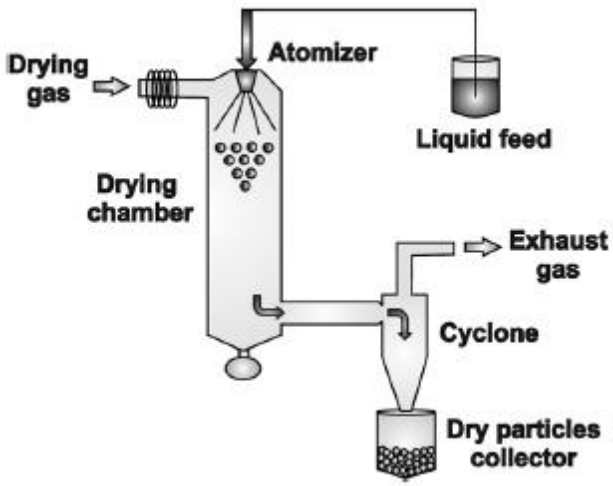

Figure 2.5. Diagram of the equipment and process of conventional spray-drying.[23]

2.1.1.7 Supercritical fluid technology (SCF)

SCF propound an attractive and exciting opportunity for the fabrication of PNPs due to its low operating conditions and potential applications for pharmaceutical research. The prescribed treatment allows the fabrication of formulations without subsidiary agents and organic solvents. Under ambient conditions, the polymer is mixed in a befitted supercritical fluid. Then the solution is sent to a pre-expansion tank through a syringe pump where it is heated isobarically to the pre-expansion temperature under pre-expansion pressure. Through nozzle, the solution is then permitted to expand into the air. The solution posed by expansion endures from rapid pressure reduction and exhibit a high degree supersaturation, resulting in fabrication and nucleation of nicely discrete

particles (Figure 2.6). At alternative fact, the solution that is pre-heated is permissible to inflate across the orifice of a nozzle into aqueous.[8,15]

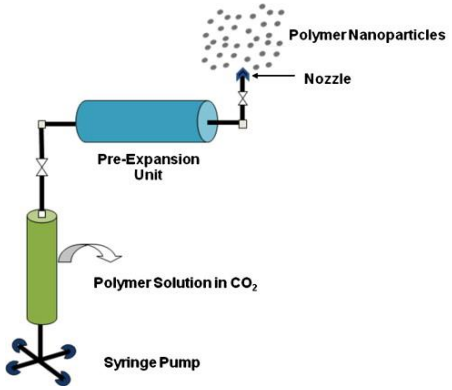

Figure 2.6. Experimental set-up for the preparation of polymer nanoparticles by rapid expansion of supercritical fluid solution.[15]

2.1.1.8 Electrospray

Electrospraying is a one-step technique which has potential to generate narrow size distributions of submicrometric particles, with limited agglomeration of particles and high yields.[24] Vonnegut and Neubauer (1952) were pioneers applying voltage to produce micrometer-sized spherical particles for application as sprays.[25] Today this technology is extending to other areas where it is booming in medicine and food technologies, because it is simple and uses low-cost equipment.[26] The principle of the electrospray is based on the ability of an electric field to deform the interface of the droplet and get droplets in the range of a micrometer or nanometer depending on the parameters to control. According to the way of collecting the droplets, there are two variants of the electrospray technique: electrospray in plates and electrospray in solution.

(1) Electrospray in plates consists of collecting charged droplets in a grounded plate, and collection can be of two forms. The first one, charged droplet, is deposited individually or can be deposited as an agglomerate of droplets on the plate (2) Electrospray in solution is based on collection of charged droplets in a cross-linking solution into a precipitate glass to facilitate the formation of micro- and nanospheres (Figure 2.7).[27]

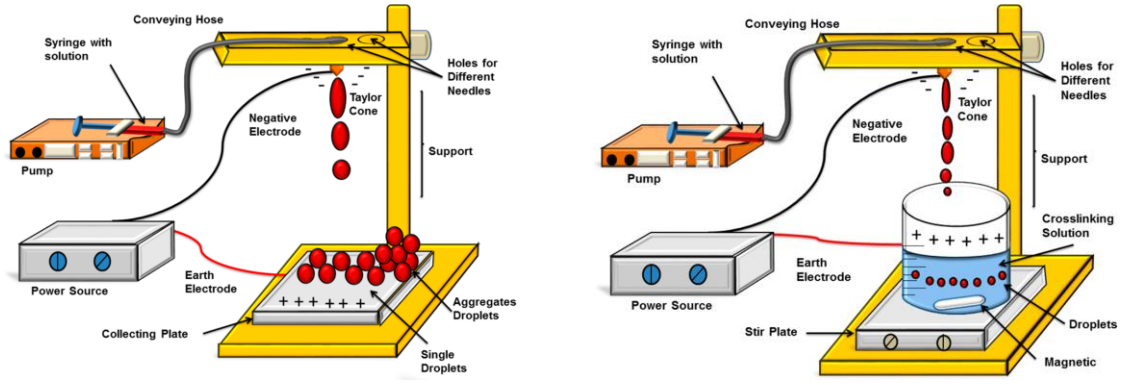

(a) (b)

Figure 2.7. Method of electrospray (a) in plates (b) in solution.[27]

The experimental set up has a syringe pump with polymer solution connected to the high voltage power supply that constitutes the functional electrode. A metal foil collector placed opposite functions as the ground electrode. The flow rate and the applied voltage were optimized depend on the type of the solution used for electrospraying. The liquid emerging from the nozzle into the electric field forms tailor cone because of the surface tension. By increasing the electric field the Taylor cone breaks into highly charged droplets, selecting the suitable conditions leads those droplets close to micro or nano size level. Solid particles can be produced by solvent evaporation. Needle gauge diameter, applied voltage, flow rate, concentration and working distance are variables that influence on the final products. The principle of electrospraying is to apply a high voltage to a polymeric solution to force the polymer to come out from the syringe in the form of nanoparticles. Electrospraying has emerged as a similar technique as the electrospinning which uses the analogous technology for the production of nanostructures. The nanoparticles can be useful for numerous biological, medicinal or pharmaceutical applications because of their zero dimensional nature, whereas the nanofibers can be only useful for their two dimensional applications. The advantages of the electrospraying include increased scalable synthesis, reproducibility and high encapsulation efficiency. This method is not only convenient for the synthesis of synthetic polymer nanoparticles but also for natural polymer nanoparticles either protein or carbohydrate and was found to produce stable nanoparticles without any loss of their bioactivity of either the drug or encapsulating biomolecules.[28]

Electrosprayed nanoparticles can encapsulate drugs and can be specific drug carriers because of their active surface absorption, binding or complexation with drug.[29] In the other hand, the nano particle size plays an important role in the therapeutic treatment, the particle size is one of the factors to decide the drug carrier velocity, specificity towards binding or adhesion and reactivity.[30] Thus the electrosprayed nanoparticle technology opens a new domain for drug delivery applications and therapeutic use. The advantages of electrospraying technique are: (1) It can produce lowest and uniform particle size as possible. (2) Easy to control the operation parameters. (3) Fast preparation and one step technique. (4) This involves simple ideology. (5) This technique can be able to extend for bulk production. On other hand, this technique may induce some macromolecule degradation due to the stress involved in the operation parameters (ex: thermal stress in drying, shear stress in the nozzle).[28]

2.2 Composite nanoparticles

Composite nanoparticles showing multiple discrete functionalities integrated into a single nano-unit have recently been the subject of intense research because they could have widespread uses in advanced medical and other technological applications. While the properties of single-phase nanoparticles depend primarily on the intrinsic properties of the material they are made of, on their size and shape, the properties of composite nanoparticles can be modified on the basis of interactions between the different properties in the materials being coupled. This coupling of the properties of different functional materials inside composite nanoparticles can lead to greatly improved or even completely new properties.

In recent years, the emergence of multifunctional nanomaterials has yielded substantial advances in the design and application of NP architectures for quantitative measurements. Of these NP architectures, at least three geometries substantially enhance NP utility for quantitative applications: (1) core–shell materials that are layered concentrically over one another, (2) composite materials comprising distinct, interspersed domains of different materials, and (3) hybrid materials comprising interspersed domains that are indistinguishable above the molecular/macromolecular level (Figure 2.8).[31]

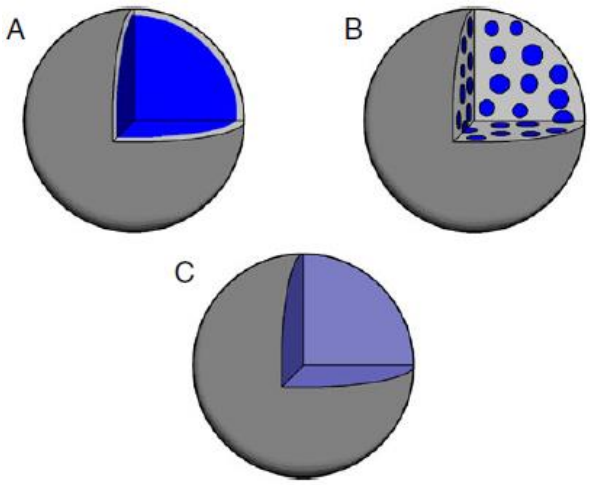

Figure 2.8. Different multifunctional nanoparticle geometries: a) core–shell, b) composite, and c) hybrid NP morphologies.[31]

The combination of multiple materials often minimizes or masks the disadvantageous properties, e.g., solubility, drug retention, and degradation, of the individual component materials to yield an optimal geometry, a clear case of the whole being greater than the sum of the parts. For example, aggregation of hydrophobic polymer or metal NPs in aqueous solutions is prevented by addition of hydrophilic silica or polymer shells, whereas drug leakage from hydrophilic architectures can be minimized by inclusion of a hydrophobic core. Additionally, mechanically fragile materials such as alginate can be reinforced by more robust polymers or silica.[32] Furthermore, compartmentalization of differing materials within distinct domains of composite NPs allows multiple, sometimes incongruous, components to be combined within one particle by providing suitable environments for each individual component. Thus, the design of composite, hybrid, and core–shell NP represents a bright future for quantitative applications of NPs.

2.2.1 Organic-Inorganic composite nanoparticles

Composite nanoparticles as core/shell nanoparticles or surface modified nanoparticles may be considered as a special type of nanocomposites. When these nanoparticles contain an inorganic core and an organic shell one may speak about hybrid nanoparticles. In this case the inorganic core may be a metal or a metal oxide, and the organic shell either a polymerized monomer, a chromophore, a detergent or surfactant, carbon, or some organic molecule. Particles of this type, consisting of a metal oxide core and a polymerizable organic shell, were reported in the mid and late-90s by Vollath,[33,34] synthesized in a microwave plasma reactor by gas phase synthesis. This concept allows the design of new functional materials with novel or modified magnetic, optical, electronic or biological properties. In the last decade, a broad portfolio of nanocomposite particles with different functional properties have been developed depending on the inorganic core and the organic shell. Many research groups worldwide are involved in this field. Chen and Somasundaran, for example described the preparation of Al_2O_3/PAA core/shell nanocomposites by a controlled polymer bridging, using commercial Al_2O_3 nanoparticles.[35] A polystyrene-based coating was used for SiO_2 nanoparticles[36] and TiO_2 nanoparticles,[37] respectively. Acrylate-based nanoparticle composites were reported from ZnO,[38] TiO_2,[39] and SiO_2.[40] Al_2O_3 nanoparticles were coated with pyrrole,[41] or in situ with polyethylene.[42] He et al. reported about ZrO_2 nanoparticles, coated with quasi-polyethylene.[43] Various oxide nanoparticles were coated with acrylic based monomers and with fluoropolymers.[44]

Schmidt developed magnetic core/shell nanoparticles based on Fe_3O_4 and ε-caprolactone[45] by surface initiated ring-opening polymerization, whereas Nan et al.[46] synthesized a similar type of nanocomposite using microwave assisted graft polymerization. Gravano et al. described the surface functionalization of Fe_2O_3 with ligands and polymers.[47]

2.2.2 Organic-Organic composite nanoparticles

Organic-organic composite nanoparticles have received increased scientific interest in terms of basic research as well as commercial applications, promising a variety of uses for nanostructures in fields including bionanotechnology and medicine. Composite nanoparticles as core/shell nanoparticles or surface modified nanoparticles may be considered as a special type of nanocomposites. A number of important synthesis methods of hybrid nanoparticles/nanostructure have been discussed yet. Recently Cory et al. fabricated uniform double-walled composite nanoparticles by using dual coaxial jets.[48] As well Yang et al, developed sequentially-controlled drug release for cancer combination chemotherapy treatment by fabrication of PVP/PLGA and PCL/PLGA nanoparticles with a distinct core–shell structure by coaxial electrospray.[49] Wen et al. developed PDVB/porous PDVB composite nanoparticles by precipitation polymerization.[50] Layer by layer deposition was employed for preparation of PLA/PEI composite nanoparticles by Trimaille et al.[51] Gulnaz et al. reported about production of stereocomplex polylactide hybrid nanoparticles by supercritical fluid technology with higher mechanical and thermal properties.[52] The other method uses for making composite nanoparticles is grafting. PLGA/chitosan hybrid nanoparticles have been demonstrated by Shailesh et al. which grafting of chitosan on PLGA surface was carried out via amide bond.[53]

2.3 Polymer nanoparticles applications

The researchers are scrutinizing materials accompanied by enhanced physicochemical features that have dimensionally better suitability in nanoscience and technology applications. In this regard, polymeric nanoparticles-based material is an important addition in the area of nanoscience, for playing a key role in modern science and technology. Among the various nanostructures, same as quantum dots, graphene, carbon nanotubes, metallic and metal oxide nanoparticles, polymeric nanoparticles, characterized by satisfying biocompatibility, have aroused great interest as the carriers for various biologically active substances such as drugs, proteins, monoclonal antibodies, biological extracts, nucleic acids, and others. polymer nanoparticles have already been reported as efficient vehicles for therapeutic agents in many disease entities. They can be delivered to the body via different administration routes.[54]

One of the most important biomedical applications of biodegradable polymeric nanomaterials can be found in the field of drug delivery. Polymeric nanomaterials offer several advantages, such as (1) provide a controlled release fashion from the matrix structure into a targeted part of the body; (2) encapsulate labile molecules (e.g., DNA, RNA, and proteins) and prevent degradation; (3) option to modify surfaces with ligands; and (4) provide excellent in vitro and in vivo stability.[54]

2.3.1 Polymeric nanoparticles as carriers for therapeutic agents

Polymer-based nanoparticles have been successfully used as carriers for antimicrobial agents. For instance, Intriguingly, Chaudhary and Kumar have demonstrated the antibacterial activity of Cefixime-loaded PLGA nanoparticles against the intracellular multidrug resistance (MDR) of Salmonella typhimurium. The results revealed a sustained release of the antibiotic from the

prepared formulation and its better permeation across rat intestines as compared to the free drug.[55] A curious instance has been explored by Hill and co-workers, who demonstrated that PLGA nanoparticles loaded with the natural antimicrobial cinnamon bark extract, are effective inhibitors of Salmonella typhimurium and Listeria monocytogenes. The authors highlighted the potential of the as-prepared system for the food industry to help prevent foodborne diseases.[56]

Polymeric nanoparticles have also been used successfully as carriers for antihypertensive drugs. As an example, pulmonary delivery of the antihypertensive drug carvedilol was the subject of studies performed by Varshosaz and co-workers. The authors prepared drug-loaded poly(ethyleneco-vinyl acetate) (PEVA) nanoparticles coated with chitosan. The system revealed mucoadhesive properties and provided prolonged drug release up to 8 h.[57]

In the anticancer therapy, one of the worst problems is the low tumor answer to treatment, because of the non-specific bioavailability of the administered anticancer agent. By using nanoparticles it is possible to achieve the bioaccumulation of the drug in the target tissue. In the most cases, the EPR (enhanced permeation and retention) effect is responsible for the accumulation of drug in the tumor tissue. Hapca et al. synthesized PLA nanoparticles on which they have grafted monoclonal antibodies with a high specificity for the treatment of ovarian cancer and lymphomas.[58]

Another field where nanoparticles are very important is gene delivery. By encapsulating the genes into nanoparticles it is possible to protect them from degradation in the presence of certain factors (pH, bile, proteolytic enzymes). The entrapment of genes into nanoparticles has encountered some problems regarding the stability of the synthesized structures during the preparation as well as after administration. One method to ensure the stability is to bind the genes to the surface of nanoparticles or nanocapsules. The binding must be reversible in order to allow the cleavage of the complex once the target has been reached.[59] A method to obtain nanoparticles without using a surfactant was proposed by Castadello et al. who obtained nanoparticles able to bind DNA without using a surfactant. The nanoparticles have a PMMA core and a shell of PEG and positively charged groups. The PEG chains are both biocompatible and biodegradable and provide steric stability while the positively charged groups bind DNA. By using these complex structures, the risk of physical desorption is greatly decreased.[60]

2.4 References

1. Hanemann T, Szabó DV. *Polymer-Nanoparticle Composites: From Synthesis to Modern Applications*. Vol 3.; 2010. doi:10.3390/ma3063468.
2. Elsabahy M, Heo GS, Lim S-M, Sun G, Wooley KL. Polymeric Nanostructures for Imaging and Therapy. *Chem Rev*. 2015;115(19):10967-11011. doi:10.1021/acs.chemrev.5b00135.
3. Wang YJ, Larsson M, Huang WT, et al. The use of polymer-based nanoparticles and nanostructured materials in treatment and diagnosis of cardiovascular diseases: Recent advances and emerging designs. *Prog Polym Sci*. 2016;57:153-178. doi:10.1016/j.progpolymsci.2016.01.002.
4. Nasir A, Kausar A, Younus A. A Review on Preparation, Properties and Applications of Polymeric Nanoparticle-Based Materials. *Polym - Plast Technol Eng*. 2015;54(4):325-341. doi:10.1080/03602559.2014.958780.
5. Mallakpour S, Behranvand V. Polymeric nanoparticles: Recent development in synthesis and application. *Express Polym Lett*. 2016;10(11):895-913. doi:10.3144/expresspolymlett.2016.84.
6. Quintanar-Guerrero D, Allémann E, Fessi H, Doelker E. Preparation Techniques and Mechanisms of Formation of Biodegradable Nanoparticles from Preformed Polymers. *Drug Dev Ind Pharm*. 1998;24(12):1113-1128. doi:10.3109/03639049809108571.
7. Lu X-Y, Wu D-C, Li Z-J, Chen G-Q. Polymer Nanoparticles. In: ; 2011:299-323. doi:10.1016/B978-0-12-416020-0.00007-3.

8. NAGAVARMA B V N, HEMANT K.S.YADAV*, AYAZ A, VASUDHA L.S SH. DIFFERENT TECHNIQUES FOR PREPARATION OF POLYMERIC NANOPARTICLES- A REVIEW. *Asian J Pharm Clin Res*. 2012;5:16-23.
9. Fessi H, Puisieux F, Devissaguet JP, Ammoury N, Benita S. Nanocapsule formation by interfacial polymer deposition following solvent displacement. *Int J Pharm*. 1989;55(1):1-4. doi:10.1016/0378-5173(89)90281-0.
10. Govender T, Stolnik S, Garnett MC, Illum L, Davis SS. PLGA nanoparticles prepared by nanoprecipitation: Drug loading and release studies of a water soluble drug. *J Control Release*. 1999;57(2):171-185. doi:10.1016/S0168-3659(98)00116-3.
11. Timko M, Koneracká M, Tomašovičová N, Kopčanský P, Závišová V. Magnetite polymer nanospheres loaded by Indomethacin for anti-inflammatory therapy. *J Magn Magn Mater*. 2006;300(1):191-194. doi:10.1016/j.jmmm.2005.10.077.
12. Legrand P, Lesieur S, Bochot A, et al. Influence of polymer behaviour in organic solution on the production of polylactide nanoparticles by nanoprecipitation. *Int J Pharm*. 2007;344(1-2):33-43. doi:10.1016/j.ijpharm.2007.05.054.
13. Lassalle V, Ferreira ML. PLA nano- and microparticles for drug delivery: An overview of the methods of preparation. *Macromol Biosci*. 2007;7(6):767-783. doi:10.1002/mabi.200700022.
14. Pinto Reis C, Neufeld RJ, Ribeiro AJ, Veiga F. Nanoencapsulation I. Methods for preparation of drug-loaded polymeric nanoparticles. *Nanomedicine Nanotechnology, Biol Med*. 2006;2(1):8-21. doi:10.1016/j.nano.2005.12.003.
15. Rao JP, Geckeler KE. Polymer nanoparticles: Preparation techniques and size-control parameters. *Prog Polym Sci*. 2011;36(7):887-913. doi:10.1016/j.progpolymsci.2011.01.001.
16. Quintanar-Guerrero D, Allémann, Eric Doelker E, Fessi H. Preparation and Characterization of Nanocapsules from Preformed Polymers by a New Process Based on Emulsification-Diffusion Technique. *Pharm Res*. 1998;15(7):1056-1062.
17. Jeong Y Il, Cho CS, Kim SH, et al. Preparation of poly(DL-lactide-co-glycolide) nanoparticles without surfactant. *J Appl Polym Sci*. 2001;80(12):2228-2236. doi:10.1002/app.1326.
18. Kostag M, Köhler S, Liebert T, Heinze T. Pure cellulose nanoparticles from trimethylsilyl cellulose. *Macromol Symp*. 2010;294(2):96-106. doi:10.1002/masy.200900095.
19. Oh I, Lee K, Kwon HY, et al. Release of adriamycin from poly(gamma-benzyl-L-glutamate)/poly(ethylene oxide) nanoparticles. *Int J Pharm*. 1999;181(1):107-115. http://www.ncbi.nlm.nih.gov/pubmed/10370207%5Cnfile:///Users/andrewmikhail/Documents/Mendeley Desktop/Oh et al/1999/International journal of pharmaceutics/Release of adriamycin from poly(gamma-benzyl-L-glutamate)poly(ethylene oxide) nanoparticles/Oh et al.
20. Lee J, Cho EC, Cho K. Incorporation and release behavior of hydrophobic drug in functionalized poly(D,L-lactide)-block-poly(ethylene oxide) micelles. *J Control Release*. 2004;94(2-3):323-335. doi:10.1016/j.jconrel.2003.10.012.
21. Paudel A, Worku ZA, Meeus J, Guns S, Van Den Mooter G. Manufacturing of solid dispersions of poorly water soluble drugs by spray drying: Formulation and process considerations. *Int J Pharm*. 2013;453(1):253-284. doi:10.1016/j.ijpharm.2012.07.015.
22. Deshmukh R, Wagh P, Naik J. Solvent evaporation and spray drying technique for micro- and nanospheres/particles preparation: A review. *Dry Technol*. 2016;34(15):1758-1772. doi:10.1080/07373937.2016.1232271.
23. Sosnik A, Seremeta KP. Advantages and challenges of the spray-drying technology for the production of pure drug particles and drug-loaded polymeric carriers. *Adv Colloid Interface Sci*. 2015;223:40-54. doi:10.1016/j.cis.2015.05.003.
24. Bock N, Woodruff MA, Hutmacher DW, Dargaville TR. Electrospraying, a reproducible method for production of polymeric microspheres for biomedical applications. *Polymers (Basel)*.

2011;3(1):131-149. doi:10.3390/polym3010131.
25. Vonnegut B, Neubauer RL. Production of monodisperse liquid particles by electrical atomization. *J Colloid Sci*. 1952;7(6):616-622. doi:10.1016/0095-8522(53)90062-2.
26. Ikeuchi M, Tane R, Ikuta K. Electrospray deposition and direct patterning of polylactic acid nanofibrous microcapsules for tissue engineering. *Biomed Microdevices*. 2012;14(1):35-43. doi:10.1007/s10544-011-9583-x.
27. Ramalho MJ, Pereira MC. Preparation and Characterization of Polymeric Nanoparticles: An Interdisciplinary Experiment. *J Chem Educ*. 2016;93(8):1446-1451. doi:10.1021/acs.jchemed.5b00837.
28. Sridhar R, Ramakrishna S. Electrosprayed nanoparticles for drug delivery and pharmaceutical applications. 2015;(September 2013):1-12.
29. De Jong WH, Borm PJA. Drug delivery and nanoparticles:applications and hazards. *Int J Nanomedicine*. 2008;3(2):133-149. doi:10.2147/IJN.S596.
30. Champion JA, Katare YK, Mitragotri S. Particle shape: A new design parameter for micro- and nanoscale drug delivery carriers. *J Control Release*. 2007;121(1-2):3-9. doi:10.1016/j.jconrel.2007.03.022.
31. Janczak CM, Aspinwall CA. Composite nanoparticles: The best of two worlds. *Anal Bioanal Chem*. 2012;402(1):83-89. doi:10.1007/s00216-011-5482-5.
32. Coradin T, Mercey E, Lisnard L, Livage J. Design of silica-coated microcapsules for bioencapsulation. *Chem Commun*. 2001;(23):2496-2497. doi:10.1039/b108324b.
33. Vollath D, Szabo DV, Fuchs J. Synthesis and properties of ceramic-polymer composits. *Nanostructured Mater*. 1999;12(1-4):433-438. doi:10.1016/S0965-9773(99)00152-X.
34. Vollath D, Szabó D V. Coated nanoparticles: a new way to improved nanocomposites. *J Nanoparticle Res*. 1999;1(2):235-242. doi:10.1023/A:1010060701507.
35. Chen T, Somasundaran P. Preparation of Novel Core-shell Nanocomposite Particles by Controlled Polymer Bridging. *J Am Ceram Soc*. 1998;81(1):40-44. doi:10.1111/j.1151-2916.1998.tb02305.x.
36. Gu S, Kondo T, Konno M. Preparation of silica-polystyrene core-shell particles up to micron sizes. *J Colloid Interface Sci*. 2004;272(2):314-320. doi:10.1016/j.jcis.2004.01.056.
37. Rong Y, Chen HZ, Wu G, Wang M. Preparation and characterization of titanium dioxide nanoparticle/ polystyrene composites via radical polymerization. *Mater Chem Phys*. 2005;91(2-3):370-374. doi:10.1016/j.matchemphys.2004.11.042.
38. Shi D, He P, Lian J, Wang L, van Ooij WJ. Plasma deposition and characterization of acrylic acid thin film on ZnO nanoparticles. *J Mater Res*. 2011;17(10):2555-2560. doi:10.1557/JMR.2002.0371.
39. Zhu F, Zhang J, Yang Z, Guo Y, Li H, Zhang Y. The dispersion study of TiO2 nanoparticles surface modified through plasma polymerization. *Phys E Low-Dimensional Syst Nanostructures*. 2005;27(4):457-461. doi:10.1016/j.physe.2005.01.004.
40. Suffner J, Schechner G, Sieger H, Hahn H. In-situ coating of silica nanoparticles with acrylate-based polymers. *Chem Vap Depos*. 2007;13(9):459-464. doi:10.1002/cvde.200606522.
41. Shi D, He P, Wang SX, et al. Interfacial Particle Bonding Via an Ultrathin Polymer Film on Al2O3 Nanoparticles by Plasma Polymerization. *J Mater Res*. 2002;17(5):981-990. doi:10.1557/JMR.2002.0146.
42. Schallehn M, Winterer M, Weirich TE, Keiderling U, Hahn H. In-situ preparation of polymer-coated alumina nanopowders by chemical vapor synthesis. *Chem Vap Depos*. 2003;9(1):40-44. doi:10.1002/cvde.200290006.
43. He W, Guo Z, Pu Y, Yan L, Si W. Polymer coating on the surface of zirconia nanoparticles by inductively coupled plasma polymerization. *Appl Phys Lett*. 2004;85(6):896-898.

doi:10.1063/1.1778470.
44. Lamparth I, Vinga Szabó D, Vollath D. Ceramic nanoparticles coated with polymers based on acrylic derivatives. *Macromol Symp*. 2002;181(1):107-112. doi:10.1002/1521-3900(200205)181:1<107::AID-MASY107>3.0.CO;2-2.
45. Schmidt AM. The synthesis of magnetic core-shell nanoparticles by surface-initiated ring-opening polymerization of ε-caprolactone. *Macromol Rapid Commun*. 2005;26(2):93-97. doi:10.1002/marc.200400426.
46. Nan A, Turcu R, Craciunescu I, Pana O, Scharf H, Liebscher J. Microwave-assisted graft polymerization of ε-caprolactone onto magnetite. *J Polym Sci Part A Polym Chem*. 2009;47(20):5397-5404. doi:10.1002/pola.23589.
47. Gravano SM, Dumas R, Liu K, Patten TE. Methods for the surface functionalization of γ-Fe_2O_3 nanoparticles with initiators for atom transfer radical polymerization and the formation of core-shell inorganic-polymer structures. *J Polym Sci Part A Polym Chem*. 2005;43:3675-3688. doi:10.1002/pola.20823.
48. Berkland C, Pollauf E, Pack DW, Kim K. Uniform double-walled polymer microspheres of controllable shell thickness. *J Control Release*. 2004;96(1):101-111. doi:10.1016/j.jconrel.2004.01.018.
49. Cao Y, Wang B, Wang Y, Lou D. Polymer-controlled core–shell nanoparticles: a novel strategy for sequential drug release. *RSC Adv*. 2014;4(57):30430-30439. doi:10.1039/C4RA03610G.
50. Li WH, St??ver HDH. Monodisperse cross-linked core-shell polymer microspheres by precipitation polymerization. *Macromolecules*. 2000;33(12):4354-4360. doi:10.1021/ma9920691.
51. Trimaille T, Pichot C, Delair T. Surface functionalization of poly(D,L-lactic acid) nanoparticles with poly(ethylenimine) and plasmid DNA by the layer-by-layer approach. *Colloids Surfaces A Physicochem Eng Asp*. 2003;221(1-3):39-48. doi:10.1016/S0927-7757(03)00105-5.
52. Bibi G, Jung Y, Lim JC, Kim SH. Novel strategy of lactide polymerization leading to stereocomplex polylactide nanoparticles using supercritical fluid technology. *ACS Sustain Chem Eng*. 2016;4(9):4521-4528. doi:10.1021/acssuschemeng.6b00446.
53. Chalikwar SS, Mene BS, Pardeshi C V., Belgamwar VS, Surana SJ. Self-Assembled, Chitosan Grafted PLGA Nanoparticles for Intranasal Delivery: Design, Development and Ex Vivo Characterization. *Polym - Plast Technol Eng*. 2013;52(4):368-380. doi:10.1080/03602559.2012.751999.
54. Moritz M, Malgorzata G-M. Recent Developments in the Application of Polymeric Nanoparticles as Drug Carriers. *Adv Clin Exp Med*. 2015;24(5):749-758. doi:10.17219/acem/31802.
55. de Carvalho RF, Ribeiro IF, Miranda-Vilela AL, et al. Leishmanicidal activity of amphotericin B encapsulated in PLGA-DMSA nanoparticles to treat cutaneous leishmaniasis in C57BL/6 mice. *Exp Parasitol*. 2013;135(2):217-222. doi:10.1016/j.exppara.2013.07.008.
56. Hill LE, Taylor TM, Gomes C. Antimicrobial Efficacy of Poly (DL-lactide-co-glycolide) (PLGA) Nanoparticles with Entrapped Cinnamon Bark Extract against Listeria monocytogenes and Salmonella typhimurium. *J Food Sci*. 2013;78(4). doi:10.1111/1750-3841.12069.
57. Varshosaz J, Taymouri S, Hamishehkar H. Fabrication of polymeric nanoparticles of poly(ethylene-co-vinyl acetate) coated with chitosan for pulmonary delivery of carvedilol. *J Appl Polym Sci*. 2014;131(1):1-8. doi:10.1002/app.39694.
58. Cirstoiu-Hapca A, Bossy-Nobs L, Buchegger F, Gurny R, Delie F. Differential tumor cell targeting of anti-HER2 (Herceptin®) and anti-CD20 (Mabthera®) coupled nanoparticles. *Int J Pharm*. 2007;331(2):190-196. doi:10.1016/j.ijpharm.2006.12.002.
59. Cismaru L, Popa M. ChemInform Abstract: Polymeric Nanoparticles with Biomedical Applications. *ChemInform*. 2011;42(27):no-no. doi:10.1002/chin.201127264.
60. Castaldello A, Brocca-Cofano E, Voltan R, et al. DNA prime and protein boost immunization

with innovative polymeric cationic core-shell nanoparticles elicits broad immune responses and strongly enhance cellular responses of HIV-1 tat DNA vaccination. *Vaccine*. 2006;24(29-30):5655-5669. doi:10.1016/j.vaccine.2006.05.058.

CHAPTER 3. Used materials

3.1 Poly (lactic acid) (PLA)

Poly(lactic acid) (PLA) belongs to the family of aliphatic polyesters, a compostable, biodegradable thermoplastic made from renewable sources. Poly(lactide) was discovered in 1932 by Carothers (at DuPont). He was only able to produce a low molecular weight PLA by heating lactic acid under vacuum while removing the condensed water. The problem at that time was to increase the molecular weight of the products; and, finally, by ring-opening polymerization of the lactide, high-molecular weight PLA was synthesized. As early as the 1970's, PLA products have been approved by the US Food and Drug Administration (FDA) for direct contact with biological fluids. PLA was first used in combination with polyglycolic acid (PGA) as suture material and sold under the name Vicryl in the U.S.A. in 1974. Four of its most attractive advantages are renewability, biocompatibility, processability, and energy saving. First of all, PLA is derived from renewable and degradable resources such as corn and rice, which can help alleviate the energy crisis as well as reduce the dependence on fossil fuels of our society; PLA and its degradation products, namely H_2O and CO_2, are neither toxic nor carcinogenic to the human body, hence making it an excellent material for biomedical applications including sutures, clips, and drug delivery systems (DDS). Moreover, contributing to its processability, PLA can be formed into any desired shape, including film, board, pellets, and fibers, by extrusion, injection molding, thermoforming, hot drawing, electrospinning and solvent casting due to high thermal processibility. These thermal properties contribute to the application of PLA in industry in fields such as textiles and food packaging. Due to the ease of synthesizing and processing, PLA is less energy consuming than other polymers, consequently reducing air and water pollution. This feature surely can relieve the global warming effect and the over-consumption of fossil energy.[1,2]

The monomer of PLA is lactic acid (2-hydroxy propionic acid), which can be taken from milk or similar dairy product. Lactic acid is the simplest hydroxy acid with an asymmetric carbon atom that has two isomers with two optically active configurations, L-lactic acid and D-lactic acid, which are shown in figure 3.1.[1]

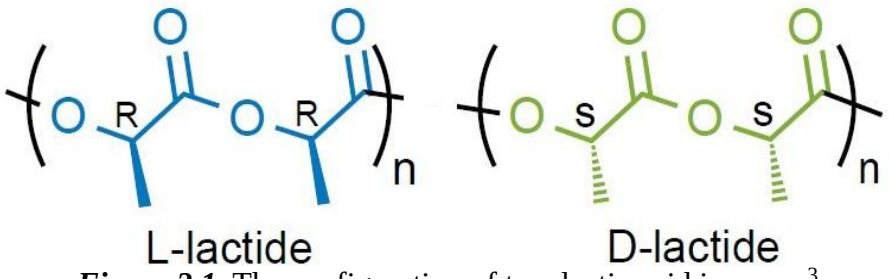

Figure 3.1. The configuration of two lactic acid isomers.[3]

With L-lactic acid and D-lactic acid isomers, four different polymers can be produced: Semi-crystalline poly (L-lactic acid) (PLLA), regular chain structure polymer synthesized solely with L-lactic; Crystalline poly (D-lactic acid) (PDLA), regular chain structure polymer synthesized solely with D-lactic; and amorphous polymer poly (D, L-lactic acid) (PDLLA). Moreover, with meso-lactide as a monomer, polymerized meso-PLA can be prepared. Figure 3.2 shows the chemical structure of PLA.[1,3]

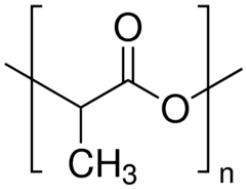

Figure 3.2. Chemical structure of PLA.[3]

In addition to the great degradability and processability, PLA also possesses another valuable physical, chemical, and mechanical properties. However, the thermal and mechanical properties of PLA primarly depend on polymer structure. PLA homopolymer has glass transition temperature (T_g) around 55 °C, and melting temperature (T_m) around 175 °C. The differences in molecular weight, crystalline structure (i.e. crystalline, semi crystalline, amorphous) and tacticity lead to differences in properties.[4]

Even though PLA can be considered as a good renewable substitute for petroleum based materials but in comparison with traditional polymer materials some properties of PLA are still inferior. For instance, PLA is brittle, showing low elongation strain at breaking point. Unless modified, it cannot be used as a proper substitute for applications requiring good elongation. In addition, the heat distortion temperature is around 55-65 °C for most pure PLA homopolymers, narrowing and limiting their utilization range.[5]

To improve their general performance, a considerable amount of research has been conducted. Perego et al. developed impact resistance of PLLA by increasing molecular weight and crystallinity. In their study, PLLA samples were prepared by injection molding method.[6]

Jonoobi et al. improved tensile strength of PLA by blending the PLA matrix with well-dispersed cellulose nanofibers via twin screw extrusion method. The tensile strength increased with nanofiber content.[7]

To modify high rigidity and brittleness of PLA at room temperature, Hassouna et al. studied the plasticizing effect on PLA of grafting by hydroxyl-functionalized using reactive extrusion. Results demonstrated an overall improvement on PLA's yield stress when plasticized with 10wt% PEG and 10wt% maleic anhydride-grafted PLA copolymer. However, the plasticizer steeply reduced the glass transition temperature, melting temperature and degree of crystallinity. Therefore the heat distortion temperature cannot be improved by this route.[8]

The modification of PLA has been considered as a practical way to enhance certain of its properties. However, improving thermal and mechanical properties without balancing compromising renewability and degradability is not a trivial task. Typically, improved thermomechanical properties are at the expense of renewability/ biodegradability. Hence, reconsideration of the approaches to improve the overall PLA performance is required.

3.1.1 Stereocomplex poly (lactic acid) (sc-PLA)

When the interaction between polymers having different tacticities or configurations prevails over that one between polymers with the same tacticity or configuration, a stereoselective association of the former polymer pair takes place. PLA stereocomplex consists of both enantiomeric poly (L-lactic acid) and poly (D-lactic acid). PLA stereocomplexation due to the peculiarly strong interaction between L-lactyl unit sequences and D-lactyl unit sequences is expected to improve PLA thermal and mechanical properties when compared to the pure form of either enantiomer. The melting temperature of stereocomplex is 50 °C higher (230°C) than that of pure PLLA or PDLA (180°C). The stereocomplex crystal has PLLA and PDLA chains packed side by side with a triclinic 31 helix.[9] Ikada et al. indicated that mixing ratio and molecular weight of

PLLA and PDLA are critical among many parameters affecting stereocomplexation.[10] Indeed, to achieve the stereocomplexation, polymers with relatively low molecular weight are required, while polymers with high molecular weights tend to hinder its formation, due to their very low macromolecular mobility.[11] As Auras et al. described, Strong shear can induce stereocomplexation, by rotating and extending macromolecular chains of PLA and facilitating the enantiomeric sequences.[9]

Considering the previous study which revealed that in the unit cell, the number of L-units and D- units should be equal, the PLLA and PDLA stereocomplex are presumed to possess a 31 helix in its crystal.[12] Using the conformational parameter equation for polymer helices composed by Miyazawa, the existence of the 31 helix has been proved.[13]

A PLLA chain is left-handed, while a PDLA chain is right-handed, both making up the helical system. When the mixing ratio of left-handed structure and right-handed structure is 1:1, the two forms the most densely packed structure. Thus when they are mixed by 1:1 ratio, the stereocomplex formed by rotating both PLLA and PDLA polymer backbones, results in a side-by-side, highly ordered stable 31 helix structure. The strong interaction between PLLA and PDLA explains why the stereocomplex has a high melting temperature, as well as better mechanical properties.[14]

To prepare PLA stereocomplex, the various methods such as compression, orientation, melt crystallization, solution casting, and precipitation were utilized which have been listed below.

a. Crystallization from Melt

Crystallization at a fixed temperature directly from the melt is the most prevalent way to obtain PLA stereocomplex crystal from the melt, and it requires an equimolar mixture of PLLA and PDLA with low molecular weights.[15]

b. Compression

Using twin screw extruder and squeezing molecular chains, PLA stereocomplex formed with following temperature profile: 200-230°C for extruder barrel; die for 220°C. The screw speed was 200 rpm.[16]

c. Orientation

By hot drawing, a large molecular surface area can be created. This increases the possibility of the interaction between PLLA and PDLA polymer chain segments. This method also increases the tensile strength.[17]

d. Solution casting

Solution casting method can be used for with higher molecular weight PLLA and PDLA, but the time given for PLA stereocomplex crystallization must be long enough, otherwise, PLLA or PDLA homocrystallites may form.[4]

e. Precipitation

By adding PLLA and PDLA mixture solution into a non-solvent, rapid crystallization of PLA stereocomplex takes place. The low concentration of polymer and the introduction of the high shear rate in the non-solvent can induce the formation of PLA stereocomplex over PLLA or PDLA homo-crystallization.[4]

3.2 Polycaprolactone (PCL)

Polycaprolactone (PCL) is aliphatic polyester composed of hexanoate repeat units which is produced from crude oil. It is a hydrophobic, semicrystalline (50%), biocompatible, and relatively slow degrading polymer, which has been widely used in the biomedical field for the last few decades. PCL biodegrades within several months to several years depending on the molecular weight, the degree of crystallinity of the polymer, and the conditions of degradation. PCL is not degraded by enzymes within human or animal bodies because of the lack of suitable enzymes, but it can be degraded by microorganisms (bacteria and fungi) as the polymer backbone has ester linkages that are hydrolysable. PCL is a thermoplastic polymer with glass transition temperature (T_g) of -60°C and melting point ranging between 59-64°C, that grant it several desirable features, including good stability under ambient conditions, ease of processaibility (thermal and solution), and has already been approved for use in a few products by the U.S. Food and Drug Administration. PCL has a wide range of application area, such as packaging, medical implant, and controlled drug delivery system, so the crystallization and the morphologic properties of PCL are very important. The mechanical and degradation properties of pure PCL are not adequate with the requirement for some kind of medical applications, such as scaffold. So, PCL can be used as one of the component of blend materials or as a copolymer. Incorporation of nanostructured filler material into the PCL material could be an important strategy to improve and modulate the mechanical and degradation properties of PCL-based materials.[18–20]

Polycaprolactone is mainly synthesized by ring opening polymerization (ROP) of ε-caprolactone and many efficient catalysts have been used for the polymerization (Figure 3.3).[21] ROP of ε-caprolactone proceeds according to the four different major mechanisms: cationic, anionic, monomeractivated, and coordination-insertion ring opening polymerization.[18] Stannous (II) 2-ethylhexanoate (or tin octoate) is a representative catalyst with high efficacy and low toxicity, which has been frequently used in ring opening polymerization of ε-caprolactone.[20]

PCL is suitable for controlled drug delivery due to a high permeability to many drugs and excellent biocompatibility. Due to the fact that PCL degrades at a slower rate than other biopolymers such as PLA, poly(glycolic acid) (PGA), poly(lactic acid-co-glycolic acid) (PLGA) and its copolymers, it is therefore originally used in drug-delivery devices.[22] PCL also has the ability to form compatible blends with other polymers, which can affect the degradation kinetics, facilitating tailoring to fulfill its applications. The advantages of PCL for these applications include tailorable degradation kinetics and mechanical properties, ease of shaping and manufacture enabling appropriate pore sizes conducive to tissue in-growth, and the controlled delivery of drugs contained within their matrix.[23] Functional groups could also be added to make the polymer more hydrophilic, adhesive, or biocompatible which enabled favorable cell responses. The applications of PCL in medical devices include sutures, wound dressings as well as in dentistry.[24–26]

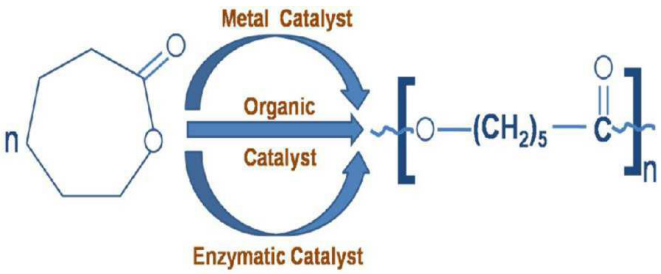

Figure 3.3. Synthesis of polycaprolactone (PCL) by ring opening polymerization.[20]

3.3 Poly styrene maleic anhydride copolymer (PSMA)

In the past few decades, chemical modifications of polymers to achieve desirable characteristics have been put into practice. This practice has led to the synthesis of polymers in which more than one monomer is used to form copolymers. A good example of a copolymer is poly (styrene-co-maleic anhydride) (PSMA).[27]

The PSMA copolymers are composed of styrene (hydrophobic) and maleic anhydride (hydrophilic) monomer units, synthesized by radical polymerization of a mixture of styrene and maleic anhydride, which largely determine their amphiphilic nature.[28]

Styrene-maleic anhydride copolymer is also regarded as a functional or reactive polymer. The functionality is brought about by the maleic anhydride in the backbone of the copolymer which is reactive towards nucleophilic reagents (H_2O, alcohols, thiols, ammonia, amines, etc). Introduction of nucleophilic compounds enables the synthesis of new materials. Figure 3.4 shows the preparation of PSMA derivatives.[28]

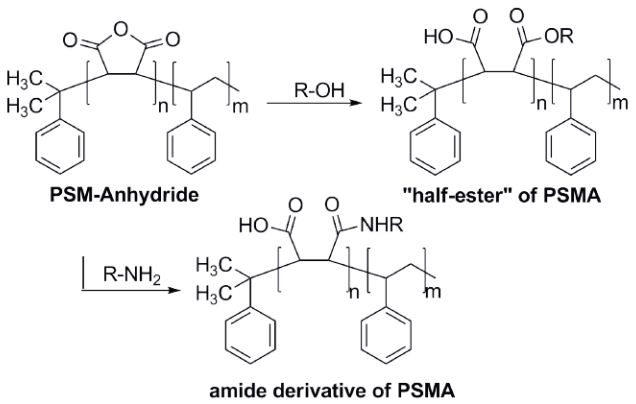

Figure 3.4. Preparation of PSMA derivatives (half-esters and amide conjugates).[28]

The physicochemical properties of PSMA copolymers are determined mainly by three factors: 1) the molecular mass distribution; 2) the molar ratio of styrene to maleic acid monomer units; and 3) the relative order of monomer units in the polymer molecule (c.a. whether it is a random, alternating or block copolymer). There are also chiral centers in the copolymer molecules and therefore a possibility for various tacticity of the molecules. The alternating copolymers with equi-molar ratio of styrene to maleic acid monomer units are usually soluble in water at pH > 5.[28]

PSMA is known to be a biocompatible polymeric material that employed within medical and pharmaceutical applications. It has been used in many applications such as drug and protein delivery vehicles to the biological environments of different pH. Yordanov et al. prepared PSMA nanoparticles as colloidal career for the anticancer drug epirubicin by nanoprecipitation method. They showed that the nanoparticles were stable in phosphate buffered saline within the pH interval from 4.5 to 9.3 and forming precipitates at lower pH and being disintegrated at higher pH.[29]

The first PSMA-drug conjugate has been reported by Maeda et al. in 1985.[30] The conjugate contained on average about two molecules of PSMA and one molecule of neocarzinostatin (an anti-cancer protein). The conjugation has been performed via amide linkage obtained after reaction between amino-groups from the protein and non-hydrolyzed anhydride groups from the copolymer.[30] Khazaei et al. studied Grafting amino drugs to poly(styrene-alt-maleic anhydride) as a potential method for drug release.[31] Maeda and coworkers demonstrated low release by doxorubicin conjugated PSMA as a new polymeric micellar drug.[32]

3.4 Other used materials

For the preparation of PAMAM-PCL: ε-caprolactone (97%), purchased from Sigma-Aldrich, was distilled under reduced pressure; second generation PAMAM dendrimer containing 16 amidoethanol surface groups, commercialized from Sigma-Aldrich as a 20 wt.% solution in methanol, was evaporated under vacuum at 50 °C for 24 h prior to use, to completely remove the solvent. Tin(II) 2-ethylhexanoate ($Sn(Oct)_2$) (95%; from Sigma-Aldrich) was used without further treatments. Anhydrous toluene (≥99.7%), chloroform and methanol were purchased from Sigma-Aldrich and used as received.

For the preparation of HBPG-PDLA: D-lactide (D-la) (purity >98%) was kindly supplied by Purac Biochem (The Netherlands). Before polymerization, the monomer was purified by three successive recrystallizations from 100% (w/v) solution in anhydrous toluene and dried under vacuum at room temperature. Fully-OH-functionalized hyperbranched polyglycerol (HPG), with number average molecular weight (Mn) of $25 \cdot 10^3$ g/mol and polydispersity of 1.7, was purchased from Nanopartica GmbH (Germany). For the sake of easy transfer, a 10% (w/v) solution of HPG in methanol was prepared. Once fed into reactor, the solution was evaporated under vacuum at 50 °C for 24 h prior to use, to completely remove methanol as well as the ~12.5 wt.% of water present in the pristine HPG. Anhydrous toluene (≥99.7%), chloroform and methanol were purchased from Sigma-Aldrich and used as received.

For the preparation of the PCL (DOXO) and PCL/PAMAM-PCL (DOXO) fibers: PCL with an average molecular weight of 80.000, N,N-dimethylformamide (DMF), dichloromethane (DCM) and doxorubicin hydrochloride (DOXO) were purchased from Sigma-Aldrich.

For the preparation of the PLLA and PLLA/HBPG-PDLA fibers: poly(L-lactide) (PLLA), with average molecular weight of $1 \cdot 10^5$ g/mol, was obtained from Purac (Synterra PLLA 1010) in pellet form, DCM and DMF were purchased from Sigma-Aldrich and used as received.

For preparation of sc-PLA/POSS/cyclodextrin fibers: Poly(L-lactide) (PLLA), PLLA 1010 Synterra (average molecular weight $1 \cdot 10^5$), and poly(D-lactide) (PDLA), PDLA 1010 Synterra (average molecular weight $1 \cdot 10^5$), purchased from Purac (The Netherland) in powder form, were used as received. Aminopropyl heptaisobutyl POSS (from now on referred as POSS-NH_2) (Figure 3.5) was purchased from Hybrid Plastics (USA) as crystalline powders and used as received.

The following solvents and reagents, all from Aldrich, were used as received: 1,1,1,3,3,3-hexafluoro-2-propanol (HFIP), chloroform ($CHCl_3$), acetonitrile, p-toluenesulfonyl chloride (TsCl), β-cyclodextrin (CD), methanol, alizarin red and 2-chlorophenol.

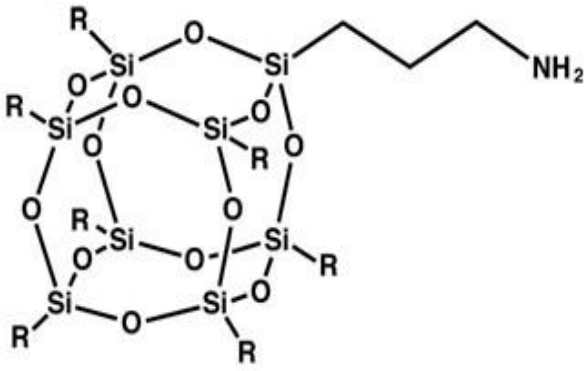

Figure 3.5. Aminopropyl heptaisobutyl POSS (POSS-NH_2).

For preparation of PSMA nanoparticles: Polystyrene-co-maleic anhydride (PSMA) (Dylark 332), kindly supplied by Nova Chemicals, was characterized by a concentration of maleic anhydride of 14 mol %, verified by NMR measurements. Dimethylfuran (DMF) and ethanol were purchased from Sigma-Aldrich and used as received. Papain (≥3 u/g, 23400 Da) from Carica papaya, casein (from bovine milk), L-cysteine, Ethylenediaminetetraacetic Acid (EDTA), trichloroacetic acid (TCA), sodium carbonate (Na_2CO_3), sodium hydroxide (NaOH), Folin & Ciocalteu's phenol reagent, dextran (DEX, Mw 9000-12000) and Poly (L) arginine (PAR, Mw 15000-70000) were purchased from Sigma-Aldrich. Calcium Chloride (CaCl2) was purchased from Riedel-de Haën. All solutions were prepared with deionized ultrapure Milli-Q (18.2 MΩ) water.

3.4 References

1. Garlotta D. A Literature Review of Poly (Lactic Acid). *J Polym Environ*. 2002;9(2):63-84. doi:10.1023/A:1020200822435.
2. Xiao L, Wang B, Yang G, Gauthier M. Poly(Lactic Acid)-Based Biomaterials: Synthesis, Modification and Applications. In: *Biomedical Science, Engineering and Technology*. InTech; 2012. doi:10.5772/23927.
3. Xiao L, Wang B, Yang G, Gauthier M. Poly(Lactic Acid)-Based Biomaterials: Synthesis, Modification and Applications. In: *Biomedical Science, Engineering and Technology*. InTech; 2012. doi:10.5772/23927.
4. Tsuji H. Poly(lactide) stereocomplexes: Formation, structure, properties, degradation, and applications. *Macromol Biosci*. 2005;5(7):569-597. doi:10.1002/mabi.200500062.
5. Auras R, Lim L-T, Selke SEM, Tsuji H, eds. *Poly(Lactic Acid)*. Hoboken, NJ, USA: John Wiley & Sons, Inc.; 2010. doi:10.1002/9780470649848.
6. Perego G, Cella G, Bastioli C. Effect of molecular weight and crystallinity on poly (lactic acid) mechanical properties. *J Appl Polym …*. 1996;59:37-43. doi:10.1002/(SICI)1097-4628(19960103)59:1<37::AID-APP6>3.0.CO;2-N.
7. Jonoobi M, Harun J, Mathew AP, Oksman K. Mechanical properties of cellulose nanofiber (CNF) reinforced polylactic acid (PLA) prepared by twin screw extrusion. *Compos Sci Technol*. 2010;70(12):1742-1747. doi:10.1016/j.compscitech.2010.07.005.
8. Hassouna F, Raquez JM, Addiego F, Dubois P, Toniazzo V, Ruch D. New approach on the development of plasticized polylactide (PLA): Grafting of poly(ethylene glycol) (PEG) via reactive extrusion. *Eur Polym J*. 2011;47(11):2134-2144. doi:10.1016/j.eurpolymj.2011.08.001.
9. Auras R, Lim L-T, Selke SEM, Tsuji H, eds. *Poly(Lactic Acid)*. Hoboken, NJ, USA: John Wiley & Sons, Inc.; 2010. doi:10.1002/9780470649848.
10. Ikada Y, Jamshidi K, Tsuii H, Hyon SH. Stereocomplex Formation between Enantiomeric Poly(lactides). *Macromolecules*. 1987;20(4):904-906. doi:10.1021/ma00170a034.
11. Tsuji H, Hyon SH, Ikada Y. Stereocomplex Formation between Enantiomeric Poly(lactic acid)s. 3. Calorimetric Studies on Blend Films Cast from Dilute Solution. *Macromolecules*. 1991;24(20):5651-5656. doi:10.1021/ma00020a026.
12. Cartier L, Okihara T, Lotz B. Triangular polymer single crystals: Stereocomplexes, twins, and frustrated structures. *Macromolecules*. 1997;30(20):6313-6322. doi:10.1021/ma9707998.
13. Miyazawa T. Molecular Vibrations and Structure of High Polymers. II. Helical Parameters of Infinite Polymer Chains as Functions of Bond Lengths, Bond Angle, and Internal Rotation Angles. *J Polym Sci*. 1961;55:215-231. doi:10.1002/pol.1961.1205516121.
14. Okihara T, Tsuji M, Kawaguchi A, et al. Crystal structure of stereocomplex of poly(L-lactide) and poly(D-lactide). *J Macromol Sci Part B*. 1991;30(1):119-140. doi:10.1080/00222349108245788.

15. Tsuji H, Ikada Y, Horii F, Nakagawa M, Odani H, Kitamaru R. Stereocomplex Formation between Enantiomeric Poly(lactic acid)s. 7. Phase Structure of the Stereocomplex Crystallized from a Dilute Acetonitrile Solution As Studied by High-Resolution Solid-State 13C NMR Spectroscopy. *Macromolecules*. 1992;25(16):4114-4118. doi:10.1021/ma00042a011.
16. Nam BU, Lee BS, Kim MH, Hong CH. Effect of a Nucleating Agent on Crystallization Behavior and Mechanical property of PLA stereocomplex. *Iccm18*. 2011:2-5.
17. Tsuji H, Ikada Y, Hyon S -H, Kimura Y, Kitao T. Stereocomplex formation between enantiomeric poly(lactic acid). VIII. Complex fibers spun from mixed solution of poly(D-lactic acid) and poly(L-lactic acid). *J Appl Polym Sci*. 1994;51(2):337-344. doi:10.1002/app.1994.070510216.
18. Mohamed RM, Yusoh K. A Review on the Recent Research of Polycaprolactone (PCL). *Adv Mater Res*. 2015;1134:249-255. doi:10.4028/www.scientific.net/AMR.1134.249.
19. Labet M, Thielemans W. Synthesis of polycaprolactone: a review. *Chem Soc Rev*. 2009;38(12):3484. doi:10.1039/b820162p.
20. Mondal D, Griffith M, Venkatraman SS. Polycaprolactone-based biomaterials for tissue engineering and drug delivery: Current scenario and challenges. *Int J Polym Mater Polym Biomater*. 2016;65(5):255-265. doi:10.1080/00914037.2015.1103241.
21. Van Natta FJ, Hill JW, Carothers WH. Studies of Polymerization and Ring Formation. XXIII. ε-Caprolactone and its Polymers. *J Am Chem Soc*. 1934;56(2):455-457. doi:10.1021/ja01317a053.
22. Armentano I, Dottori M, Fortunati E, Mattioli S, Kenny JM. Biodegradable polymer matrix nanocomposites for tissue engineering: A review. *Polym Degrad Stab*. 2010;95(11):2126-2146. doi:10.1016/j.polymdegradstab.2010.06.007.
23. Woodruff MA, Hutmacher DW. The return of a forgotten polymer - Polycaprolactone in the 21st century. *Prog Polym Sci*. 2010;35(10):1217-1256. doi:10.1016/j.progpolymsci.2010.04.002.
24. Sowmya S, Bumgardener JD, Chennazhi KP, Nair S V., Jayakumar R. Role of nanostructured biopolymers and bioceramics in enamel, dentin and periodontal tissue regeneration. *Prog Polym Sci*. 2013;38(10-11):1748-1772. doi:10.1016/j.progpolymsci.2013.05.005.
25. Li Z, Tan BH. Towards the development of polycaprolactone based amphiphilic block copolymers: Molecular design, self-assembly and biomedical applications. *Mater Sci Eng C*. 2015;45:620-634. doi:10.1016/j.msec.2014.06.003.
26. Jin G, Prabhakaran MP, Kai D, Annamalai SK, Arunachalam KD, Ramakrishna S. Tissue engineered plant extracts as nanofibrous wound dressing. *Biomaterials*. 2013;34(3):724-734. doi:10.1016/j.biomaterials.2012.10.026.
27. Baruah SD, Laskar NC. Styrene-maleic anhydride copolymers: Synthesis, characterization, and thermal properties. *J Appl Polym Sci*. 1996;60:649-656. doi:10.1002/(SICI)1097-4628(19960502)60:5<649::AID-APP1>3.3.CO;2-T.
28. Angelova N, Yordanov G. Nanopharmaceutical formulations based on poly (styrene-co-maleic acid). 2014;3(January):33-43.
29. Angelova N, Yordanov G. Nanoparticles of poly(styrene-co-maleic acid) as colloidal carriers for the anticancer drug epirubicin. *Colloids Surfaces A Physicochem Eng Asp*. 2014;452(1):73-81. doi:10.1016/j.colsurfa.2014.03.106.
30. Maeda H, Ueda M, Morinaga T, Matsumoto T. Conjugation of Poly(styrene-co-maleic acid) Derivatives to the Antitumor Protein Neocarzinostatin: Pronounced Improvements in Pharmacological Properties. *J Med Chem*. 1985;28(4):455-461. doi:10.1021/jm00382a012.
31. Khazaei A, Saednia S, Saien J, et al. Grafting amino drugs to poly(styrene-alt-maleic anhydride) as a potential method for drug release. *J Braz Chem Soc*. 2013;24(7):1109-1115. doi:10.5935/0103-5053.20130145.
32. Greish K, Sawa T, Fang J, Akaike T, Maeda H. SMA-doxorubicin, a new polymeric micellar

drug for effective targeting to solid tumours. *J Control Release*. 2004;97(2):219-230. doi:10.1016/j.jconrel.2004.03.027.

CHAPTER 4. *ad-hoc*-synthesized star polymers as novel additives for tuning PLLA and PCL electrospun fiber properties

In this chapter two different research projects have been presented. They are focused on the development of novel *ad-hoc*-synthesized polymeric additives suitable to modifying the properties of electrospun fibers based on bio-polymers, namely poly(ε-caprolactone) (PCL) and poly(L-lactide) PLLA (Figure 5.1). Indeed, the synthesis of two different dendritic macromolecules was set up: a star-like polymer, made up of a PAMAM core and PCL arms (PAMAM-PCL) and an hyperbranched polymer made up of a high molecular mass hyperbranched polyglicerol (HBPG) core and poly(D-lactide) PDLA arms (HBPG-PDLA). The above molecules were designed by taking into account both the features of the polymer matrix and the specific applications of the final materials. In particular, in order to enhance their dispersion, the dendritic molecules were characterized by arms whose chemical nature was identical to that of the polymer matrix. Moreover, in the case of the dispersion of HBPG-PDLA, the arms might promote the stereocomplexation with the polymer matrix, consisting of PLLA. Concerning the core of the dendritic structures, for PAMAM-PCL-based systems the hydrophilic dendrimer core may promote specific interactions with hydrophilic molecules, such the drug used in our work, namely doxorubicin (DOXO), which is a clinically used anticancer drug. In the case of the fibers based on HBPG, the hyperbranched core may modify the hydrophilicity of the polymer, increasing its tendency to absorb water or hydrophilic molecules as well as change the enzymatic degradation rate.

Indeed, new materials offer many advantages related to the employment of dendritic-based systems: i) the lower solubility in water or organic solvent with respect to the pristine dendritic core, which limit their leaching in the used medium, ii) their immobilization onto an insoluble solid support and iii) the easy processability of the support as a polymer, with some resistential characteristics, and having a “bio” nature.

In detail, the preparation of electrospun fibers was set up by mixing in solution the high molecular mass commercially available PCL and PLLA with the here-synthesized dendritic polymers (Figure 4.1).

In the case of the fibers containing PAMAM-PCL, DOXO was directly introduced in the electrospinning solution and the obtained fibers were characterized in terms of morphology, thermal properties and water absorption. The cytotoxicity tests, performed at IIT(Genova), were carried out on tumor cells for a period of 9 days. For the fibers based on HBPG-PDLA, we explored the influence of the dendritic polymer on the features of the electrospun PLLA fibers in terms of morphology, thermal and mechanical properties, water uptake and enzymatic degradation.

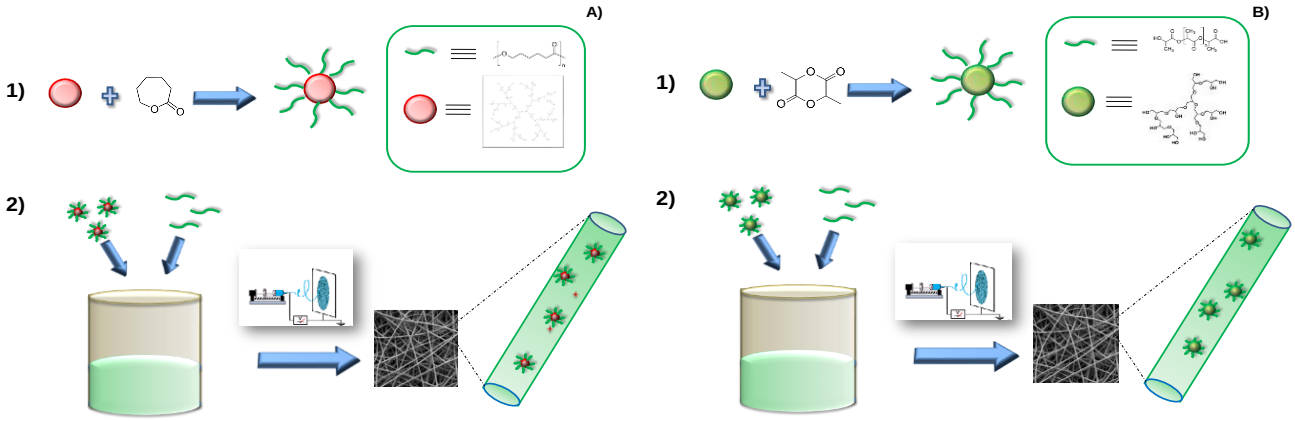

Figure 4.1. *Scheme of the preparation of: (a) PCL/PAMAM-PCL and (b) PLLA/HBPG-PDLA electrospun fibers.*

4.1 Introduction

Polymer nanofibers and nanoparticles have gained increasing interest in the biomedical field as carriers of drugs and enzyme, for their high surface area-to-volume ratio, flexibility, easy processability, tuneable size and porosity, modifiable chemical structure and in the case of the application of bio-polymers for their biodegradability and biocompatibility.[1] Although the potentialities of these materials, in relation to their specific applications, some issues have to be taken into account mainly connected to their interactions with the drugs as well as to their mechanical, thermal and degradation properties. Some of these aspects were considered during my Ph.D. work, by modifying the properties of electrospun fibers using *ad-hoc*-synthesized additives. In general, in the case of application of nanofibers as controlled/localized delivery of anticancer drugs, which was the field considered in this Ph.D. project, the peculiar architecture of the support, characterized by a highest surface/contact area, and its robust drug loading capability favors from one side the killing of the tumor cells and from the other, promotes tissue reconstruction of damaged areas.[2,3] Moreover, the delivery of the drugs can be controlled by tuning the fiber morphology, porosity and composition. Electrospun polymer fibers have been widely applied as delivery devices of several anticancer drugs such as carmustine,[4] paclitaxel,[5] cisplatin,[4] and DOXO[5] (that is the drug selected in the present work). Despite the potentialities of these systems, the simple electrospinning of the drug and the polymer mixture leads to an undesirable initial burst release of the drug, which is frequently inevitable. In order to overcome this limitation and attain a slow, sustainable release, several inorganic nanocarriers were inserted into the electrospun nanofibers. In particular, composite nanofibers were developed by combining the polymer with silica based nanoparticles,[6] - in systems where the drug was either loaded into the pre-formed nanocarriers or introduced into the nanoparticles during their growth under controlled conditions - hydroxyapatite,[7] as well as a combination of silica and hydroxyapatite.[8] Even though such nanofillers can be considered as ideal drug carriers, mainly due to their high surface area and good biocompatibility, their application in designing composite nanofibers for the drug delivery implies facing some drawbacks. Indeed, the weak interactions between the drug molecules and the inorganic nanoparticles as well as the not always easy dispersibility of the nanofillers into the polymer matrix and their slow bio-absorption capacity are important issues to be taken into account. Clearly, the development of nanofibrous scaffold containing more specific drug carriers, as an alternative to the classical inorganic nanofillers, characterized by a good affinity with both the drug molecules and the polymer matrix, represents an ideal target in the development of materials to be applied as local drug delivery system. With this in mind, we have developed a novel drug delivery system, consisting of fibers, based on a biocompatible and re-absorbable polymer, namely PCL, and containing as a drug carrier an *ad-hoc*-synthesized star polymer, designed taking into account the specific characteristics of the polymer matrix, and the chosen drug, that is DOXO (Figure 4.1A).

Another specific aspect which was considered during my work was the modification of the bio-polymer degradation feature. Indeed, the investigation and the tuning of the degradation of biodegradable and biocompatible polymers, represent important issues for their exploitation.[9] In particular, in the case of PLA, one of the most promising bio-polymers and object of the present study, the decomposition, which can be mainly induced by thermal activation,[10] hydrolysis and biological activity,[11] has been regulated by applying different approaches. Indeed, from one side the degradation turns out to depend on the intrinsic features of the polymer such the chemical composition (homo and copolymers), tacticity and physical properties (molecular weight, crystallinity, ect.).[9] Moreover, the introduction into the polymer matrix of proper additives, both organic (molecules or macromolecules) and inorganic, was found to be a valid method to modify the properties and, in particular, the degradation of PLA.[12] Indeed, as far as the latter approach is

concerned, various types of fillers/nanofillers were used, such as layered silicates, carbon nanotubes, graphite/graphene, which were capable of increasing or reducing thermal- or bio-degradation.[12] Nevertheless, some issues have to be considered, which are mainly related to the dispersion of the inorganic phase into the polymer matrix, whose quality depends the material final properties, and the filler biocompatibility. On the other hand, organic molecules/macromolecules, characterized by a better compatibility with PLA and capable of modifying the polymer degradation, generally decrease its mechanical properties. Among the organic additives, which can be used to change linear polymer features, star polymers represent ideal fillers because of their compact shape and elevated concentration of functional end groups.[13] However, as the above macromolecules are characterized by a higher solubility than the linear homologous their leaching from the polymer matrix can limit the application of the related composite material. On this basis, in this work a novel dendritic polymer has been designed and synthesized, which was made up of a high molecular mass hyperbranched polyglicerol (HBPG) core and PDLA arms (HBPG-PDLA) (Figure 4.1B). Then, the preparation of electrospun fibers, based on a high molecular mass commercial PLLA and containing the synthesized star polymer, was set up by mixing both the components in a solution. We explored the influence of HBPG-PDLA on the electrospun PLLA fibers in terms of morphology, thermal and mechanical properties, water uptake and enzymatic degradation.

4.2 Experimental section

For the preparation of PAMAM-PCL: ε-caprolactone (97%), purchased from Sigma-Aldrich, was distilled under reduced pressure; second generation PAMAM dendrimer containing 16 amidoethanol surface groups, commercialized from Sigma-Aldrich as a 20 wt.% solution in methanol, was evaporated under vacuum at 50 °C for 24 h prior to use, to completely remove the solvent. Tin(II) 2-ethylhexanoate ($Sn(Oct)_2$) (95%; from Sigma-Aldrich) was used without further treatments. Anhydrous toluene (≥99.7%), chloroform and methanol were purchased from Sigma-Aldrich and used as received.

For the preparation of HBPG-PDLA: D-lactide (D-la) (purity >98%) was kindly supplied by Purac Biochem (The Netherlands). Before polymerization, the monomer was purified by three successive recrystallizations from 100% (w/v) solution in anhydrous toluene and dried under vacuum at room temperature. Fully-OH-functionalized hyperbranched polyglycerol (HPG), with number average molecular weight (Mn) of 25·103 g/mol and polydispersity of 1.7, was purchased from Nanopartica GmbH (Germany). For the sake of easy transfer, a 10% (w/v) solution of HPG in methanol was prepared. Once fed into reactor, the solution was evaporated under vacuum at 50 °C for 24 h prior to use, to completely remove methanol as well as the ~12.5 wt.% of water present in the pristine HPG. Anhydrous toluene (≥99.7%), chloroform and methanol were purchased from Sigma-Aldrich and used as received.

For the preparation of the PCL (DOXO) and PCL/PAMAM-PCL (DOXO) fibers: PCL with an average molecular weight of 80.000, N,N-dimethylformamide (DMF), dichloromethane (DCM) and doxorubicin hydrochloride (DOXO) were purchased from Sigma-Aldrich.

For the preparation of the PLLA and PLLA/HBPG-PDLA fibers: poly(L-lactide) (PLLA), with average molecular weight of 1·105 g/mol, was obtained from Purac (Synterra PLLA 1010) in pellet form, DCM and DMF were purchased from Sigma-Aldrich and used as received.

Synthesis of PAMAM-PCL

Star-like PCL was synthesized by ring-opening polymerization of ε-caprolactone, at 120 °C, using the hydroxyl-terminated PAMAM dendrimer as macroinitiator and $Sn(Oct)_2$ as a catalyst. In detail, 1.14 ml of PAMAM solution (corresponding to 0.2 g of PAMAM) were introduced into a 50-ml two-neck round-bottomed flask equipped with a magnetic stirrer and in-situ dried; then, 3 g of ε-caprolactone (previously distilled) were charged into the flask under argon flow. The reaction vessel was immersed into a thermostatically controlled oil bath (initially set at 140 °C, in order to favour the solubilisation of the dendrimer in the monomer), under vigorous stirring: as soon as the mixture was completely homogenized, about 0.3 ml of a freshly prepared solution of $Sn(Oct)_2$ in toluene ([ε-caprolactone]/[$Sn(Oct)_2$] = 5.103) was added through a micropipette. The reaction was then allowed to proceed for 24 hours at 120 °C, always under inert atmosphere. After this time, the polymerization was stopped by cooling down the reaction mixture, which was subsequently dissolved in chloroform and poured into an excess of cold methanol. The as-purified polymer (PAMAM-PCL) was recovered as white fine powder by filtration and dried in vacuum at 40 °C till constant weight.

Synthesis of HBPG-PDLA

Dendritic poly(D-lactide) (HBPG-PDLA) was synthesized by ring-opening polymerization (ROP) of D-lactide using HBPG polyol as a multifunctional macroinitiator and $Sn(Oct)_2$ as a catalyst, in bulk at 120 °C. In detail, about 3 g of D-la (previously recrystallized and dried) were charged under argon flow into the reactor (i.e., a 50-ml two-neck round-bottomed flask equipped with a magnetic stirrer) containing a predetermined amount of accurately weighed and in-situ dried HPG. The feeding ratio of the D-la monomer to the HPG initiator was adjusted to about 1500 to 1. After the introduction of D-la, the flask was evacuated for 15 minutes and purged with argon, and the exhausting/refilling process repeated three times in order to fully dry the reaction environment. The reaction vessel was then immersed into a thermostatically controlled oil bath set at 120 °C, under vigorous stirring: as soon as the mixture was completely molten and homogenized, about 0.15 ml of a freshly prepared solution of $Sn(Oct)_2$ in toluene ([D-la]/[$Sn(Oct)_2$] = 103) were added under argon through a micro-pipette, and the reaction allowed to proceed for 24 hours under inert atmosphere, before cooling it down. The crude product was dissolved in chloroform and poured into an excess of cold methanol: after filtering and drying in vacuum at 40 °C to constant weight, the as-purified polymer (designated as HBPG-PDLA) was obtained as a fine, white powder, with a gravimetric yield of ~80%.

Electrospun fiber preparation

Electrospinning solutions for PCL-based fibers were prepared by dissolving 15 wt.-% of PCL or PCL containing 10 wt.-% of PAMAM-PCL (PCL/PAMAM-PCL fibers) in the solvent mixture DMF and DCM with a 30:70 v/v ratio. In the case of the preparation of fibers containing the drug, the concentration of DOXO in the polymer solution was 0.015 mg/ml to have a final total amount in the electrospun mats, used per each of the well in the cytotoxicity tests, of 0.5 μg.

Electrospinning solutions for PLLA-based fibers were prepared by dissolving 14 wt.-% of PLLA in the solvent mixture DMF and DCM with a 30:70 v/v ratio. In the case of the fibers based on the dendritic polymer, the concentration of PLLA and HBPG-PDLA were 11.25 wt-% and 3.75 wt.-%, respectively.

The fibers were electrospun using a conventional electrospinning system. The solutions were loaded in a syringe (model Z314544, diameter d=11.6 mm, Aldrich Fortuna Optima) placed in the horizontal direction. A Gamma high-voltage research power supply (Model ES30P-5W) was used to charge the solution in the syringe with a positive DC voltage. The positive electrode was connected to the needle (diameter d=0.45mm) of the syringe and the negative electrode was attached to the grounded collector, an aluminium sheet wrapped on a glass cylinder (height 4 cm, diameter 14.5 cm). The distance between the tip and the collector was 20cm. A syringe pump (Harvard Apparatus Model 44 Programmable Syringe Pump) was used to feed the needle. The needle tip and the ground electrode were contained in a hollow plastic cylinder (height 30.5 cm, inner diameter 24 cm, and thickness 3.5 mm), internally coated with a polytetrafluoroethylene sheet (thickness 1 mm). A glass Brooks rotameter was used to keep constant the air flow in the enclosed electrospinning space. The air flow was fed in the chamber at atmospheric pressure from an inlet placed behind the collector.

The established conditions for producing PCL-based fibers were: voltage tension = 15 kV, tip-collector distance = 20 cm, air flow = 2 l/min and temperature =21 °C, while in the case of PLLA-based fibers the following conditions were applied: voltage tension = 20 kV, tip-collector distance = 20 cm, air flow = 2 l/min and temperature =21 °C. In addition, the PLLA-based fibers underwent an annealing treatment at 80°C for 4 hours.

Characterization

FTIR spectra were recorded on a Bruker IFS66 spectrometer in the spectral range 400-4000 cm^{-1}. ^1H NMR spectra were collected with a Varian NMR Mercury Plus instrument, at a frequency of 300 MHz, in $CDCl_3$ solutions containing tetramethylsilane as internal standard.

Differential scanning calorimetry (DSC) measurements were performed with a Mettler-Toledo TC10A calorimeter calibrated with high purity indium and operating under flow of nitrogen. The sample weight was about 5 mg and a scanning rate of 10 °C/min was employed in all the runs. The samples were heated from 25 °C to 100 °C, at which temperature the melt was allowed to relax for 1 minute, then cooled down to -100 °C, and finally heated up again to 100 °C (second heating scan). The degree of crystallinity (X_c) was calculated by using an enthalpy of fusion for a 100% crystalline PCL of 136 J/g, PLLA of 93 J/g and stereocomplex PLA of 143 J/g.

Thermal gravimetrical analysis (TGA) was performed with a Mettler-Toledo TGA 1 thermogravimetric analyzer, under a flow of nitrogen of 80 ml/min. The weight loss of the samples (having initial masses of ca. 10 mg) was measured in isothermal mode at a holding temperature of 230 °C.

Wide-angle X-ray diffraction (WAXD) measurements were performed in reflection mode using a Philips PW 1830 powder diffractometer equipped with a nickel-filtered Cu-Kα source (λ = 0.1542 nm) in a 2θ angle range of 5-30°. The crystalline phase content was calculated after deconvolution of the WAXD patterns (using the software package Peak-Fit) as the ratio between the areas of the crystalline peaks to the total area under the curve.

The tensile properties of the electrospun mats, based on PLLA and PLLA/HBPG-PDLA, were determined at room temperature by an Instron Mechanical Tester (Instron 5565), at a crosshead speed of 5 mm/min, using rectangular specimens with dimension of 10×25×0.5 mm. The values reported represent an average of the results for tests run on six specimens, along with experimental deviation.

The water absorption was measured by immersing electrospun mat specimens having area of 1.5× 1.5 cm^2 in distilled water at room temperature for 24 h, and expressed as increase in weight percent according to the formula:

$$\text{water adsorption } (\%) = [(W_{wet} - W_{dry_0})/W_{dry_0}] \times 100 \quad (4.1)$$

where W_{wet} is the wet weight measured (immediately – to avoid evaporative losses) after withdrawing the films from water and gently wiping off the surface water with a tissue, and Wdry0 is the initial weight of the specimens, measured after vacuum-drying the films for 24 h at 40 °C. For each sample, at least five replicates were analyzed

To study the sample surface morphology, a Zeiss Supra 40 VP field emission scanning electron microscope (FE-SEM) was used to examine the fiber morphologies. All samples were thinly sputter-coated with carbon using a Polaron E5100 sputter coater. The fiber diameters and their distribution were measured using an image analyzer, with ImageJ 1.41 software.

Confocal analysis was performed to check the presence of DOXO in the PCL and PCL/PAMAM-PCL mats. The DOXO-loaded-PCL and DOXO-loaded-PCL/PAMAM-PCL mats were cut into 1×1 cm^2 pieces. Each piece was then mounted on a flat sample holder and viewed under confocal microscope Nikon Eclipse Ti microscope equipped with an argon laser source with excitation and emission wavelength of 488 and 530 nm, respectively, to view the doxorubicin loading in the electrospun mats.

The tensile properties of the electrospun mats, based on PLLA and PLLA/HBPG-PDLA, were determined by an Instron Mechanical Tester (Instron 5565) at a crosshead speed of 10 mm/min at room temperature using rectangular specimens with dimension of 10×25×0.5 mm. Property values reported represent an average of the results for tests run on six specimens, along with experimental deviation.

Degradation test

To test their resistance to hydrolysis by the enzyme proteinase K, small pieces of PLLA and PLLA/HBPG-PDLA nanofiber mats (previously dried overnight) having area of 1×1 cm^2 were immersed into 2 ml of enzyme solution (containing 0.2 mg/ml of proteinase K in 0.1 M phosphate buffer solution at pH = 7.4) at 37 °C. At intervals of 1, 3, 6, 24, 48 and 120 hours, the mats (two replicates per each incubation period) were removed from the enzyme solution and washed with water and ethanol, and then vacuum dried. It is worth underlining that, to avoid loss in enzyme activity with the progress of the reaction, the enzyme solution was replaced with a freshly prepared one each day. The (dry) sample weights were determined both before and after the immersion and washing and the extent of degradation was measured as percentage weight loss of the nanofiber mat as:

$$\text{Weight loss } (\%) = [(W_{dry0} - W_{dry})/W_{dry0}] \times 100 \quad (4.2)$$

where W_{dry0} is the initial weight of the specimens and W_{dry} is the dry weight of the specimens as measured after the treatment with the proteinase K enzyme solution for a given time lapse.

In-vitro viability assay for testing of toxicity caused by pristine and DOXO-loaded PCL or PCL/PCL-PAMAM electrospun mats

Three different cancer cell lines - A431 epidermoid carcinoma cells (ATCC® CRL-1555™), HeLa-WT cervical cancer cells (ATCC® CCL-2™) and MCF-7 breast cancer cells (ATCC® HTB-22™) were used. All these cell lines were cultured using DMEM media supplemented with 10% Fetal Bovine Serum, 2% Penicillin-streptavidin and 1% L-Glutamine (Gibco™) under 37ºC, 5%

CO_2 and 95% relative humidity. These cells were then harvested and plated in 24 multi-well-plate at a cell number of 100,000 cells in 1 mL cell media per well and allowed to adhere overnight. Given the interference of phenol-red in the optical read out of the cytotoxicity assay, prior to performing the viability assays applied in this work, the media in the well plates was replaced with 1 mL of freshly prepared Phenol-Red free DMEM media supplemented with 10% Fetal Bovine Serum, 2% Penicillin-streptavidin and 1% L-Glutamine. Meanwhile the electrospun mats, pristine PCL, pristine PCL/PAMAM-PCL, DOXO-loaded-PCL and DOXO-loaded-PCL/PAMAM-PCL were cut into 1×1 cm^2 pieces (each single piece of scaffold was manipulated to contain 0.5 µg DOXO during electrospinning process). These 1×1 cm^2 scaffold pieces were peeled off from their aluminum substrate and dropped on top of the media in 24 multi-well-plate containing the cells and incubated for 1, 3, 5, 7 and 9 days. After the respective incubation periods, PrestoBlue® and AlamarBlue® Cell Viability Reagents (Molecular Probes™) were used to access the viability of the cancer cells. For each condition, the assays were performed in triplicate.

PrestoBlue® Viability Assay

The 24 multi-well-plates containing the cells incubated with the scaffolds floating in their media, after their incubation periods were washed with Phosphate Buffer Saline (PBS) and incubated with fresh Phenol-Red free media containing 10% PrestoBlue reagent for 30-40 minutes at 37 °C. Then 100 µL of supernatants from each well were transferred in a new 96 multi-well-plate and absorbance was read using a Multiskan™ GO Microplate Spectrophotometer (ThermoFisher Scientific™) at 570 and 600nm. The viability of each experimental condition was normalized to the viability of the control untreated cells considering them to be 100% viable.

AlamarBlue® Viability Assay

After the respective incubation periods as mentioned earlier, 100µL of AlamarBlue reagent (10% AlamarBlue reagent in media) was added to each of the 24 multi well-plate containing the cells incubated with the floating scaffolds. The well plates were then incubated at 37ºC for 4h. Next, 100 µL of supernatants from each well were collected in a new 96 multi well-plate and absorbance was read using a Multiskan™ GO Microplate Spectrophotometer (ThermoFisher Scientific™) at 570 and 600nm (Ab570-Ab600). The viability of each experimental condition was normalized to the viability of the control untreated cells considering them to be 100% viable.

Confocal Microscopy characterization to study the attachment and proliferation of adult human dermal fibroblasts (HDFa) on PCL/PAMAM-PCL electrospun scaffolds

The HDFa Adult human dermal fibroblasts (ThermoFisher ScientificTM C0135C) were grown in special fibroblast media, Medium 106 (M106500) supplemented with 10 mL low serum growth supplement (LSGS_S00310). The cells were maintained in culture at 37ºC in a sterile incubator and 5% CO_2 and 95% relative humidity. These cells were then harvested using 0.1% trypsin-EDTA, counted and plated in 24 MW-plate containing the PCL/PAMAM-PCL scaffolds at density of 10,000 cells/well in 1mL complete media to check for the ability of this normal and healthy cell line to attach and proliferate on the drug free-PCL/PAMAM-PCL scaffolds. In order for the scaffolds to remain at the bottom of the well, soft PDMS ring prepared by us was placed over the scaffold. These cells after 24h, were washed carefully with PBS and fixed using 4% sterile formaldehyde (Sigma) for 10min, washed thoroughly and permeated with 0.1% Triton X-100 for 2-3min. Followed by fixation and permeation, the scaffold containing the cells were washed 3X with

PBS. They were the incubated with 1% bovine serum albumin (BSA) for 30-40min; this step provides a blocking step for the upcoming F-actin staining. Then they were stained using Alexa Fluor® 488 phalloidin (InvitrogenTM A12379) for 30min, washed with PBS 3X and stained using NucBlu® Fixed Cell ReadyProbes® Reagent (InvitrogenTM R37606) for 15min. Then the scaffolds containing cells were washed and carefully inverted in the same 24 MW-plate and filled with 1mL fresh PBS for the purpose of imaging using Confocal Microscope (Nikon) at excitation and emission wavelength of 495/518nm for F-actin phalloidin and 360/460nm for nuclei DAPI. The same was repeated after 48 and 72h. The analysis was done in triplicate.

4.3 Results and discussions

Synthesis and characterization of PAMAM-PCL

At first, the star-like polymer, made up of a PAMAM core and PCL arms, was synthesized via ROP of ε-caprolactone using as macro-initiator the generation 2 PAMAM (fitted with 16 hydroxyl end groups). The dendrimer-graft architecture of the obtained product was established through spectroscopic measurements. Figure 4.2(a) shows the FTIR spectrum of PAMAM-PCL: together with the intense absorption band for the stretching of the ester carbonyl at 1720 cm^{-1}, characteristic of PCL, two new peaks of lower intensity can be observed at 1650 and 1545 cm^{-1} (corresponding to amide carbonyl stretching and amide N-H bending, respectively), to be related to the poly-(amidoamine) structure of the PAMAM molecule. Since the sample was purified by precipitation in methanol, which is a good solvent for PAMAM, the presence of these peaks is indicative of the successful incorporation of PAMAM as the core onto which the PCL arms were grown.

This was further confirmed by means of ^{1}H NMR spectroscopy (Figure 4.2(b)), where the characteristic peaks of PCL (at δ 1.40, 1.65, 2.31, 3.64 and 4.06 ppm – assigned to CH_2-CH_2-C*H*$_2$-CH_2-CH_2, CH_2-C*H*$_2$-CH_2-C*H*$_2$-CH_2, CO-C*H*$_2$, terminal C*H*$_2$-OH, and C*H*$_2$-O-CO protons, respectively) are accompanied by several signals in the region at δ 2.60-3.60 ppm, ascribable to the presence of the PAMAM units. Furthermore, the triplet at δ 3.60 ppm for the terminal methylene protons of unbound PAMAM becomes hardly discernible, while a signal appears at δ ~4.12 ppm (see the insets of Figure 4.2 (b)), which is consistent with the resonance shift upon formation of ester linkages. This confirms the formation of the desired star-like PCL with the ROP started from the hydroxyl end groups of PAMAM, and also indicates that all of these groups were active initiators, thus giving rise to a dendritic star-like PCL having on average 16 polyester arms. Finally, ^{1}H NMR spectroscopy was exploited to calculate the mean degree of polymerization of the PCL arms, by comparing the peak integral of the methylene protons in the PCL chain with those at the chain end (at δ 2.31 and δ 3.64 ppm, respectively), ascertaining it is about 18. Thus, spectroscopic measurements enabled assessing the successful preparation of a dendritic PCL star product, having 16 arms, each one with an average length of about 2000 g/mol, and thence an overall number average molecular weight of about 35000 g/mol – corresponding to a PAMAM content of about 9 wt.%.

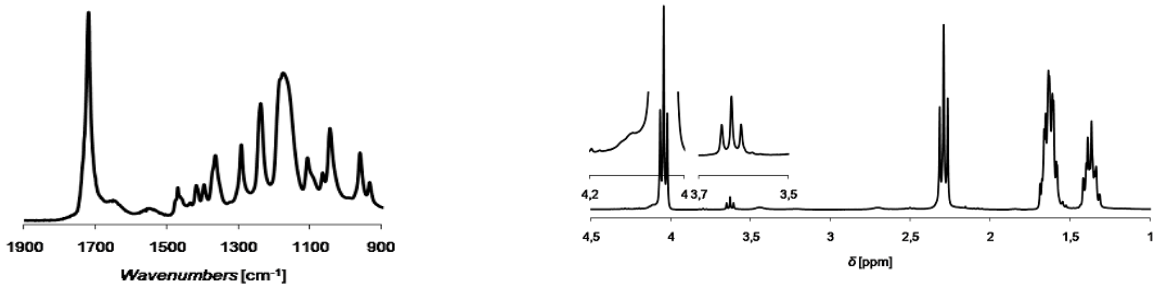

(a) (b)

Figure 4.2. *(a) FTIR spectra of the sample PAMAM-PCL in the spectral region 1900-900 cm^{-1} and (b) ^{1}H NMR spectrum of PAMAM-PCL (region at δ 4.5-1.0 ppm) with enlargement insets (at δ 3.7-3.5 and 4.2-4.0 ppm).*

The thermal behaviour of PAMAM-PCL, together with that of the linear high-molecular-weight PCL employed for electrospinning, were studied by means of the DSC (results not shown). In spite of the branched nature of PAMAM-PCL, which would be expected to disturb ordering, its crystallizability is enhanced with respect to PCL, while the melt-crystallization is anticipated, as well as the final crystallinity is found higher (X_c ~55% against ~37%) than for the linear polymer. This suggest that the improved chain mobility is promoted in the short-armed star system, as compared to high-molecular-weight PCL and prevails over the hindering effect caused by branching. Contrariwise, the temperature of melting is lower for PAMAM-PCL than for linear PCL (T_m ~51 °C against ~56 °C) – that is a general observation for star polymers, and it would be imputed to the short arm length and branched architecture of PAMAM-PCL, both of which factors negatively affect crystal thickness and perfection.

Synthesis and characterization of HBPG-PDLA

The $Sn(Oct)_2$-catalyzed ROP of D-la employing HBPG as the macroinitiator was carried out as described in the Experimental Section. The FTIR spectrum of the crude reaction product (not shown) was recorded to verify that the conversion of D-la was close to completion.

After purification, the polymerization product was characterized by means of ^{1}H NMR spectroscopy (see Figure 4.3(a)) and the signals identified according to the literature.[14–16] In addition to the peaks characteristics of PLA (at δ 1.50-1.58 ppm, 4.35 ppm and 5.16 ppm – assigned as methyl protons, methine protons at the chain ends and methine protons in the chain, respectively) the spectrum exhibits a broad, featureless signal in the range 3.2-3.8 ppm for the methylene and methine core protons of HBPG,[3,4] while the peak at about 2.7 ppm may be assigned to the free (unreacted) hydroxyl groups of HBPG.[4] As the sample had been purified with methanol, so as to remove eventual residues of unbound HBPG (aside from unreacted D-la), this result seems substantiating the successful linkage of the PDLA arms and the HBPG core. Indeed, a closer look to the spectrum (see the inset) reveals the presence of a small signal around 4.17 ppm, partially overlapping with the PDLA resonance at 4.35 ppm and belonging to the esterified hydroxymethylene protons of HBPG. This evidence definitively allows assessing the successful preparation of the dendritic HBPG-PDLA, with the ROP of D-la effectively induced from the hydroxyl groups of the HBPG initiator. The mean degree of polymerization (DP) of the PDLA arms, based on ^{1}H NMR spectroscopy, was calculated by comparison of the peak integral of the methine protons in the polylactide chain with those at the chain end (at δ 5.16 and δ 4.35 ppm,

respectively): the number average molecular weight (M_n) per arm was estimated to be about 1100 g/mol (see Table 4.1).

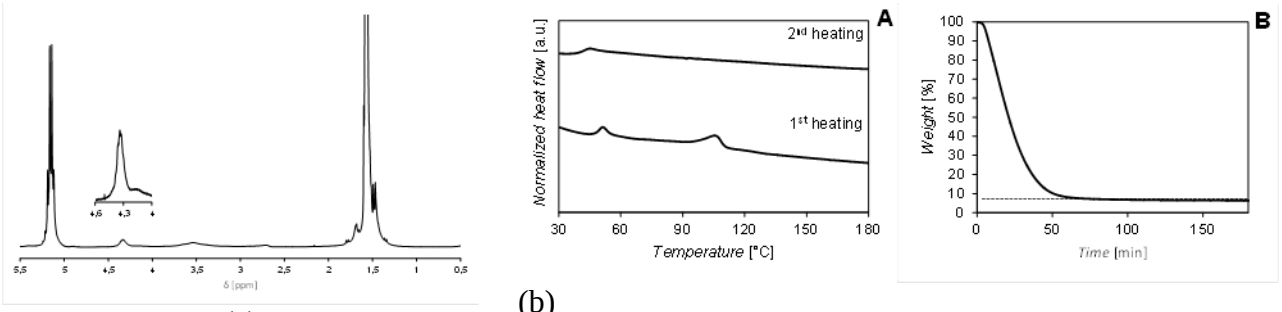

(a) (b)

Figure 4.3. *(a) ^{1}H NMR spectrum (region at δ 5.5-0.5 ppm) of purified HPG-PDLA with enlargement inset (at δ 4.6-4.0 ppm) and (b) DSC thermograms of HPG-PDLA both as-prepared (first heating scan) and after melt-cooling (second heating scan)(A), and its TGA curve recorded on isothermal holding at 230 °C (B).*

In order to derive the average number of arms of HBPG-PDLA (n), the information from ^{1}H NMR was combined with that from thermal gravimetric analysis. Indeed, since the two structural parts (the polyester branches and the HBPG core) have very different thermal stabilities (with HBPG being more thermally resistant), by isothermal holding at 230 °C it was possible to degrade selectively only the PDLA component. Figure 4.3(B) shows the TGA curve of the HPG-PDLA sample during the isothermal measurement: the mass loss corresponds to the degradation of the PDLA arms, while the remaining weight (dashed lines drawn to guide the eyes) belongs to the HBPG core, thus allowing quantifying its mass percentage in the sample, that is, about 7% (see Table 4.1). From this value, the overall M_n of HBPG-PDLA was obtained (about $350 \cdot 10^3$ g/mol, see Table 4.1), and, on the basis of the arm length calculated from ^{1}H NMR spectroscopy, it was estimated that HPG-PDLA has an average number of polylactide arms of about 300. Unfortunately, as we did not know the exact degree of hydroxyl functionalization of the HBPG core, we could not to estimate how many of them effectively took part in the polymerization.

The molecular characteristics of the synthesized product are summarized in Table 4.1: by means of ROP of D-la with HBPG initiator, a core-shell structure, that is, a multi-arm star PDLA with hyperbranched polyglycerol core ("dendritic PDLA"), was obtained.

Table 4.1*. Molecular characteristics of the synthesized dendritic PDLA.*

Sample	**$DP_{NMR(arm)}$[a]**	**$Mn_{NMR(arm)}$[b] [g/mol]**	**wt% HPG_{TGA}[c]**	**Mn_{TGA}[d] [10^3 g/mol^{-1}]**	**n[e]**
HBPG-PDLA	8	1100	7	357	300

[a] Average degree of polymerization of D-la (per arm) evaluated from ^{1}H NMR spectroscopy [by comparing the peak integral of the methine protons in the chain (at δ 5.16 ppm) with that of the methine protons at the chain end (at δ 4.35 ppm)]. [b] Numeric average molecular weight of each PDLA arm calculated as: $Mn_{NMR(arm)} = DP_{NMR(arm)} \times 144.13$, where 144.13 is the molecular mass of D-la. [c] Measured by TGA analysis. [d] Numeric average molecular weight of HPG-PDLA calculated as: $Mn_{TGA} = (25000 \times 100)/wt\%\ HPG_{TGA}$, where 25000 is the Mn of HPG. [e] Average number of PDLA arms calculated as: $n = (Mn_{TGA} - 25000)/DP_{NMR(arm)}$, where 25000 is the Mn of HPG.

The thermal properties of the synthesized dendritic PDLA have been characterized by means of DSC. Figure 4.3(A) shows the DSC thermograms during both the first and the second heating scans (that is, on heating the as-prepared sample and following cooling from the relaxed melt to -10 °C). While during the first heating scan there is trace of some crystalline order (as signaled by the

small melting peak at about 106 °C, corresponding to a crystallinity of ~ 7%), only PDLA glass transition at about 41 °C can be detected in the second heating run, without any sign of cold crystallization nor melting phenomena. Indeed, this was expected based on the well-known fact that star-like topology makes regular packing challenging, the more the greater the number of arms.

Preparation, characterization and properties of PCL, PCL/PAMAM-PCL, PCL/PAMAM-PCL/DOXO and PCL/PAMAM-PCL/DOXO fibers

The electrospinning conditions were tailored in order to obtain defect-free and homogeneous fibers. Indeed, in Figure 4.4(a) the micrograph of a PCL mat, prepared by applied the optimized electrospinning conditions, is shown. The fibers, which result to be defect-free, are characterized by an average diameter of 1.5 μm. Indeed, the addition of PAMAM-PCL (10 wt.-%) turned out not to modify the fibers morphology, as by applying the same conditions used in the preparation of the neat PCL fibers, those based on the star polymer were found to be homogeneous with an average diameter similar to that reported for the PCL fibers (Figure 4.4(b)).

Concerning the morphology of the mats containing the drug, as shown in Figure 4.4(c) and 4.4(d), the above fiber morphology does not change by adding DOXO into the electrospinning solution, both in the case of PCL/DOXO and PCL/PAMAM-PCL/DOXO fibers.

To incorporate the standard chemotherapeutic agent, DOXO was mixed with the electrospinning solutions containing PCL and the mixture PCL and PCL-PAMAM. The dispersion of the drug into the fibers was investigated by confocal microscopy. Considering the confocal microscopy images, shown in Figure 4.5, the DOXO-loaded-PCL/PAMAM-PCL fibers result to be characterized by a more uniform red fluorescence than the DOXO-loaded-PCL fibers. This result may be correlated with the good distribution of the star PCL-based molecule inside the PCL fibers, which dispersion promotes also the homogeneous distribution of DOXO, thanks to the specific interactions occurring between the drug and the PAMAM core.

Indeed, the incorporation of the hydrophilic PAMAM moieties into the hydrophobic PCL fibers is expected to enhance the hydrophilicity of the resulting materials, which should be reflected in their capability to absorb water and, at the same time, interact with hydrophilic drug molecules like DOXO. The percentage of water absorbed by the mats containing PAMAM-PCL resulted to be 30 %, while the neat PCL fibers do not show any tendency to uptake water. This finding points out to the capacity of the star PAMAM-PCL polymer to modify the performances of the fibers, increasing their affinity for hydrophylic molecules, which feature turns out to be relevant for the formulation of the novel drug delivery system based on the hydrophylic DOXO.

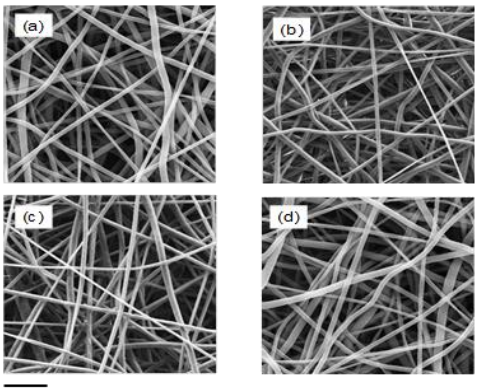

Figure 4.4. *FE-SEM micrographs of: (a) PCL, (b) PCL/PAMAM-PCL, (c) PCL/DOXO and (d) PCL/PAMAM-PCL/DOXO fibers. Scale bar represents 5 μm.*

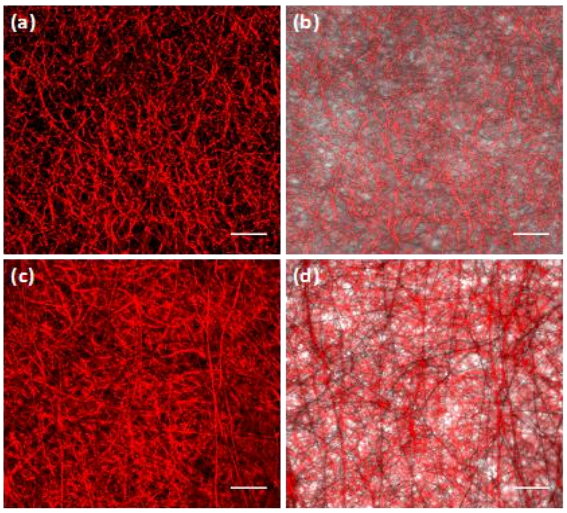

Figure 4.5. *Confocal microscopy images of PCL/DOXO electrospun mats red (a) and transmission + red channel (b) and PCL/PCL-PAMAM/DOXO electrospun mats, red (c) and transmission + red channel (d). Scale bars in all figures represent 50µm.*

To test the drug release from the various mats, an indirect cell viability study was performed on different cancer cell lines (A431 adenocarcinoma, HeLa-WT cervical cancer and MCF-7 breast cancer cells). The cytotoxicity effects of the DOXO was tested by using two sensitive resazurin based-viability assay kits (PrestoBlue® and AlamarBlue®), that assess the mitochondrial activity of cells exposed to the scaffolds at different time points post-incubation (1, 3, 5, 7 and 9 days). To demonstrate that the toxicity was caused by the release of DOXO and not by the materials constituting the electrospun mat itself, the pristine PCL and PCL/PAMAM-PCL fibers were tested in parallel with the corresponding DOXO-loaded fibers (PCL/DOXO and PCL/PCL-PAMAM/DOXO). From Figure 4.6, PCL and PCL/PAMAM-PCL showed good biocompatibility with all the cancer cells lines studied, up to 9 days of incubation. The HeLa-WT cells showed abrupt reduction in viability from day 1 to 9 when treated with PCL/DOXO fibers whereas the same cell-line treated with PCL/PAMAM-PCL/DOXO showed a subtler profile in the reduction of viability over days (Figure 4.6(b) and 4.6(c)). Controls were untreated cells grown in cell media and kept under the same culture conditions. In case of A431 cancer cells, also a similar trend was observed (Figure 4.7). The prolonged and slow release of the new fibers could be due to the fact that the amphiphilic nature of the PAMAM-PCL, contained in the mats, increases the interactions and good mixing of the hydrophilic drug that in turn, was released in a more controlled manner over days, with respect to the most hydrophobic PCL mats. Indeed, the latter released DOXO at a much higher rate causing such sudden decrease in viability. We also tested the scaffolds on DOXO resistant MCF-7 cell line and when compared to the other two cell lines studied, the MCF-7 cells showed much more resistance to toxicity caused by the release of DOXO, but a gradual reduction in viability was also observed following the same comparative trends as for the other two cell lines (Figure 4.6(d) and 4.6(e)). Overall the cytotoxicity study suggests that the PCL/PCL-PAMAM scaffolds enable a slower release of the drug with respect to the PCL mats thus allowing a prolonged drug treatment. When considering the drug release profile with other hydrid-based fibers prepared by electro-spun techniques, we could assess that in our study we had a look at longer period of drug release (up 9 days) than the case of polyethylene oxide/chitosan/graphene oxide fibers (up to 48 hours)[17] and to the polymeric-based fibers (72 h)[18]. The drug release profile of our

hybrid system was more in line with that of multiwall carbon nanotubes/poly(lactic-co-glycolic acid) polymer fibers in which several days of release have been considered (up to 42 days)[19] This prolonged release feature makes the system appealing as implantable post-surgical drug delivery scaffold.

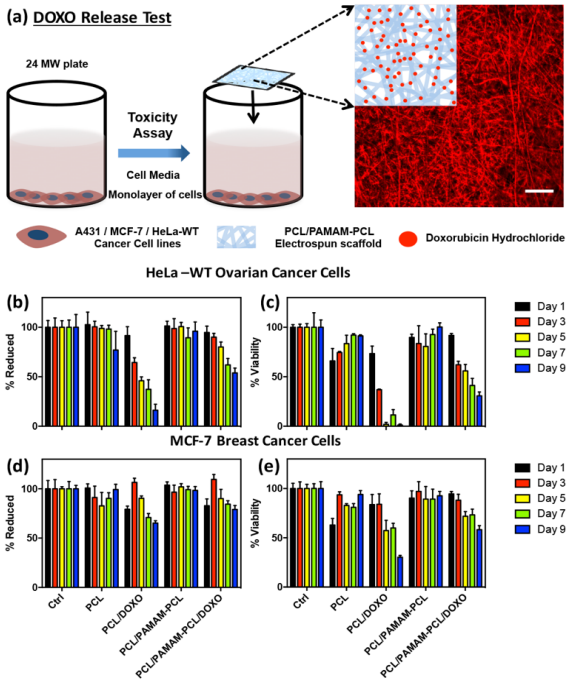

Figure 4.6. *Scheme representing the drug release assay when using the mats as drug scaffolds and typical confocal imaging of a red fluorescent DOXO loaded PCL/PAMAM-PCL fibers ((a) - scale bar corresponds to 50μm). AlamarBlue® Viability assay on HeLa-WT (b) and MCF-7 (d) tumor cells treated with pristine and DOXO-loaded PCL or PCL/PCL-PAMAM mats. PrestoBlue® Viability assay on HeLa-WT (c) and MCF-7 (e) tumor cells treated with pristine and DOXO-loaded PCL or PCL/PCL-PAMAM mats.*

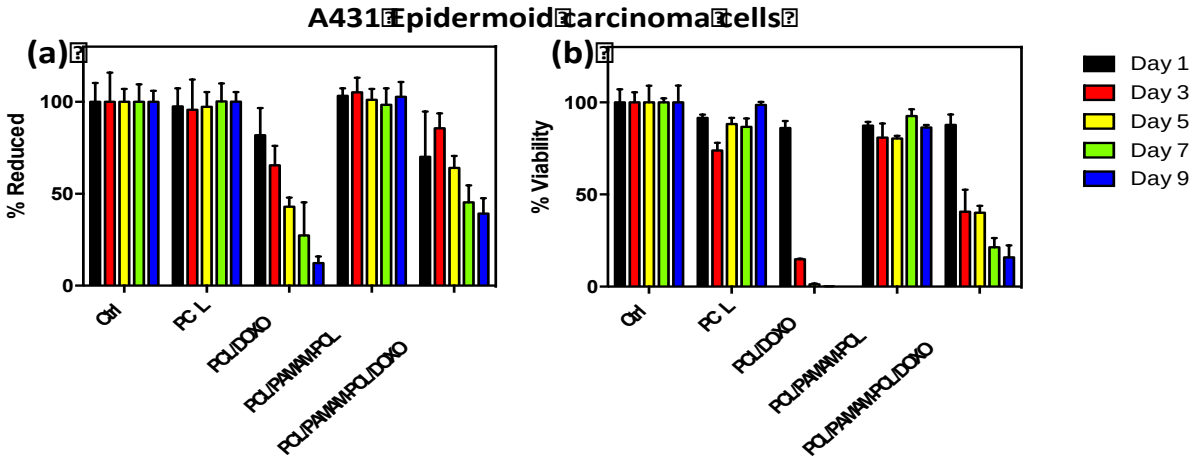

Figure 4.7. *AlamarBlue® Viability assay (a) and PrestoBlue® Viability assay (b) on A431 epidermoid carcinoma cells treated with pristine and DOXO-loaded PCL or PCL/PCL-PAMAM mats, showing similar trend as that of the other cell lines studied. The PCL/PAMAM-PCL scaffold loaded with DOXO showed a gradual cancer cell kill when compared to the abrupt toxicity behavior shown by PCL/DOXO.*

The drug-free PCL/PCL-PAMAM scaffolds did not show any toxicity towards all the tumor cell lines. This prompted us to investigate the biocompatibility of the mats with healthy cells in the view to apply such mats as tissue scaffolds. To this aim adult human dermal fibroblasts (HDFa) were grown directly on PCL/PAMAM-PCL scaffolds. Confocal imaging characterization was done to study the attachment and growth of these cells (Figure 4.8 and Figure 4.9). It was evident that HDFa cells attached firmly already after day 1 of incubation, being characterized by the multiple finger-like projection (F-actin stained in green by Alexa Fluor® 488 phalloidin, Figure 4.8(b)). By day 3 these cells were proliferating rapidly and by day 5, they spread well and formed their typical bipolar shape. An interesting note is that, these cells were able to penetrate deep into the scaffold, as shown in zeta-stack analysis of the fibers (Figure 4.10).

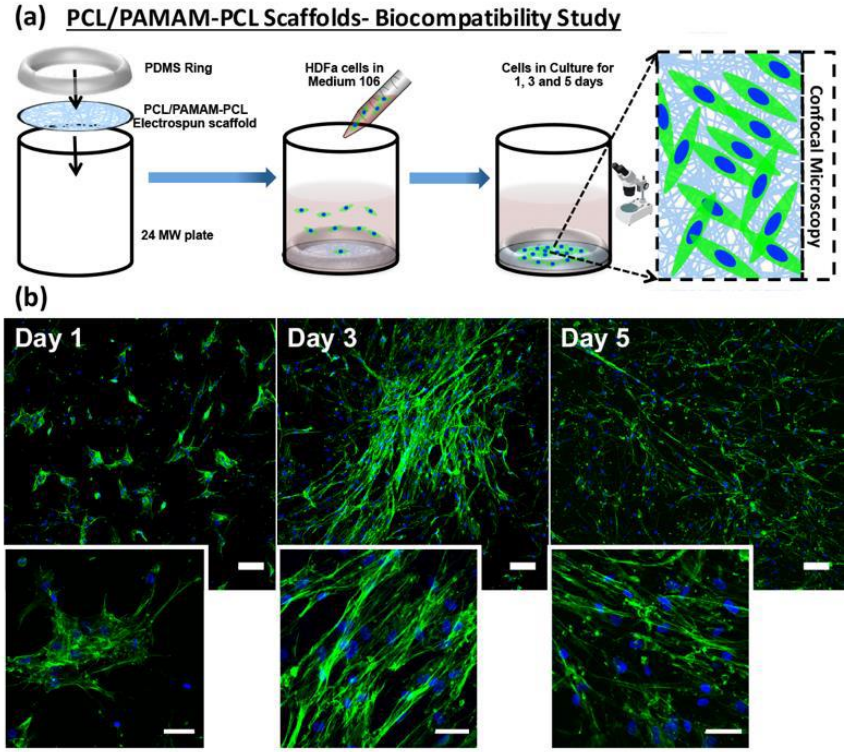

Figure 4.8. *Scheme representing the culturing of healthy dermal fibroblast (HDFa) cells on PCL/PAMAM-PCL scaffold (a). Confocal images showing the attachment and growth of HDFa cells on PCL/PAMAM-PCL scaffold between 1 and 5 days (b). Scale bar represents 100μm (50μm in the inserts). F-Actin stained using Alexa Fluor® 488 Phalloidin (green) and nuclei stained with DAPI (blue).*

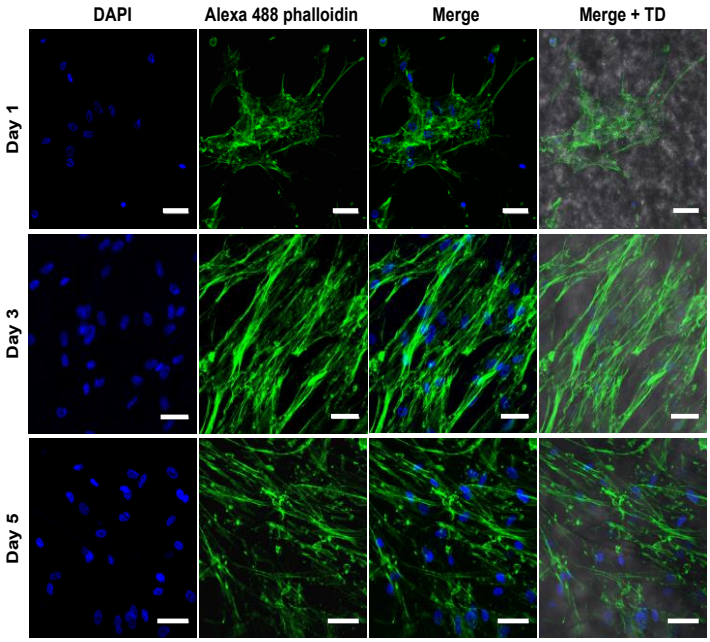

Figure 4.9. *Confocal microscopic image showing the attachment and proliferation of adult human dermal fibroblasts (HDFa) on PCL/PAMAM-PCL scaffolds on day 1, 3 and 5 post cell seeding. Panel 1: DAPI nuclear stain (blue), Panel 2: Alexa Fluor 488 Phalloidin for F-actin filaments (green), Panel 3: Merge of DAPI and Phalloidin, Panel 4: Merge of panel 3 and transmission image showing the PCL/PAMAM-PCL scaffold. Scale bar represents 50µm.*

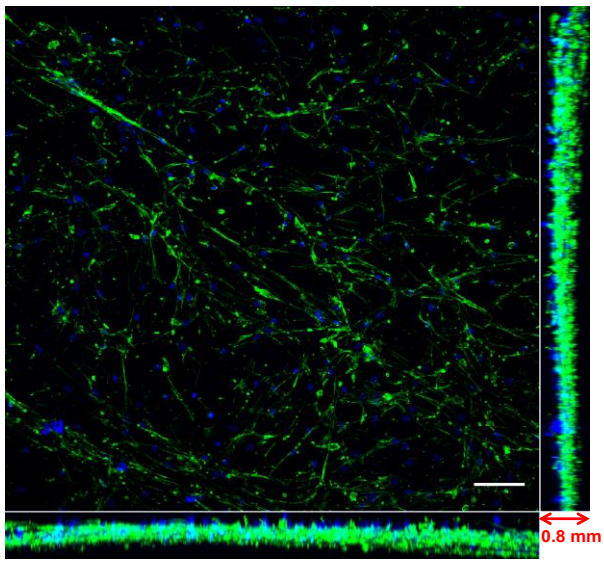

Figure 4.10. *Maximum intensity projection image achieved from Z-stalking using confocal microscopy techniques showing the growth of HDFa cells in different planes of the scaffold, which suggest the penetration of these cells throughout the PCL/PAMAM-PCL scaffold.*

Preparation, characterization and properties of PLLA and PLLA/HBPG-PDLA fibers

FE-SEM micrograph of the PLLA (Figure 4.11(a)) mat, prepared by applying the conditions already reported, evidenced the formation of defect-free fibers characterized by an average dimension of ca. 700 nm. Moreover, the thermal treatment (4 hours at 80 °C), accomplished to allow the polymer structuration, was found not to alter significantly the morphology (Figure 4.11(b)).

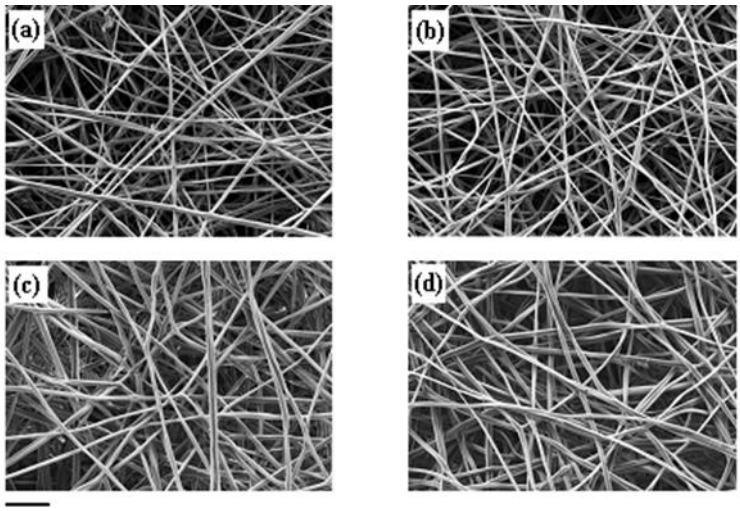

Figure 4.11. *FE-SEM micrographs of: (a) PLLA, (b) PLLA after annealing, (c) PLLA/HBPG-PLLA and (d) PLLA/HBPG-PDLA after annealing fibers. Scale bar represents 2 µm.*

FE-SEM micrographs of the fibers based on HBPG-PDLA, with and without thermal treatment, are shown in Figure 4.11(c) and 4.11(d). The morphology and the dimensions of the above fibers turn out to be similar to those of the PLLA mats. Moreover, they do not present micrometer aggregates, thus it demonstrating the fine dispersion of the polymer additive. It is worth underling that in the case of the system containing the dendritic polymer, in order to obtain defect-free fibers, the polymer concentration was modified. Indeed, as widely reported, hyperbranched polymers are capable to changing the viscosity of the polymer solution, which parameter can strongly influence the final morphology of the fibers.[20]

The thermal properties of the prepared fibers were studied by means of DSC and the results, shown in Figure 4.12, are summarized in Table 4.2. The thermogram of the neat PLLA fibers shows an enthalpic relaxation peak, followed by a cold crystallization exotherm around 80°C and an endotherm of fusion at about 180 °C.

The crystallinity data, reported in Table 4.2, demonstrate that the extent of crystallinity in the electrospun PLLA fibers before annealing is lower than that of the mat which underwent a thermal treatment. The above results indicate that the fast evaporation of the solvent during the electrospinning process hampers the macromolecules crystallization. Conversely, in the thermogram of the PLLA fibers, subjected to the annealing treatment, no cold crystallization events can be detected on heating and as reported in Table 4.2, the maximum crystallinity is ca. 54 %.

The thermograms of the mats containing the dendritic additive are similar to those of the neat PLLA fibers. Moreover, the crystallinity of PLLA, calculated considering its content in the composite fibers, results to be the same as that found in the case of the neat PLLA fibers. On the basis of these findings, it is possible to infer that the presence of the dendritic molecules does not limit the structuring of the polymer matrix. Moreover, in both the above thermograms, it is possible

to notice the presence of a very small and broad signal at around 190 °C, which can be ascribed to a limited amount of stereocomplex crystals, whose formation may occur thanks to the arrangement of the PLLA chains of the polymer matrix with the PDLA-type arms of the dendritic additive.[21]

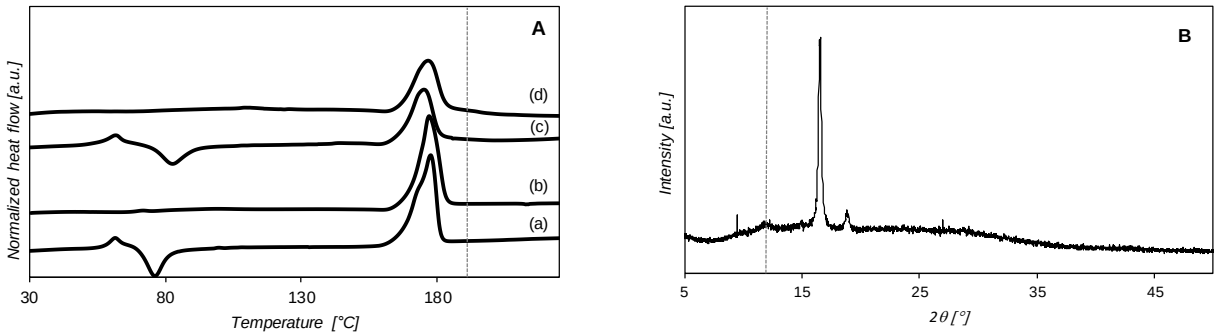

Figure 4.12. *(a) DSC of the neat PLLA and of PLLA/HBPG-PDLA fibers and (b) WAXD profile of the PLLA/HBPG-PDLA annealed fibers.*

Table 4.2. *Thermal properties of the neat and annealed PLLA and PLLA/HBPG-PDLA fibers.*

Sample	T_{cc} [°C]	ΔH_{cc} [J/g]	T_m [°C]	ΔH_m[a] [J/g]	X_c [%]
PLLA	76	16	177	50	36
PLLA (annealed)	-	-	177	50	54
PLLA/HBPG-PDLA	80	15	175	50	38
PLLA/HBPG-PDLA (annealed)	-	-	177,190	46	50

The subscripts m and cc indicate the values measured during melting and cold-crystallization, respectively. [a] ΔH is the enthalpy, normalized to the PLLA content.

In order to validate the above finding, the crystallinity structure of the HBPG-PDLA-based fibers was studied by means of WAXD measurements (Figure 4.12(b)). The pattern of the annealed mat based on HBPG-PDLA, together with an intense peak at 2θ of 17° and a smaller one at 2θ of 19° belonging to homocrystal PLLA, exhibits a signal at 2θ of 12° characteristic of the stereocomplex crystallites.[21] Indeed, in the light of the above results, it is possible to infer that the stereocomplexation promote PLLA crystallization.

The electrospun mats, which underwent an annealing treatment, were also characterized by mechanical tests and the results are given in Table 4.3 and in Figure 4.13. PLLA mats show a relatively high modulus (30 MPa) associated with a low deformation at break, namely about 20%.

Table 4.3. *Mechanical properties of neat PLLA and PLLA/HB-PDLA fibers which underwent an annealing treatment*

Sample	E [MPa]	ε_{break} [%]
PLLA (annealed)	24±3	24±4
PLLA/HBPG-PDLA (annealed)	44±4	20±5

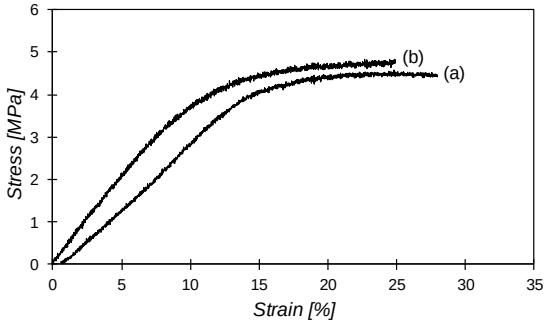

Figure 4.13. *Stress-strain curves of: (a) PLLA (annealed) and (b) PLLA/HBPG-PDLA (annealed) fibers.*

The fibers containing the dendritic additive exhibit a modulus which is even higher than that of the neat mat and a similar deformation at break. This finding can be related to the crystallinity of the polymer matrix, which is not altered by the addition of the dendritic additive and to the stereocomplexation, which is known to increase PLA mechanical properties.[21] It is relevant to underline that these results point out the benefits of having a partial stereocomplex material as most of the organic additives, used as modifier of PLLA, produce a reduction of the polymer crystallization and a decrease of its mechanical properties.

Taking into the account the chemical nature of the synthesized dendritic molecules, HBPG-PDLA, also in the case of the fibers containing the above additive it was analysed the capacity of this material to absorb water. Unlike the neat PLLA fibers, whose tendency to absorb water is negligible, the mats based on HBPG-PDLA show an intrinsic absorbency capacity, up to 30 %. As for the fibers containing PAMAM, this result can be ascribed to the hydrophilicity of the hyperbranched core of the dendritic additive, whose dispersion in the polymer matrix modifies its water absorption capacity.

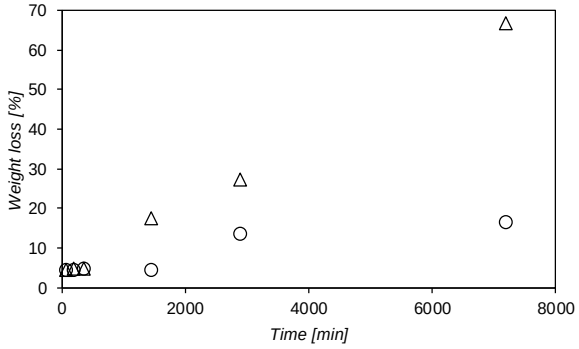

Figure. 4.14. *Weight loss as a function of time during enzymatic degradation tests: ○ neat PLLA fibers, Δ PLLA/HBPG-PDLA.*

In order to verify the influence of the synthesized additive on the polymer matrix degradation properties, enzymatic degradation tests were carried out on both the neat PLLA fibers and on those containing HBPG-PDLA by using proteinase K as enzyme. Figure 4.14 shows the weight loss of the analyzed samples as a function of time during these tests. The curves indicate that at low contact time (t_c) the weight loss is similar for both the samples, while increasing t_c the degradation of the sample containing the dendritic additive results to be faster. This finding is supported by FE-SEM analysis of the samples which were put in contact with proteinase K for ca. 8000 min. Indeed, while the surface of the neat PLLA fibers (Figure 4.15(a)) have a perfectly smooth surface, those based on

HBPG-PDLA (Figure 4.15(b)) are characterized by a considerable rough surface, which phenomenon can be related to a more pronounced degradation in the latter sample. Moreover, as shown in the histograms of the diameter distribution (calculated based on the SEM micrographs of the PLLA and PLLA/HBPG-PDLA mats that underwent the degradation test) the average dimension of the fibers based on the dendritic additive was lower than that of the PLLA fibers. Indeed, in the case of the latter sample the calculated average diameter was ca. 500 nm, while for the PLLA/HBPG-PDLA fibers it was ca. 300 nm, this result supporting the trend of the weight loss.

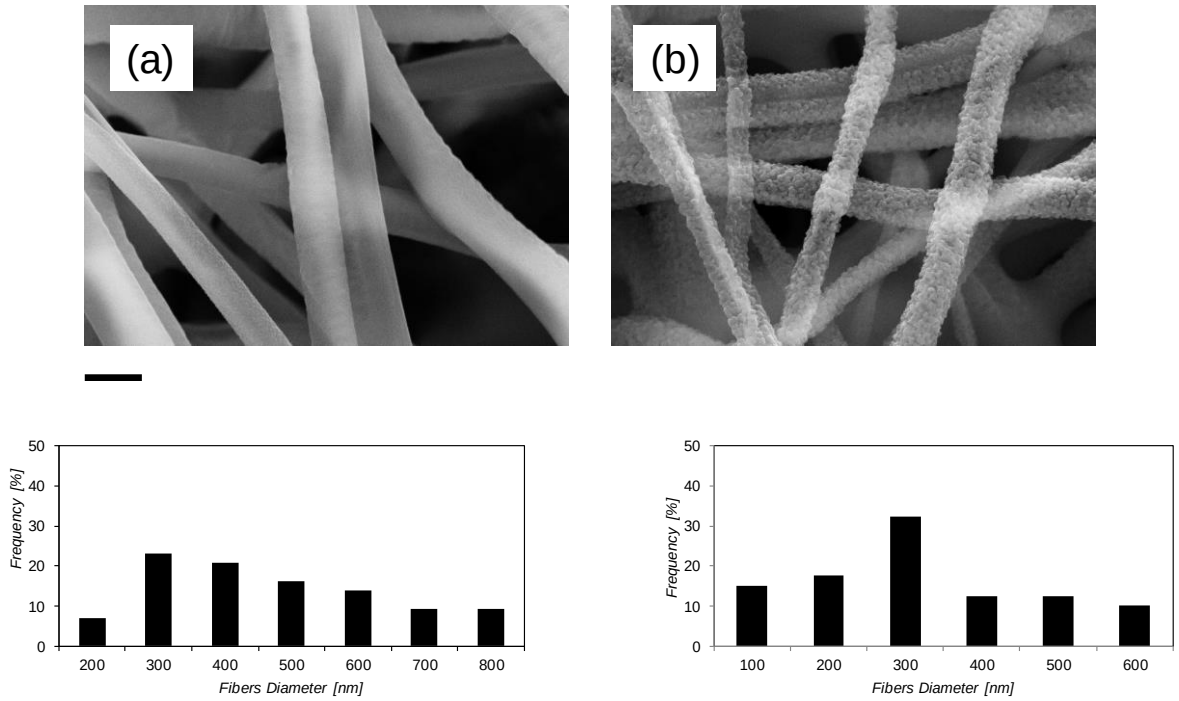

Figure 4.15. *FE-SEM micrographs of: (a) neat PLLA fibers which underwent an enzymatic degradation test (tc = 120 h) and the relative diameter distribution, (b) PLLA/HBPG-PDLA fibers which underwent an enzymatic degradation test (tc = 120 h) and the relative diameter distribution. Scale bar represents 300nm.*

This behaviour can be explained by considering the higher hydrophilicity of the composite fibers, as demonstrating by the water absorption analysis. Indeed, the relation between the hydrophilicity and the enzymatic degradation rate was already demonstrated in the literature. As an example, Tsuji et al. verified that the surface hydrophilicity is crucial to determine the enzymatic hydrolyzability, as the enzymatic hydrolysis rates of PLLA films was found to increase by enhancing the surface hydrophilicity, through an alkaline treatment, irrespective of the crystallinity.[22]

4.4 References

1. Yoo HS, Kim TG, Park TG. Surface-functionalized electrospun nanofibers for tissue engineering and drug delivery. *Adv Drug Deliv Rev*. 2009;61(12):1033-1042. doi:10.1016/j.addr.2009.07.007.
2. Zong S, Wang X, Yang Y, et al. The use of cisplatin-loaded mucoadhesive nanofibers for local chemotherapy of cervical cancers in mice. *Eur J Pharm Biopharm*. 2015;93:127-135. doi:10.1016/j.ejpb.2015.03.029.
3. Xie J, Ruo ST, Wang CH. Biodegradable microparticles and fiber fabrics for sustained delivery

of cisplatin to treat C6 glioma in vitro. *J Biomed Mater Res - Part A*. 2008;85(4):897-908. doi:10.1002/jbm.a.31499.
4. Xu X, Chen X, Xu X, et al. BCNU-loaded PEG-PLLA ultrafine fibers and their in vitro antitumor activity against Glioma C6 cells. *J Control Release*. 2006;114(3):307-316. doi:10.1016/j.jconrel.2006.05.031.
5. Ma G, Liu Y, Peng C, Fang D, He B, Nie J. Paclitaxel loaded electrospun porous nanofibers as mat potential application for chemotherapy against prostate cancer. *Carbohydr Polym*. 2011;86(2):505-512. doi:10.1016/j.carbpol.2011.04.082.
6. Qiu K, He C, Feng W, et al. Doxorubicin-loaded electrospun poly(l-lactic acid)/mesoporous silica nanoparticles composite nanofibers for potential postsurgical cancer treatment. *J Mater Chem B*. 2013;1(36):4601. doi:10.1039/c3tb20636j.
7. Zheng F, Wang S, Shen M, Zhu M, Shi X. Antitumor efficacy of doxorubicin-loaded electrospun nano-hydroxyapatite–poly(lactic-co-glycolic acid) composite nanofibers. *Polym Chem*. 2013;4(4):933-941. doi:10.1039/C2PY20779F.
8. Chen M, Feng W, Lin S, He C, Gao Y, Wang H. Antitumor efficacy of a PLGA composite nanofiber embedded with doxorubicin@MSNs and hydroxycamptothecin@HANPs. *Rsc Adv*. 2014;4(95):53344-53351. doi:10.1039/c4ra09122a.
9. Madhavan Nampoothiri K, Nair NR, John RP. An overview of the recent developments in polylactide (PLA) research. *Bioresour Technol*. 2010;101(22):8493-8501. doi:10.1016/j.biortech.2010.05.092.
10. Signori F, Coltelli MB, Bronco S. Thermal degradation of poly(lactic acid) (PLA) and poly(butylene adipate-co-terephthalate) (PBAT) and their blends upon melt processing. *Polym Degrad Stab*. 2009;94(1):74-82. doi:10.1016/j.polymdegradstab.2008.10.004.
11. Müller R-J. Biodegradability of Polymers: Regulations and Methods for Testing. In: Steinbüchel A, ed. *Biopolymers Online*. Weinheim, Germany: Wiley-VCH Verlag GmbH & Co. KGaA; 2005:366–388. doi:10.1002/3527600035.bpola012.
12. Raquez JM, Habibi Y, Murariu M, Dubois P. Polylactide (PLA)-based nanocomposites. *Prog Polym Sci*. 2013;38(10-11):1504-1542. doi:10.1016/j.progpolymsci.2013.05.014.
13. Inoue K. Functional dendrimers, hyperbranched and star polymers. *Prog Polym Sci*. 2000;25(4):453-571. doi:10.1016/S0079-6700(00)00011-3.
14. de Jong SJ, van Dijk-Wolthuis WNE, Kettenes-van den Bosch JJ, Schuyl PJW, Hennink WE. Monodisperse Enantiomeric Lactic Acid Oligomers: Preparation, Characterization, and Stereocomplex Formation. *Macromolecules*. 1998;31(19):6397-6402. doi:10.1021/ma980553i.
15. Gottschalk C, Wolf F, Frey H. Multi-arm star poly(L-lactide) with hyperbranched polyglycerol core. *Macromol Chem Phys*. 2007;208(15):1657-1665. doi:10.1002/macp.200700168.
16. Adeli M, Namazi H, Du F, et al. Synthesis of multiarm star copolymers based on polyglycerol cores with polylactide arms and their application as nanocarriers. *RSC Adv*. 2015;5:14958-14966. doi:10.1039/C4RA14619K.
17. Ardeshirzadeh B, Anaraki NA, Irani M, Rad LR, Shamshiri S. Controlled release of doxorubicin from electrospun PEO/chitosan/graphene oxide nanocomposite nanofibrous scaffolds. *Mater Sci Eng C*. 2015;48:384-390. doi:10.1016/j.msec.2014.12.039.
18. Salehi R, Irani M, Rashidi MR, et al. Stimuli-responsive nanofibers prepared from poly(N-isopropylacrylamide- acrylamide-vinylpyrrolidone) by electrospinning as an anticancer drug delivery. *Des Monomers Polym*. 2013;16(6):515-527. doi:10.1080/15685551.2013.771303.
19. Qi R ling, Tian X jiao, Guo R, et al. Controlled release of doxorubicin from electrospun MWCNTs/PLGA hybrid nanofibers. *Chinese J Polym Sci (English Ed*. 2016;34(9):1047-1059. doi:10.1007/s10118-016-1827-z.
20. Gao C, Yan D. Hyperbranched polymers: From synthesis to applications. *Prog Polym Sci*.

2004;29(3):183-275. doi:10.1016/j.progpolymsci.2003.12.002.
21. Tsuji H. Poly(lactide) stereocomplexes: Formation, structure, properties, degradation, and applications. *Macromol Biosci*. 2005;5(7):569-597. doi:10.1002/mabi.200500062.
22. Tsuji H, Ishida T, Fukuda N. Surface hydrophilicity and enzymatic hydrolyzability of biodegradable polyesters: 1. Effects of alkaline treatment. *Polym Int*. 2003;52(5):843-852. doi:10.1002/pi.1199.

CHAPTER 5. On a new bio-based system composed of electrospun sc-PLA/POSS/cyclodextrin fibers to remove water pollutants

This chapter deals with the development of novel bio-based system, characterized by specific features suitable for the removal of water pollutants. Indeed, the system consists of electrospun stereocomplex polylactide (sc-PLA)-based fibers, prepared from solutions containing equimolar amounts of high-molecular-weight poly(L-lactide) (PLLA) and poly(D-lactide) (PDLA), functionalized by the presence of an amino polyhedral oligomeric silsesquioxanes (POSS-NH_2), which was added directly into the electrospinning solution. The sc-PLA/POSS-NH_2 fibers, characterized by a submicrometric dispersion of the silsesquioxanes underwent a grafting reaction with β-cyclodextrin molecules, activated to nucleophilic substitution *via* monotosylation (CD-O-Ts). The surface reaction was investigated by IR and ^{1}H-NMR and obtained β-CD-grafted fibers were characterized in terms of grafting reaction and morphology by IR, XPS, TGA and SEM analysis. Moreover, the surface wettability and absorb capacity of water pollutants were measured.

5.1 Introduction

As previously mentioned, nanofibers mainly fabricated by electrospinning, have a great potential, but so far largely unrealized, for many emerging environmental applications.[1] One of the most important features of the above engineered nanomaterials, is the large surface area-to-volume ratio, which potentially could allow greater surface absorption of contaminants from air and water.[1] Moreover, unlike inorganic nanofibers - those based on ZnO[2,3] and TiO_2[4–6] being the most extensively applied for water or air treatment - polymer nanofibers are flexible. Since the above characteristic is highly appealing for the practical exploitation of these systems, the inorganic phase is generally combined with polymer nanofibers in order to take advantage simultaneously of both the organic and inorganic materials, the latter having in general a catalytic effect on the pollutant molecules. Indeed, in the field of water remediation, TiO_2 nanoparticles, immobilized using layer by layer electrostatic assembly onto porous dimethylsiloxane-block-etherimide (PSEI) nanofibers exhibited a high degree of bisphenol A decomposition.[7] Nanofibrous mat of poly (L-lactic acid) was used as substrate for the growth of radially oriented ZnO nanowires by chemical bath deposition and the PLLA/ZnO systems were applied for decomposition of several organic contaminants.[8] ZnO, in the form of nanocrystals were also grown on cellulose acetate butyrate (CAB) nanofibers and the photocatalytic activity of the CAB-ZnO system was proved.[9] Another method applied to obtain ZnO-based systems was the atomic layer deposition, used by Kayaci et al.[10] to prepare ZnO/nylon 6,6 nanofibes, which allowed to obtain a layer of the oxide of about 90 nm.

Despite the potentialities of the above systems, their application is limited because of some specific drawbacks, such as the tricky inorganic phase dispersion/deposition, the accessibility of the catalytic sites, the possible inorganic phase leaching and the need to activate the process by UV radiation.

Another potential and effective approach for the removal of pollutants, in view of the high surface area of the electrospun nanofibers, is that based on the adsorption of contaminants. In general, this method consists in the dispersion of particular adsorbing systems, both inorganic[11–13] and organic[14,15] species in the polymer nanofibers. As for the former described organic/inorganic nanofibers, also in this case the possible leaching of the absorption molecules and the incomplete accessibility of the absorption sites are limiting factors for the application of the process. In this

light, the development of nanofibers based on polymer systems enabling surface grafting of active species that is molecules with a high tendency to interact with/absorb contaminants, represents a significant current research issue.

Among the molecules applicable as absorber of contaminants, cyclodextrins (CD) - natural cyclic oligosaccharides derived from starch[16,17]- show suitable features as they are characterized by a significant capacity of forming inclusion complexes with several molecules through non-covalent host-guest interactions, thanks to their peculiar toriodal-shape.[18,19] So far, in the field of water treatment, they have been mainly applied in powder form or crossliked granules,[18–20] while in the case of CD/nanofibers systems, they were physically blended with the polymer matrices.[21,22]

It is worth underlining that the few attempts performed in the literature to graft CD on the surface of polymer nanofibers[14,23] implied the laborious and not always feasible chemical modification of the nanofiber surface, as the polymer matrices, generally used to prepare the nanofiber mats, do not hold reactive functionalities.

Our system, which is alternative to the conventional materials applied for environmental applications and possesses properties potentially exploitable in the field of water treatment, takes advantage of the capability of cyclodextrin molecules, covalently linked to the surface of nanofibers based on stereocomplex polylactide (sc-PLA) and polyhedral oligomeric silsesquioxanes (POSS), to absorb/complexate organic molecules. It is worth underlining that sc-PLA nanofibers combine the properties of the peculiar polymer matrix with those of POSS molecules. Indeed, as reported in the introduction, stereocomplex PLA, formed by mixing poly(L-lactide) (PLLA) and poly(D-lactide) (PDLA), has a melting temperature 50 °C higher than that of PLLA and PDLA homo-crystals, a higher stability and crystallization rate as well as lower solubility in solvents and resistance to hydrolysis enhanced compared with the two single polymers.[24–26] Moreover, it was recently reported on a method to improve the performances of the above nanofibers by introducing functionalized POSS - in our case POSS bearing an amino group attached to the siliceous cage ($POSS\text{-}NH_2$)[27] - into the electrospinning solution.[28] Indeed, the electrospinning process turned out to allow a nanometric dispersion of the silsesquioxane[29–32] and, consequently, in the case of the exploitation of functionalized POSS, an homogenous distribution on the polymer nanofiber surface of the reactive groups, which were found to be accessible but simultaneously strongly linked to the polymer matrix.[28]

The developed system shows peculiar and functional properties connected to both the chemical and structural features of the components, that is: i) the bio-based and bio-degradable polymer matrix, ii) the stereocomplexation of PLA, which gives the polymer support higher thermal/chemical resistance with respect to the tradition used PLLA or PDLA single polymers, iii) the high surface area-to-volume ratio, characteristic of the nanofibers and iv) the high accessibility of the cyclodextrin molecules, which should not undergo any leaching process, they being covalently linked to the nanofiber surface. Indeed, in this work, the novel system consisted of electrospun sc-PLA-based fibers, prepared from solutions containing equimolar amounts of high-molecular-weight poly(L-lactide) (PLLA) and poly(D-lactide) (PDLA), functionalized by the dispersion of $POSS\text{-}NH_2$ which underwent a grafting reaction with *ad hoc* functionalized CD. The reaction between the CD and $POSS\text{-}NH_2$ as well as the characteristics of the sc-PLA/POSS-NH-CD fibers, were studied in detail. The capacity of the novel hybrid molecule POSS-NH-CD and that of the prepared fibers to absorb water pollutants was evaluated.

5.2 Experimental section

Nanofiber preparation

As previously reported,[28] PLLA/PDLA-based POSS solutions were prepared by using a mixture HFIP/$CHCl_3$ (1/2), equal amounts of PLLA and PDLA to a final polymer concentration of 12 w/v and 5 wt.-% of POSS-NH_2. The nanofibers were electrospun using a conventional electrospinning system. The solutions were loaded in a syringe (model Z314544, diameter d=11.6 mm, Aldrich Fortuna Optima) placed in the horizontal direction. A Gamma high-voltage research power supply (Model ES30P-5W) was used to charge the solution in the syringe with a positive DC voltage. The positive electrode was connected to the needle (diameter d=0.45mm) of the syringe and the negative electrode was attached to the grounded collector, an aluminium sheet wrapped on a glass cylinder (height 4 cm, diameter 14.5 cm). The distance between the tip and the collector was 20 cm. A syringe pump (Harvard Apparatus Model 44 Programmable Syringe Pump) was used to feed the needle. The needle tip and the ground electrode were contained in a hollow plastic cylinder (height 30.5 cm, inner diameter 24 cm, and thickness 3.5 mm), internally coated with a polytetrafluoroethylene sheet (thickness 1 mm), which was supplied with a XS Instruments digital thermohygrometer (model UR100, accuracy ±3% RH and ±0.8 °C) as humidity and temperature sensor to monitor and control the ambient parameters (temperature around 21 °C). A glass Brooks rotameter was used to keep constant the air flow in the enclosed electrospinning space. The air flow was fed in the chamber at atmospheric pressure from an inlet placed behind the collector.

The established conditions are: solution flow rate 0.004 mL/min, tip-collector distance 20 cm, air flow rate 3.5 l/min and temperature 21 °C. The fibers were subjected to an annealing treatment at 100°C for 4 hours.

Synthesis of mono-6-deoxy-(p-tolylsulfonyl)-β-cyclodextrin (CD-O-Ts)

Mono-6-deoxy-(p-tolylsulfonyl)-β-cyclodextrin (CD-O-Ts) was prepared following the procedure reported elsewhere.[33,34] The typical procedure was carried out as follows: 2 g of CD were suspended in 17 mL of water and 0.2 g of NaOH in 0.7 mL of water were added dropwise. The solution was immersed into an ice-water bath and 0.5 g of TsCl in 1 mL of acetonitrile were dripped slowly with the formation of a white precipitate. After further stirring for 2 h at room temperature, the suspension was refrigerated at 4 °C. The precipitate was recovered by filtration and recrystallized from hot water three times. The product was dried under vacuum at 50 °C.

Synthesis of POSS-NH-CD

0.1 g of POSS-NH_2 was dispersed in 10 mL of methanol and 0.1 g of CD-O-Ts dissolved in 10 mL of methanol was added dropwise. The reaction was conducted for 24 hours under stirring at 60 °C. Then, the product was recovered by centrifugation and washed several times with hot methanol. The product was dried under vacuum at 50 °C.

Preparation of sc-PLA/POSS-NH-CD nanofibers

2.9 mg of sc-PLA/POSS-NH_2 nanofibers were immersed in 10 mL of methanol and 2.9 mg of CD-O-Ts dissolved in 10 mL of methanol was added dropwise. The reaction was conducted for 24 hours at 60 °C. Finally, the fibers were recovered, washed several times with hot methanol and dried under vacuum at 50 °C.

Characterization

To study the sample surface morphology, a Leica Stereoscan 440 scanning electron microscope was used. All the samples were thinly sputter-coated with carbon using a Polaron E5100 sputter coater. The fiber diameters and their distribution were measured using an image analyzer, with ImageJ 1.41 software.

TGA measurements were performed using a Star^e System Mettler thermobalance, under nitrogen flow, at a heating rate of 10°C/min.

XPS characterization was performed with a Kratos Axis Ultra spectrometer using a monochromatic Al Kα source (10mA, 15kV). High resolution analyses were carried out with pass energy of 40 eV. Binding energy scale has been charge corrected to have the well resolved C 1s peak of carboxylic groups (C=OO) of sc-PLA at 289 eV.

FTIR spectra were recorded on a Bruker IFS66 spectrometer in the range 400-4000 cm^{-1}.

^1H NMR spectra were collected with a Varian NMR Mercury Plus instrument at a frequency of 300 MHz in $CDCl_3$ solutions containing tetramethylsilane as internal standard.

Contact angle measurements were performed at room temperature with an Erma G-1 contact angle meter using pure distilled water as probe liquid. The average static water contact angles were obtained by measuring at least three droplets on each film specimen (two films for sample).

To perform absorption experiments, stock solutions (10 mg/L) of alizarin red and 2-chlorophenol in ultra-pure water were prepared. The experiments were carried out by adding ca. 0.020 g of POSS-based powder (POSS-NH_2 or POSS-NH-CD) and 0.001 g of fibers (sc-PLA/POSS-NH_2 fibers or sc-PLA/POSS-NH-CD) in contact with 10 mL of the above solution at room temperature for a predetermined time interval. After a specific time, the adsorbent systems were separated from the solutions and the residual concentration were determined by a by UV-vis spectrophotometer (Varian Cary 100 spectrometer). The equilibrium sorption capacity, namely the sorption value constant with time, was determined using equation (1):

$$q_e = \frac{(C_0 - C_e)}{m} V \qquad (5.1)$$

Where q_e is the equilibrium amount of absorbed material per unit mass of adsorbent (mg/g), C_0 and C_e are the initial and equilibrium absorbate concentration, respectively, in mg/L, V is the sample volume and m is the adsorbent mass in mg. The absorption was also calculated as mole of absorbate per unit mass of absorbent. In the case of alizarin red, the absorbance intensity was calculated using the reading at 521 nm (molar absorption coefficient = 2328 $L \cdot mol^{-1} \cdot cm^{-1}$), while in the case of 2-chlorophenol at 272 nm (molar absorption coefficient = 1920 $L \cdot mol^{-1} \cdot cm^{-1}$).

5.3 Results and discussion

The work has been preliminary focused on the activation of the cyclodextrin by the reaction with p-toluenesulfonyl chloride (p-TsCl). The FTIR results for the β-CD and mono-6-deoxy-(p-tolylsulfonyl)-β-cyclodextrin (CD-O-Ts) are shown in figure 5.1 (c)(d). For the spectrum of β-CD (Figure 5.1(c)), the O-H stretching and bending are observed at 3307 cm^{-1} and 1651 cm^{-1}, respectively. The absorption around 2925 cm^{-1} indicates the presence of $–CH_2$ group, and the band at 1021 cm^{-1} is the characteristic absorption of C-O-C asymmetric stretching. In the spectrum of CD-O-Ts (Figure 5.1(d)), the peaks at 3343 cm^{-1} and 1659 cm^{-1} are attributable to stretching and the bending, respectively, of the O-H groups of β-CD. The peaks at 2927 cm^{-1} and 1029 cm^{-1} are, respectively, ascribed to the $–CH_2$ stretching and the C-O-C asymmetric stretching. In addition, the

characteristic peaks of O=S=O at 1364 cm^{-1} and 1156 cm^{-1} can be also observed. All the significant absorption bands of β-CD and CD-O-Ts indicate that p-TsCl was successfully reacted with β-CD.

This was further confirmed by means of ^{1}H NMR spectroscopy (Figure 5.1(a)(b)), where the characteristic peaks of β-CD (at δ 4.82, 3.25, 2.32, 3.55, 3.60, 3.64, 4.45, and 5.56- 5.80 ppm – assigned to OC*H*O-CH, CH-C*H*OH-CH, CH-C*H*OH-CH, CH-C*H*O-CH, CH-C*H*O-CH_2, CH_2-OH, CH_2-O*H*, CH-O*H* respectively) are accompanied by several signals in the region at δ 2.47 and 7.30-7.80 ppm, ascribable to the presence of the CH_3-CH and CH-CH_2-CH_2 units of tosyl.

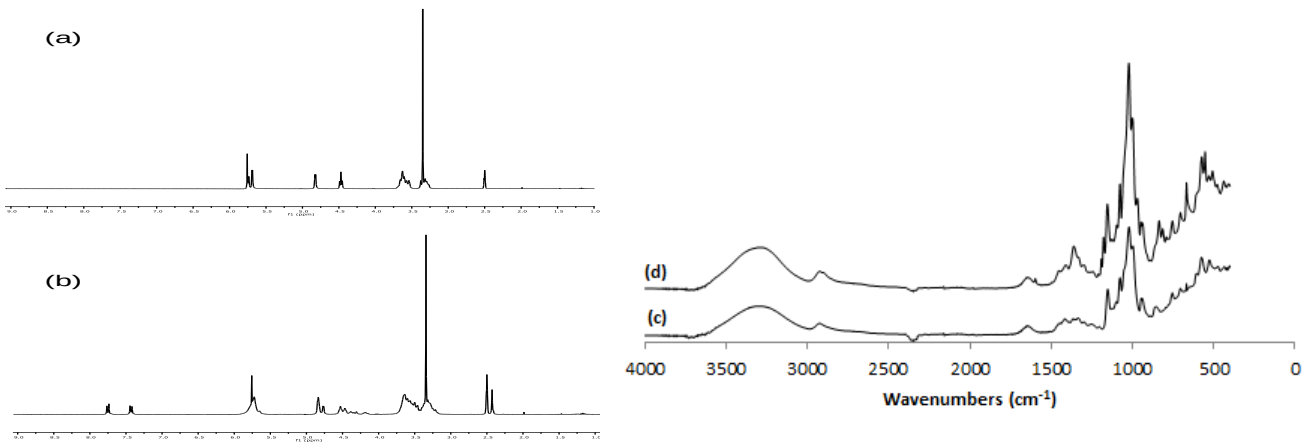

Figure 5.1. *^{1}H-NMR and FTIR spectra of: (a) β-cyclodextrin (CD), (b) mono-6-deoxy-(p-tolylsulfonyl)-β-cyclodextrin (CD-O-Ts) (c) β-cyclodextrin (CD) and (d) mono-6-deoxy-(p-tolylsulfonyl)-β-cyclodextrin (CD-O-Ts).*

In order to verify the specific reactivity of the above molecule towards the -NH_2 group of the amino POSS, the silsesquioxane was reacted with CD-O-Ts. After various attempts, methanol was used as the solvent of choice due to its ability to solubilize only β-cyclodextrin at high temperature -POSS is insoluble-, and 60 °C was found optimal to drive the substitution to completion after 24 hrs. In figure 5.2, the FTIR spectrum of POSS-NH-CD is compared with those of CD-O-Ts and POSS-NH_2.

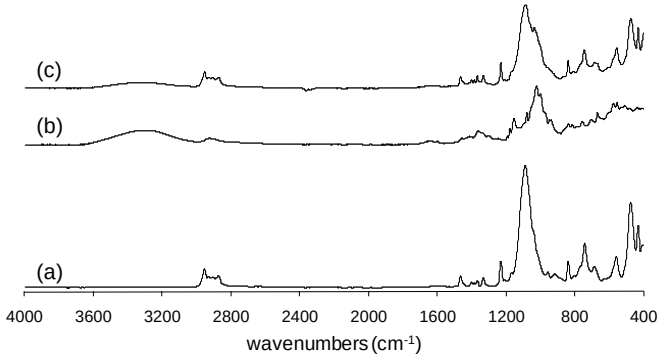

Figure 5.2. *IR spectra of: (a) POSS-NH_2, (b) CD-O-Ts and (c) POSS-NH-CD.*

The neat POSS (Figure 5.2a) shows a strong Si-O-Si stretching absorption band at *ca.* 1100 cm^{-1}, which is the typical absorption peak of the silsesquioxane inorganic framework. CD-O-Ts

holds two characteristic absorption peaks at 3343 and 1659 cm^{-1}, due to stretching and the bending, respectively, of the O-H groups of β-CD, as well as a peak at 2927 attributed to the $-CH_2$ and at 1029 cm^{-1} due to the C-O-C asymmetric stretching. Moreover, the characteristic peaks of O=S=O at 1364 cm^{-1} and 1156 cm^{-1} can be also observed.

In the spectrum of POSS-NH-CD systems, together with the peaks characteristics of the neat silsesquioxane, two new bands at *ca*. 3240 and 1030 cm^{-1} appear, which should originate from the O-H groups and C-O-C bond of β-CD moieties of POSS-NH-CD. Indeed, as the excess of CD-O-Ts was eliminated by washing, the above finding suggests the effective reaction of POSS-NH_2 with CD-O-Ts, which is illustrated in Figure 5.3. Indeed, it is of utmost relevance that the developed reaction allows to produce a new POSS-based molecule, characterized by the direct linkage of the cyclodextrin to the siliceous cage, which combines the features of the silsesquioxane (high thermal and chemical resistance) with those of cyclodextrin that is the capacity to absorb/complexate organic molecules. Clearly, the peculiar properties of the above hybrid molecule could be exploited in different fields, such as that of nanocomposite materials and for biomedical applications.

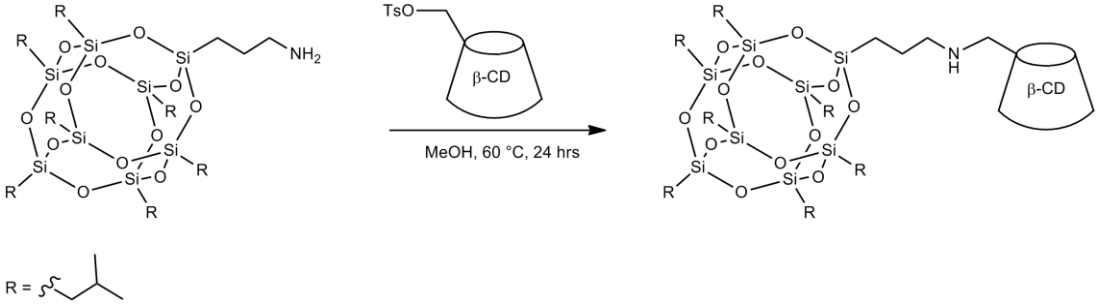

Figure 5.3. *Reaction between POSS-NH_2 and CD-O-Ts.*

To further prove the reaction between the cyclodextrin and POSS-NH_2, XPS experiments were run on both the neat silsesquioxane and CD-NH-POSS, focusing on the chemical environment of N atoms. As we already shown,[28] POSS-NH_2 is characterized by the presence of a single N 1s peak centered at (399.7 ± 0.2) eV, indicative of the presence of $–NH_2$ functionalities. In the case of CD-NH-POSS, the N 1s XP-spectrum is clearly characterized by two N species: one, centered at (399.8 ± 0.2) eV, while the second, centered at (401.6 ± 0.2) eV and accounting for approx. one third of the total N content, suggests the change of N chemical environment, which is likely due to the reaction between the POSS-NH_2 and CD-O-Ts (Figure 5.4).

In order to verify the tendency of the hybrid molecule to absorb organic water contaminants, the powder of POSS-NH-CD was contacted with a water solution of Alizarin red, namely a dye which can be considered a pollutant model molecule. A preliminary observation concerns the change of color of the solution, which passes from pink pale in the neat solution to yellow pale in that containing alizarin red (Figure 5.5). This behaviour can be related to specific interactions occurring between the hybrid molecule and the dye. Indeed, this effect was already reported with other dyes systems, capable of interacting with CD molecules. In particular, it was demonstrated that, as the result of inclusion complexes formation, the guest molecule is surrounded by the hydrophobic microenvironment of the CD cavity.[35–38] This environmental change causes some modification of the chemical and physical properties of the guest molecule, such as equilibria and kinetic parameters and absorption coefficient. As an example, it was found that upon binding of phenolphthalein to β-CD cavity in aqueous solution at pH 10.5, the red-colored dianion form is rapidly transformed into a colorless lactonoid form.[35] This effect and some other similar spectral changes were ascribed to the altered polarity of the cavity microenvironment and preferential or

specific guest–host interactions and stabilization of the preferred form and suppression of the other forms in equilibrium.

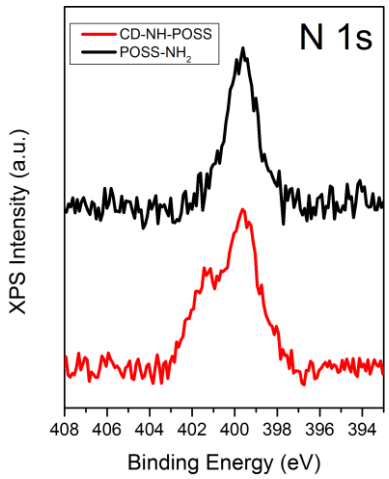

Figure 5.4. *XPS spectra collected on POSS-NH_2 and CD-NH-POSS powders. The data are shown in the energy region typical for N 1s photoelectrons after subtraction of Shirley-type background. Data are shown after normalization.*

Considering our system, besides the modification of the solution color, the extend of alizarin red absorption was evaluated by means of UV measurements (Figure 5.5B). As reported in table 5.1, unlike POSS-NH_2, which showed no tendency to retain the dye, the modification of the silsesquioxane with CD turned out to promote specific interactions between the hybrid molecule and the alizarin red, increasing, in this way, its absorption capacity. Indeed, the quantity of alizarin absorbed by POSS-NH-CD, was found to be constant after 4 hours.

(A) (B)

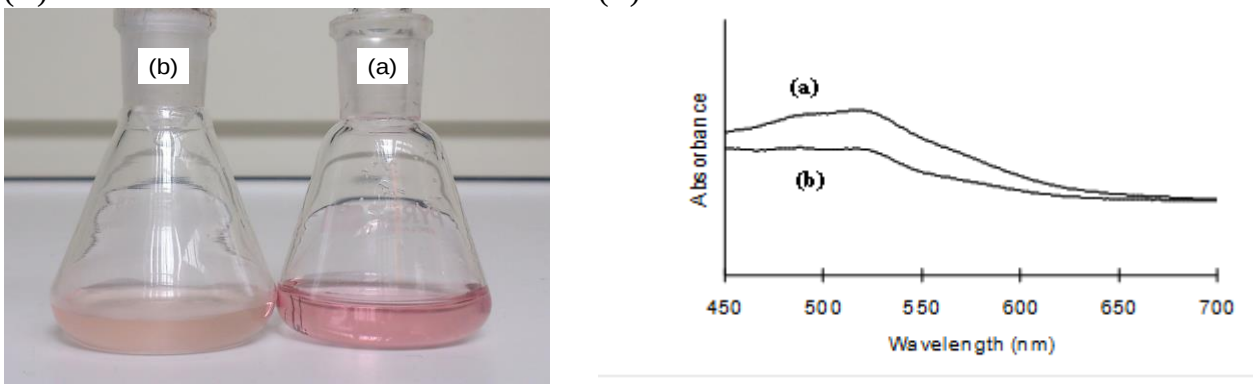

Figure 5.5. *(A) Photos of: (a) alizarin red solution at the initial time and (b) alizarin red solution with POSS-NH-CD after 4 hours. (B) UV spectra of: (a) alizarin red solution at the initial time and (b) alizarin red solution with POSS-NH-CD after 4 hours.*

Table 5.1. *Absorption capacity of the different studied systems*

System	Pollutant	Absorption capacity mol pollutant/g system	Absorption capacity mg pollutant/g system
POSS-NH_2 (powder)	Alizarin red	-	-
POSS-NH-CD (powder)	Alizarin red	$1.15 \cdot 10^{-5}$	2.8
POSS-NH_2 (powder)	2-cholorophenol	-	-
POSS-NH-CD (powder)	2-chlorophenol	$3.27 \cdot 10^{-5}$	4.2
sc-PLA/POSS-NH_2 fibers	Alizarin red	-	-
sc-PLA/POSS-NH-CD fibers	Alizarin red	$4.83 \cdot 10^{-5}$	12
sc-PLA/POSS-NH_2 fibers	2-cholorophenol	-	-
sc-PLA/POSS-NH-CD fibers	2-chlorophenol	$32.5 \cdot 10^{-5}$	42
sc-PLA/POSS-NH_2 fibers	2-chlorophenol	-	-

Besides alizarin red, it was evaluated the capacity of POSS-NH-CD to absorb another typical organic pollutant, that is 2-chlorophenol. By comparing the results reported in Table 5.1, the capacity of the POSS-NH-CD powder to absorb the above molecule, which became constant after 24 hours, turns out to be higher than that found for alizarin red. This finding can be related to the chemical-physical characteristics of the two studied contaminants and in particular to their different steric hindrance, which being higher for alizarin red, might limit its absorption inside the CD cages.

Although these results demonstrate a good capacity of the hybrid POSS-based molecule to absorb water pollutants, which in the case of phenol is of the same order of magnitude as that of other types of absorbent, such as bentonite,[39] coal[40] and wood,[41] clearly the dispersion of the molecule on a support characterized by a high surface area, such as polymer nanofibers, could increase the efficiency of its absorption.

On this basis, it was attempted to graft CD molecules on the surface of electrospun stereocomplex polylactide (sc-PLA)-based fibers, prepared from solutions containing equimolar amount of high-molecular-weight poly(L-lactide) (PLLA) and poly(D-lactide) (PDLA) and functionalized by the dispersion of a POSS-NH_2, added directly into the electrospinning solution. The reaction between sc-PLA/POSS-NH_2 and CD-OTs was carried out under the same conditions previously optimized, the fibers were then recovered, washed several times with hot methanol, dried under vacuum at 50 °C and analyzed.

FE-SEM micrograph of the sc-PLA/POSS-NH_2 (Figure 5.6(a)) mat, prepared by applying the conditions already reported,[28] evidences the formation of defect-free fibers characterized by an average dimension of 1 μm. Moreover, no POSS aggregates are present, the submicrometer dispersion of the silsesquioxane being favored, as already highlighted,[28–32] by the fast solvent evaporation occurring during the electrospinning process. The morphology and the average diameter of the treated fibers (Figure 5.6(b)) are similar to those of the neat sc-PLA/POSS-NH_2 fibers, this finding highlighting that the treatment process does not alter the fibrous structure. Nevertheless, considering the high magnification micrographs, reported in figure 5.6(c) and figure 5.6(d), the surface of the fibers completely changed. Indeed, while the neat fibers have a perfectly smooth surface, those treated are characterized by a considerable rough surface. It is worth underlining that the modification of the polymer surface caused by the introduction of CD was observed with other systems, such as cotton fabric grafted with glycidyl methacrylate-CD[42,43] or monochlorotriazinyl-CD/butylacrylate and hydroxypropyl-CD grafted woven polyethylene terephthalate (PET) vascular prosthesis.[44,45] Moreover, the increase of surface roughness was also

observed in PET fiber grafted with cyclodextrin polymer.[14] Indeed, the rough surface of the treated nanofiìbers can be consider an indication of the CD attachment to the polymer surface.

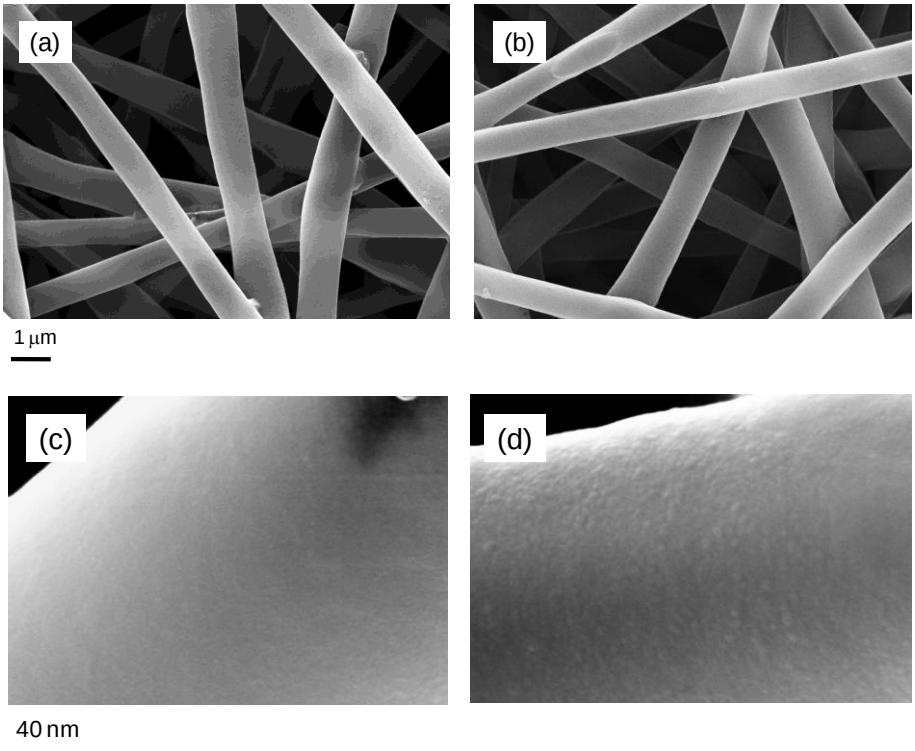

Figure 5.6. *FE-SEM micrographs of: (a) sc-PLA/POSS-NH$_2$ fibers, (b) sc-PLA/POSS-NH-CD fibers, (c) high magnification FE-SEM micrographs of: (c) sc-PLA/POSS-NH$_2$ fibers, (d) sc-PLA/POSS-NH-CD fibers.*

The fiber thermal degradation was studied by means of TGA analysis, by comparing the thermal degradation curves of the neat sc-PLA/POSS-NH$_2$ (Figure 5.7(a)) mat with that of the treated fibers (Figure 5.7(b)). As already reported,[28] the degradation of PLA occurs in one step in a temperature range between 300 and 400 °C.

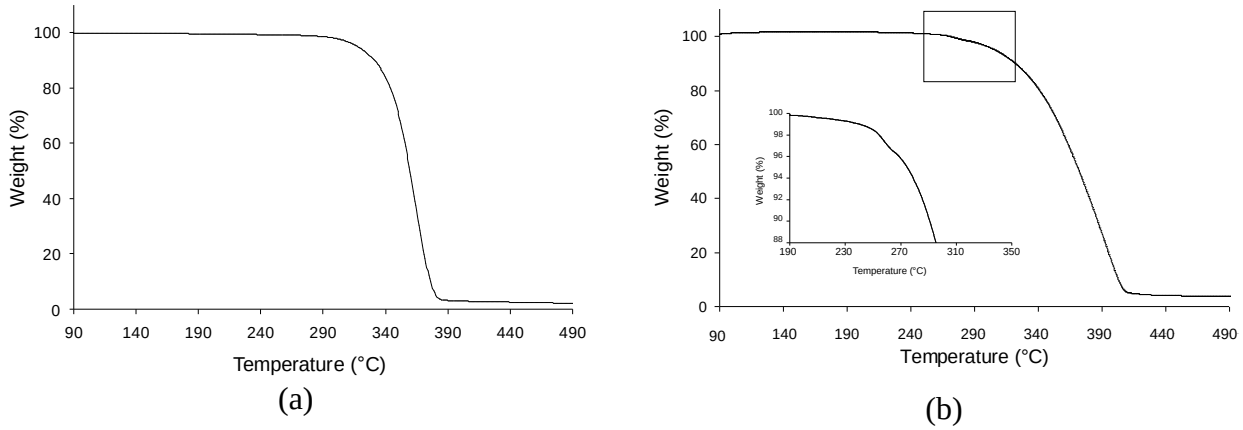

Figure 5.7. *TG curve of (a) sc-PLA/POSS-NH$_2$ fibers and (b) sc-PLA/POSS-NH-CD fibers.*

Indeed, the TGA curve of the treated fibers overlaps that of the neat mat in the range of decomposition of the PLA, thus demonstrating that the process does not alter significantly the structure of the polymer. Nevertheless, in the curve of sc-PLA/POSS-NH-CD fibers, a degradation step was observed in the temperature range between 250-270 °C (see insert of Figure 5.7 (b)), which might be attributed to the degradation of CD moieties, which typically occurs between 220-300 °C.[46,47] Based on TGA data, the grafting percentage of CD results to be 3 wt.-%, quantity which can be related with the amount of silsesquioxane dispersed in the fiber, that is 5 wt.-%.

In order to evaluate the electrospun mat wettability and study the influence of the cyclodextrin grafting on this feature, water contact angle measurements were carried out. These measurements are considered to be important to assess the surface properties, or the wettability of the solid surface, governed by both the surface chemical composition and by its geometrical microstructure.[48] Indeed, while the contact angle of sc-PLA/POSS-NH_2 fibers is 130°±2°, that of the electrospun sc-PLA/POSS-NH-CD mats is lower, 120±2°. Although the variation is small, the increase of the surface hydrophilicity of the treated mat can be ascribed to the grafting reaction and in particular to the hydrophilicity of the molecules of cyclodextrin.

The capacity of the fibers to absorb water pollutants was studied by examining the same molecules already considered in the case of POSS-NH-CD, namely alizarin red and 2-cholorophenol. The results, summarized in Table 5.1, show, as underlined for the absorbent in the powder form, that the treatment of the fibers with CD, promotes their ability to retain the contaminants and that the specific capacity of the sc-PLA/POSS-NH-CD fibers to absorb the phenol-based molecule is higher than that to retain alizarin red. Furthermore, it is of utmost relevance that the absorption capacity of the fibers towards both the contaminant molecules is much higher for the mats than for the powder, the absorption capacity passing from 2.8 to 12 mg/g for alizarin red (from $1.15 \cdot 10^{-5}$ mol/g to $4.83 \cdot 10^{-5}$ mol/g) and from 4.2 to 42 mg/g (from $3.27 \cdot 10^{-5}$ mol/g to $32.5 \cdot 10^{-5}$ mol/g) for 2-chlorophenol, in the case of POSS-NH-CD powder and sc-PLA/POSS-NH-CD fibers, respectively. The above finding can be related to the availability of the absorption sites, which are clearly more accessible in the case of CD grafting on the surface of the fibers with respect to the direct exploitation of POSS-NH-CD in the powder form.

5.4 References

1. Sahay R, Kumar PS, Sridhar R, et al. Electrospun composite nanofibers and their multifaceted applications. *J Mater Chem*. 2012;22(26):12953. doi:10.1039/c2jm30966a.
2. Yousef A, Barakat NAM, Amna T, Unnithan AR, Al-Deyab SS, Yong Kim H. Influence of CdO-doping on the photoluminescence properties of ZnO nanofibers: Effective visible light photocatalyst for waste water treatment. *J Lumin*. 2012;132(7):1668-1677. doi:10.1016/j.jlumin.2012.02.031.
3. Mali SS, Kim H, Jang WY, Park HS, Patil PS, Hong CK. Novel Synthesis and Characterization of Mesoporous ZnO Nanofibers by Electrospinning Technique. *ACS Sustain Chem Eng*. 2013;1(9):1207-1213. doi:10.1021/sc400153j.
4. Wang D, Li Y, Li Puma G, et al. Mechanism and experimental study on the photocatalytic performance of Ag/AgCl @ chiral TiO2 nanofibers photocatalyst: The impact of wastewater components. *J Hazard Mater*. 2015;285:277-284. doi:10.1016/j.jhazmat.2014.10.060.
5. Nalbandian MJ, Greenstein KE, Shuai D, et al. Tailored synthesis of photoactive TiO2 nanofibers and Au/TiO2 nanofiber composites: Structure and reactivity optimization for water treatment applications. *Environ Sci Technol*. 2015;49(3):1654-1663. doi:10.1021/es502963t.
6. Yu J, Yu H, Cheng B, Zhao X, Zhang Q. Preparation and photocatalytic activity of mesoporous anatase TiO2 nanofibers by a hydrothermal method. *J Photochem Photobiol A Chem*.

2006;182(2):121-127. doi:10.1016/j.jphotochem.2006.01.022.
7. Lee JA, Nam YS, Rutledge GC, Hammond PT. Enhanced photocatalytic activity using layer-by-layer electrospun constructs for water remediation. *Adv Funct Mater*. 2010;20(15):2424-2429. doi:10.1002/adfm.201000418.
8. Sugunan A, Guduru VK, Uheida A, Toprak MS, Muhammed M. Radially oriented ZnO nanowires on flexible poly-L-lactide nanofibers for continuous-flow photocatalytic water purification. *J Am Ceram Soc*. 2010;93(11):3740-3744. doi:10.1111/j.1551-2916.2010.03986.x.
9. Olaru N, Calin G, Olaru L. Zinc oxide nanocrystals grown on cellulose acetate butyrate nanofiber mats and their potential photocatalytic activity for dye degradation. *Ind Eng Chem Res*. 2014;53(46):17968-17975. doi:10.1021/ie503139a.
10. Kayaci F, Ozgit-Akgun C, Donmez I, Biyikli N, Uyar T. Polymer-inorganic core-shell nanofibers by electrospinning and atomic layer deposition: Flexible nylon-ZnO core-shell nanofiber mats and their photocatalytic activity. *ACS Appl Mater Interfaces*. 2012;4(11):6185-6194. doi:10.1021/am3017976.
11. Bhaumik M, Choi HJ, McCrindle RI, Maity A. Composite nanofibers prepared from metallic iron nanoparticles and polyaniline: High performance for water treatment applications. *J Colloid Interface Sci*. 2014;425:75-82. doi:10.1016/j.jcis.2014.03.031.
12. Pant HR, Kim HJ, Joshi MK, et al. One-step fabrication of multifunctional composite polyurethane spider-web-like nanofibrous membrane for water purification. *J Hazard Mater*. 2014;264:25-33. doi:10.1016/j.jhazmat.2013.10.066.
13. Dasari A, Quirós J, Herrero B, Boltes K, García-Calvo E, Rosal R. Antifouling membranes prepared by electrospinning polylactic acid containing biocidal nanoparticles. *J Memb Sci*. 2012;405-406:134-140. doi:10.1016/j.memsci.2012.02.060.
14. Kayaci F, Aytac Z, Uyar T. Surface modification of electrospun polyester nanofibers with cyclodextrin polymer for the removal of phenanthrene from aqueous solution. *J Hazard Mater*. 2013;261:286-294. doi:10.1016/j.jhazmat.2013.07.041.
15. Kayaci F, Umu OCO, Tekinay T, Uyar T. Antibacterial electrospun poly(lactic acid) (PLA) nanofibrous webs incorporating triclosan/cyclodextrin inclusion complexes. *J Agric Food Chem*. 2013;61(16):3901-3908. doi:10.1021/jf400440b.
16. Szejtli J. Introduction and General Overview of Cyclodextrin Chemistry. *Chem Rev*. 1998;98(5):1743-1754. doi:10.1021/cr970022c.
17. Del Valle EMM. Cyclodextrins and their uses: A review. *Process Biochem*. 2004;39(9):1033-1046. doi:10.1016/S0032-9592(03)00258-9.
18. Schofield WCE, Bain CD, Badyal JPS. Cyclodextrin-functionalized hierarchical porous architectures for high-throughput capture and release of organic pollutants from wastewater. *Chem Mater*. 2012;24(9):1645-1653. doi:10.1021/cm300552k.
19. Crini G, Morcellet M. Synthesis and applications of adsorbents containing cyclodextrins. *J Sep Sci*. 2002;25(13):789-813. doi:10.1002/1615-9314(20020901)25:13<789::AID-JSSC789>3.0.CO;2-J.
20. Morin-Crini N, Crini G. Environmental applications of water-insoluble β-cyclodextrin-epichlorohydrin polymers. *Prog Polym Sci*. 2013;38(2):344-368. doi:10.1016/j.progpolymsci.2012.06.005.
21. Uyar T, Havelund R, Hacaloglu J, Besenbacher F, Kingshott P. Functional Electrospun Polystyrene Nanofibers Incorporating α-, β-, and γ-Cyclodextrins: Comparison of Molecular Filter Performance. *ACS Nano*. 2010;4(9):5121-5130. doi:10.1021/nn100954z.
22. Uyar T, Havelund R, Nur Y, Hacaloglu J, Besenbacher F, Kingshott P. Molecular filters based on cyclodextrin functionalized electrospun fibers. *J Memb Sci*. 2009;332(1-2):129-137. doi:10.1016/j.memsci.2009.01.047.

23. Celebioglu A, Demirci S, Uyar T. Cyclodextrin-grafted electrospun cellulose acetate nanofibers via "click" reaction for removal of phenanthrene. *Appl Surf Sci*. 2014;305:581-588. doi:10.1016/j.apsusc.2014.03.138.
24. Tsuji H. Poly(lactide) stereocomplexes: Formation, structure, properties, degradation, and applications. *Macromol Biosci*. 2005;5(7):569-597. doi:10.1002/mabi.200500062.
25. Gardella L, Basso A, Prato M, Monticelli O. On stereocomplexed polylactide materials as support for PAMAM dendrimers: synthesis and properties. *RSC Adv*. 2015;5(58):46774-46784. doi:10.1039/C5RA05295E.
26. Gardella L, Furfaro D, Galimberti M, Monticelli O. On the development of a facile approach based on the use of ionic liquids: preparation of PLLA (sc-PLA)/high surface area nano-graphite systems. *Green Chem*. 2015;17:4082-4088. doi:10.1039/C5GC00964B.
27. Valentini L, Bon SB, Monticelli O, Kenny JM. Deposition of amino-functionalized polyhedral oligomeric silsesquioxanes on graphene oxide sheets immobilized onto an amino-silane modified silicon surface. *J Mater Chem*. 2012;22(13):6213. doi:10.1039/c2jm16111g.
28. Monticelli O, Putti M, Gardella L, et al. New stereocomplex PLA-based fibers: Effect of POSS on polymer functionalization and properties. *Macromolecules*. 2014;47(14):4718-4727. doi:10.1021/ma500528a.
29. Cozza ES, Monticelli O, Marsano E. Electrospinning: A novel method to incorporate POSS into a polymer matrix. *Macromol Mater Eng*. 2010;295(9):791-795. doi:10.1002/mame.201000214.
30. Cozza ES, Monticelli O, Cavalleri O, Marsano E. Preparation, characterization, and properties of nanofibers based on poly(vinylidene fluoride) and polyhedral oligomeric silsesquioxane. *Polym Adv Technol*. 2012;23(9):1252-1257. doi:10.1002/pat.2037.
31. Cozza ES, Ma Q, Monticelli O, Cebe P. Nanostructured nanofibers based on PBT and POSS: Effect of POSS on the alignment and macromolecular orientation of the nanofibers. *Eur Polym J*. 2013;49(1):33-40. doi:10.1016/j.eurpolymj.2012.10.006.
32. Gardella L, Basso A, Prato M, Monticelli O. PLA/POSS nanofibers: A novel system for the immobilization of metal nanoparticles. *ACS Appl Mater Interfaces*. 2013;5(16):7688-7692. doi:10.1021/am402280j.
33. Liu YY, Fan XD, Gao L. Synthesis and Characterization of β-Cyclodextrin Based Functional Monomers and its Copolymers with N-isopropylacrylamide. *Macromol Biosci*. 2003;3(12):715-719. doi:10.1002/mabi.200300052.
34. Kang Y, Zhou L, Li X, Yuan J. β-Cyclodextrin-modified hybrid magnetic nanoparticles for catalysis and adsorption. *J Mater Chem*. 2011;21(11):3704. doi:10.1039/c0jm03513k.
35. Taguchi K. Transient Binding Mode of Phenolphthalein-β-Cyclodextrin Complex: An Example of Induced Geometrical Distortion. *J Am Chem Soc*. 1986;108(10):2705-2709. doi:10.1021/ja00270a032.
36. Khalafi L, Rafiee M, Mahdiun F, Sedaghat S. Investigation of the inclusion complex of β-cyclodextrin with mycophenolate mofetil. *Spectrochim Acta - Part A Mol Biomol Spectrosc*. 2012;90:45-49. doi:10.1016/j.saa.2012.01.012.
37. Afkhami A, Khalafi L. Spectrophotometric determination of conditional acidity constant as a function of β-cyclodextrin concentration for some organic acids using rank annihilation factor analysis. *Anal Chim Acta*. 2006;569(1-2):267-274. doi:10.1016/j.aca.2006.03.054.
38. Ghosh BC, Deb N, Mukherjee AK. Determination of individual proton affinities of ofloxacin from its UV-Vis absorption, fluorescence and charge-transfer spectra: Effect of inclusion in β-cyclodextrin on the proton affinities. *J Phys Chem B*. 2010;114(30):9862-9871. doi:10.1021/jp103014b.
39. Banat FA, Al-Bashir B, Al-Asheh, Hayajneh O. Adsorption of phenol by bentonit. *Environ Pollut*. 2000;107:391-398.

40. Ahmaruzzaman M, Sharma DK. Adsorption of phenols from wastewater. *J Colloid Interface Sci*. 2005;287(1):14-24. doi:10.1016/j.jcis.2005.01.075.
41. Daifullah AE-H, Gad H. Sorption of Semi-Volatile Organic Compounds by Bottom and Fly Ashes Using HPLC. *Adsorpt Sci Technol*. 1998;16(4):273-283. doi:10.1177/026361749801600404.
42. Abdel-Halim ES, Fouda MMG, Hamdy I, Abdel-Mohdy FA, El-Sawy SM. Incorporation of chlorohexidin diacetate into cotton fabrics grafted with glycidyl methacrylate and cyclodextrin. *Carbohydr Polym*. 2010;79(1):47-53. doi:10.1016/j.carbpol.2009.07.050.
43. Hebeish A, El Shafei A, Shaarawy S. Synthesis and characterization of multifunctional cotton containing cyclodextrin and butylacrylate moieties. *Polym - Plast Technol Eng*. 2009;48(8):839-850. doi:10.1080/03602550902994904.
44. Blanchemain N, Laurent T, Haulon S, et al. In vitro study of a HPγ-cyclodextrin grafted PET vascular prosthesis for application as anti-infectious drug delivery system. *J Incl Phenom Macrocycl Chem*. 2007;57(1-4):675-681. doi:10.1007/s10847-006-9264-1.
45. Blanchemain N, Haulon S, Boschin F, et al. Vascular prostheses with controlled release of antibiotics. Part 1: Surface modification with cyclodextrins of PET prostheses. *Biomol Eng*. 2007;24(1 SPEC. ISS.):149-153. doi:10.1016/j.bioeng.2006.05.012.
46. Yang JY, Jung B Te, Suh DH. A simple attempt to change the solubility of polyimide by physical inclusion with β-cyclodextrin and its derivatives. *Polymer (Guildf)*. 2001;42(20):8349-8354. doi:10.1016/S0032-3861(01)00337-8.
47. Bryce DJ, Greenwood CT. Aspects of the Thermal Degradation of Starch. *Starch -Sätrke*. 1963;15(5):166-170. doi:10.1002/star.19630150503.
48. Monticelli O, Bocchini S, Gardella L, Cavallo D, Cebe P, Germelli G. Impact of synthetic talc on PLLA electrospun fibers. *Eur Polym J*. 2013;49(9):2572-2583. doi:10.1016/j.eurpolymj.2013.05.017.

CHAPTER 6. Poly(styrene-co-maleic anhydride) nanoparticles: Microencapsulation and protein conjugation

This chapter describes the preparation, characterization and application of a novel protein carrier. Indeed, papain-conjugated poly(styrene-co-maleic anhydride) (PSMA) nanoparticles were prepared by combining nanoprecipitation and electrospray technique. Different experimental conditions were tested in order to optimize nanoparticles dimensions and production yields. The nanoparticles were characterized by Infrared Spectroscopy (IR), Field Emission Scanning Electron Microscopy (FE-SEM) and Dynamic Light Scattering (DLS). The obtained nanoparticles were then used for the conjugation of a functional protein to their surface. The proteolytic enzyme papain was chosen as model protein. The successful papain-nanoparticle conjugation was demonstrated by zeta potential, IR and FE-SEM measurements.

6.1 Introduction

The search for new approaches for the immobilization of proteins on solid matrices is a highly active field of research, having perspective impact on different areas. In this respect, immobilized functional proteins, such as enzymes, are required for their use in industrial processes in order to permit the re-use of the expensive enzyme molecules and to improve many enzyme properties, such as stability, resistance to inhibitors and selectivity.[1,2] A number of biotechnological products are based on immobilized proteins with applications in diagnostics, bioaffinity chromatography, and biosensors.[3,4] Moreover, proteins, due to their high specificity, have emerged as promising therapeutics for the prevention and treatment of various diseases ranging from cancer, diabetes, cystic fibrosis, autoimmunity, protein deficiencies and infectious diseases.[5–7] Again the in vivo delivery of proteins requires their immobilization onto a carrier in order to overcome problems related to protein susceptibility to denaturation and poor bioavailability.[8–10] In this framework, polymeric nanoparticles are seen as ideal protein nanocarriers due to high surface area to volume ratios, to their stability and versatility, which give the possibility of incorporating functional groups reactive, as an example, towards primary amines on lysine residues, so that proteins can be either entrapped inside or conjugated to their surface.[11–14]

In this work, we proposed the design and fabrication of polymeric nanoparticles based on poly(styrene-co-maleic anhydride) (PSMA), namely a synthetic copolymer with amphiphilic properties. Generally, the above polymer, which is characterized by a good biocompatibility, has been used as a support for the covalent immobilization of proteins and drugs in the biomedical filed in the acid form, poly(styrene-co-maleic acid), as colloidal carrier of various type of drugs.[15] The possibility to covalently conjugate proteins with the PSMA functional groups was firstly investigated in 1990[16] and its use was proposed for hepatoma treatment in 1993 in Japan.[17] PSMA is soluble in organic solvent, and its characteristic of low toxicity, together with good mechanical stability make it an ideal candidate for the fabrication of nanoparticles.[18,19]

Here, the electrospray technique, which is a simple and widely used method for the fabrication of uniform samples with high yield, was chosen for the fabrication of PSMA nanoparticles.[20]

The PSMA nanoparticles were then characterized by Scanning Electron Microscopy (SEM), Fourier Transform Infrared spectroscopy (FTIR) and Dynamic Light Scattering (DLS).

The model protein papain was then conjugated to PSMA nanoparticles.

Papain is a proteolytic enzyme (EC 3.4.22.2) present in the latex of Carica papaya, and it is one of the most important industrial proteases, used in protein hydrolysate, juice and beer clarification, bakery and dairy products.[21] Moreover, papain has been demonstrated to have antibacterial, anti-inflammatory and mucolytic properties. In this respect, papain conjugation with nanoparticles has been proposed as a strategy for overcoming the mucus barrier in oral and pulmonary delivery, increasing drug permeation.[16–18,22–24]

Papain was conjugated with the surface of the PSMA nanoparticles by a one-step procedure and the modified PSMA nanoparticles were characterized by zeta potential measurements and by uv-vis spectroscopy in terms of efficiency of enzyme immobilization and of residual catalytic activity.

Finally, we preliminarily evaluated the possibility of microencapsulating PSMA nanoparticles. This study was carried out in the view of a perspective application of PSMA nanoparticles in processes based on enzymatic cascade reactions, where reactions should be carried out in confined environments,[25] or in protein delivery applications, where microencapsulation is required to control drug release profiles in oral or pulmonary delivery.[26–29] To this purpose, nanostructured polyelectrolyte capsules (NPCs) were selected as ideal microcarriers, due to their versatility and wide applicability.[30–32] NPCs are fabricated, with nanometer precision, through the electrostatic layer-by-layer (LbL) self-assembly of a multilayered shell [33] onto a sacrificial micro-core.[34,35] In this work, polyarginine and dextran were used, as polycation and polyaninion respectively, for the formation of the shell,[36] while calcium carbonate microparticles ($CaCO_3$), co-precipitated with PSMA nanoparticles, were used as sacrificial cores.[37] Scanning electron microscopy was used to characterize the morphology of PSMA/$CaCO_3$ microparticles while optical microscopy was used to visualize the formation the NPCs.

6.2 Experimental section

PSMA nanoparticle preparation by electrospray nanoprecipitation

Solutions were prepared by dissolving different amounts of PSMA in DMF. The polymer solution was introduced to a nozzle, at a constant flow rate of 2 mL/h using a syringe pump. The nozzle was connected to the positive electrode of a high-voltage supply. Ethanol, a non-solvent of PSMA but miscible with DMF, was used as the collection medium. Electrosprayed droplets were collected in a beaker containing 80 mL of ethanol stirred by a magnetic stirrer at a constant rotary speed. The beaker was placed on a grounded aluminium foil with a deposition distance of 5 cm between the charged nozzle exit and the collecting ethanol surface. Experiments were conducted at room temperature. The applied voltage, that is 20 kV, was optimized to maintain a stable cone-jet over the duration of particle collection (Figure 6.1).

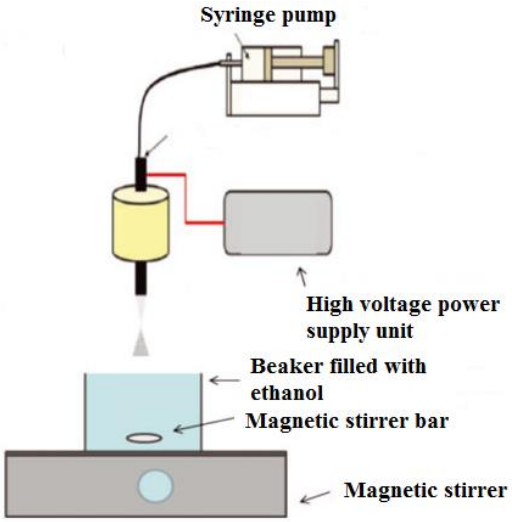

Figure 6.1. Schematic of electrospray nanoprecipitation process.

Conjugation of enzyme with PSMA nanoparticles

The conjugation of the enzyme with PSMA nanoparticles was obtained by exploiting the covalent bonding between the amino groups of the enzyme molecules and the maleic units of the polymeric chain. Specifically, Papain was used at the concentration of 0,1mg/ml in water.

PSMA nanoparticles were dispersed in the enzymatic solution and stirred for 24 hours at room temperature. Three washings at 14000 rpm for 5 minutes in water were carried out in order to remove the unbound enzyme molecules.

The enzymatic activities of the starting enzymatic solution and the residual enzymatic solution, after the removal of the nanoparticles by centrifugation, were measured, in order to evaluate the amount of conjugated enzyme (Eq. 6.1).

$$Conjugated\ enzyme\ [ug] = Starting\ enzymatic\ solution\ [ug] - Residual\ enzymatic\ solution\ [ug] \quad (6.1)$$

To this purpose, the catalytic activity of the free enzyme solution at different concentrations was determined, and the masses were calculated from the respective calibration curve (R2 = 0.9914, data non-reported).

The immobilization yield was defined as the percentage of the ratio of the previously calculated conjugated enzyme to the starting enzymatic solution (Eq. 6.2).

$$Immobilization\ yield\ (\%) = \frac{Conjugated\ Enzyme\ [ug]}{Starting\ enzymatic\ solution\ [ug]} \times 100 \quad (6.2)$$

Enzymatic activity tests

The enzymatic activity of free and immobilized papain was determined using casein assay, without addition of L-cystein as activator.[24] Specifically, either 100 µl of free papain solution or PSMA-papain nanoparticle suspension were incubated with 200 µl of 3 mM EDTA as reducing agent at 37° for 30 minutes. The mixture was added to 500 µl of 2% (w/v) casein solution in PBS pH 7.4, and the reaction was carried out for 15 minutes at 37° C. Afterward, the reaction was stopped by addition of 2 ml of 10% (w/v) TCA acid solution. After centrifugation for 5 min at 14000 rpm, the supernatant was removed and added to 1 ml of 0.5 M Na_2CO_3 and 200 µl of Folin's reagent, and the absorbance was measured at 660 nm. Since the L-cystein was found to react with Folin's reagent, it wasn't added to the reaction mixture. Briefly, when casein is digested, the amino acid tyrosine is liberated along with other amino acids and peptide fragments. Folin's reagent reacts with free tyrosine to produce a blue coloured chromophore, which is quantifiable as an absorbance value on the spectrophotometer. The more tyrosine is released from casein, the more the chromophores are generated and the stronger the activity of the protease. In order, not to overstate the specific papain catalytic activity, the addition of L-cysteine was avoided, without significantly affecting the enzyme efficiency.[38] Finally, the residual enzymatic activity for the immobilized enzyme was calculated as percentage (Eq. 6.3), in terms of resulting conjugated enzyme, due to the possible partial loss of activity after immobilization,[39,40] with respect to the expected conjugated enzyme (previously calculated with Eq. 6.1), used as 100% value.

$$Residual\ activity\ (\%) = \frac{Resulting\ Conjugated\ Enzyme\ [ug]}{Conjugated\ Enzyme\ [ug]} \times 100 \qquad (6.3)$$

PSMA nanoparticles encapsulation in polyelectrolyte microcapsules

The PSMA nanoparticles were encapsulated in $CaCO_3$ microparticles following a two-step procedure, based on the combination of complexation and mineralization processes.[41,42] The first step consisted in the complexation between 2 ml of 0.66 M $CaCl_2$ solution and 2 ml 20 mg/ml nanoparticle dispersion, which were initially mixed together by ultrasounds for 5 minutes, to homogeneously disperse the nanoparticles in the $CaCl_2$ solution. Secondly, 4 ml of 0.33 M Na_2CO_3 were added to the obtained complexes, leading to their mineralization and resulting in micro-sized PSMA loaded-$CaCO_3$ microparticles. Finally, the microparticles were washed three times with water and coated by a polyelectrolyte multi-layered shell. Briefly, the microparticles were alternatively immersed in 0.5 mg/ml negatively charged DEX solution and 0.5 mg/ml positively charged PAR solution, with 0.15 M NaCl. Three washings with water followed each adsorption step, in order to remove the excess of not adsorbed polyelectrolyte. Once the final $(DEX/PAR)_4$ multilayered structure was obtained, the coated microparticles were immersed in 0.2 M EDTA solution for 30 minutes, and $CaCO_3$ was dissolved, in order to obtain empty capsules. Three washings with water followed, and the empty capsules were kept in fridge until their further use.

Characterization

FTIR spectra were recorded on a Bruker IFS66 spectrometer in the spectral range 400-4000 cm^{-1}.

The morphology of PSMA and sc-PLA nanoparticles were analyzed by a Zeiss Supra 40 VP Field Emission Scanning Electron Microscope (FE-SEM) was used. All samples were thinly sputter-coated with carbon using a Polaron E5100 sputter coater.

Nanoparticle size distribution was further investigated by DLS using a Malvern Zetasizer Nano ZS (Malvern Instruments, Worcestershire, U.K). This instrument was also used to measure the Zeta Potential of PSMA and enzyme-conjugated PSMA nanoparticles. An inverted IX-51 Olympus optical microscope, equipped with a DP70 digital camera and with a CPlan 103 objective, was used to visualize the removal of the $CaCO_3$ microparticles.

6.3 Results and discussions

This work was accomplished assessing first the preparation of nanoparticles based on styrene-maleic anhydride copolymers by combining the nanoprecipitation method with the electrospray technique. The influence of several preparation parameters, such as voltage, distance between the collector and the tip as well as the solution concentration, on the particle features was studied. In particular, the latter parameter turned out to strongly affect the morphology and dimensions of the prepared particles. The size of particles prepared with various percentages of polymer was evaluated by using SEM and DLS. Figure 6.2(a) and 6.2(b) shows SEM micrographs of PSMA particles, together with the histograms of the diameter distributions, obtained for two different relative polymer amounts (0.5 wt % and 1.5 wt %) as significant examples.

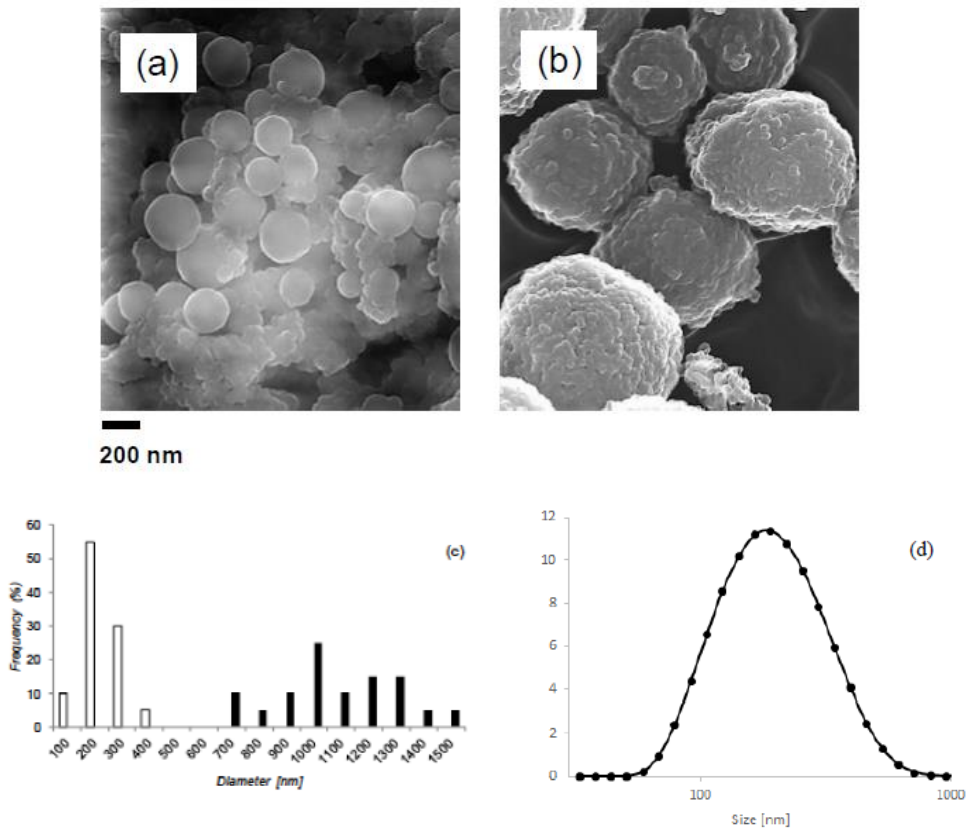

Figure 6.2. SEM images of PSMA nanoparticles with (a) 0.5% wt of polymer, (b) 1.5% wt of polymer, (c) particle diameters distribution (white bars for 0.5% wt, black bars for 1.5% wt), (d) diameter size distribution by DLS.

By decreasing the polymer concentration in the solution, the dimensions of the particles significantly diminished (Figure 6.2(c)).[43,44] Since the polymer concentration of 0.5 wt% produced nanometric particles, with an acceptable yield of 50 mg/ml, it was used for all the further preparations. As shown by DLS measurements, the dimension distribution of the produced nanoparticles was found to be relatively narrow having a polydispersity index (PI) of 0.2.[45] The mean diameter size was found to be 176 nm (Figure 6.2(d)) in good agreement with the value calculated analysing the SEM micrographs.

The conjugation of the enzyme papain with the nanoparticle surface should affect its surface charge since PSMA and Papain have different isoelectric points, at pH 5 and 9 respectively. At the pH of unbuffered water (about 5.5), their net charges are negative and positive respectively. Therefore, Zeta Potential measurements provide a check of effective conjugation. Figure 6.3 reports the results of Zeta potential measurements performed by DLS.

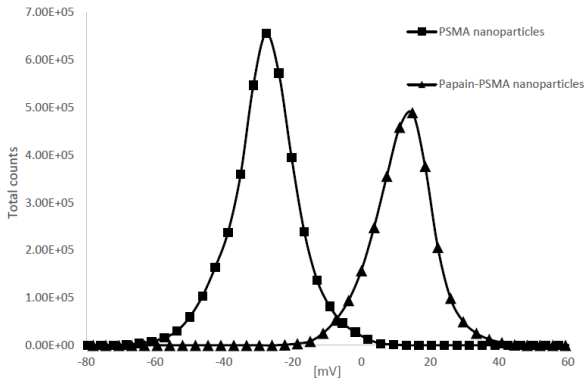

Figure 6.3. Zeta potential values of PSMA nanoparticles (■) and Papain-PSMA nanoparticles (▲).

The Zeta potential of PSMA nanoparticles was found to be (-27.9 ± 2.2) mV, while papain-PSMA nanoparticles had Zeta potentials equal to (+12.0 ± 1.9) mV in unbuffered water. These values are qualitatively in agreement with PSMA and papain electric charges in unbuffered water, thus demonstrating the modification of the chemical features of the nanoparticle surface as a consequence of the conjugation with the enzyme molecules.

In order to further validate the above findings, the IR spectra of papain, PSMA and papain-PSMA nanoparticles, were acquired (Figure 6.4).

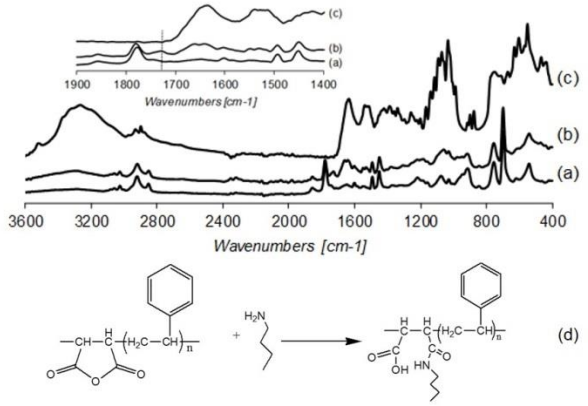

Figure 6.4. IR spectra of: (a) PSMA nanoparticles, (b) papain-PSMA nanoparticles and (c) papain; (d) scheme of the reaction between PSMA and amino groups of papain.

PSMA holds two characteristic absorption peaks at 1772 and 1850 cm^{-1} due to symmetric and antisymmetric stretching vibrations of the anhydride carbonyl group as well as a peak at 1213 cm^{-1} attributed to the stretching vibration C-O-C of maleic anhydride units. In the spectra of the particles treated with the enzymes, together with the peaks characteristics of the neat polymer matrix, new bands at ca. 3200 and 1630 cm^{-1} appear, which can be assigned to the stretching vibration of OH and to bending of NH groups, respectively. These bands, characteristic of the IR patterns of the enzymes, (Figure 6.4(c)) give evidence of the presence of above molecules on the polymer surface. Moreover, in the spectra of the treated nanoparticles a new band at ca. 1720 cm^{-1}(see insert of figure 6.4), which does not belong to Papain, is visible. The above signal, which can be assigned to the carbonyl group stretching vibration of a carboxyl acid, might be related to the surface reaction between the MA group of PSMA and the amino group of enzyme molecules (Figure 6.4(d)). Indeed, as previously reported,[46,47] the mild conditions used to combine PSMA nanoparticles with the enzyme, might promote the maleic group opening with the amine functionalities of enzymes, leading to the formation of COOH groups.

The conjugation of an enzyme with a solid support, including polymeric nanoparticles, could affect the three-dimensional structure of the protein leading to the loss of its catalytic activity.[48] The extent of the catalytic activity loss depends on the chemical interactions established between enzyme molecules and polymer functional groups. To assess the impact of the conjugation of papain with PSMA nanoparticles, the enzymatic activity was spectrophotometrically evaluated by investigating the hydrolysis of casein as substrate in the presence of free papain and of papain conjugated with PSMA nanoparticles under identical assay conditions.

The stability of papain after its immobilization was evaluated in terms of residual catalytic activity. The quantification of the superficial density of conjugated enzyme onto the total surface of the nanoparticles was calculated as well. Papain residual catalytic activity at 37°C in phosphate buffer (pH 7.4) was found to be 79 (±11)% with respect to the same amount of free papain, with a density of conjugated enzyme equal to 27 ± 4 mg/cm^2, corresponding to a 71(±10)% of immobilization yield.

In a previous work [49] electrospun PSMA nanofibers were used as support for the immobilization of the enzyme horseradish peroxidase and the residual catalytic activity was fond to be 21% compared to the free enzyme. This difference between the residual catalytic activity of the two enzymes could be due both to the different structure of the enzymes, and thus to the different interactions between the enzymes molecules with PSMA, and to the different geometry of PSMA systems. For comparison with other immobilizing supports, the immobilization of papain on magnetic gold nanocomposites was reported to lead to a residual catalytic activity of 47 (±5)% compared to native papain [50] whereas the covalent conjugation with poly(acrylic acid) nanoparticles was found to lead to a residual catalytic activity of 42.21 (±19.54)% [17] and 47.8 (±0.64)% [24] in a different work.

Overall, the obtained results showed that a papain can be efficiently immobilized by a simple protocol on PSMA nanoparticles.

Finally, the possibility to microencapsulate PSMA nanoparticles was evaluated. This study was carried out for the perspective use of the developed nanoparticles to carry out confined enzymatic reactions or for the delivery of therapeutic proteins via administration routes requiring a fine control over release profile and the protection of the payload. In this view, NPCs, obtained by the LbL self-assembly technique, were selected as micro-carriers due to their versatility, which makes these systems very interesting for different applications, including biomedical ones. One of the advantages of NPCs relies in the possibility of loading the species of interest under mild conditions into a sacrificial template, which is then used as micro-support for the LbL assembly. Specifically, it has been demonstrated that biomacromolecules can be co-precipitated in $CaCO_3$

microparticles in the process of growth from the mixture of aqueous solutions of $CaCl_2$ and Na_2CO_3.[37]

Following this approach PSMA nanoparticles were loaded in $CaCO_3$ microparticles taking advantage of the electrostatic interaction between Ca^{2+} cations of $CaCl_2$ and the negatively charged PSMA nanoparticles. This electrostatic interaction induces the self-assembly of coacervate droplets, which are finally stabilized by the addition of Na_2CO_3, leading to the final mineralization of the complex.[41] The obtained PSMA loaded-$CaCO_3$ microparticles were characterized by FE-SEM. Figure 6.5 shows $CaCO_3$ microparticles unloaded (left) and loaded (right) with PSMA nanoparticles. The presence of PSMA nanoparticles turned out to change the dimension of the resulting $CaCO_3$ microparticles from 3 μm in the case of unloaded $CaCO_3$ microparticles to 7 μm for the PSMA loaded ones. Moreover, SEM images showed a different roughness of the PSMA loaded-$CaCO_3$ microparticles respect to the unloaded ones. The obtained results seemed to confirm the successful inclusion of PSMA nanoparticles into $CaCO_3$ microparticles. The microparticles were then used for template-assisted LbL assembly of four bilayers of oppositely charged PAR and DEX. The following dissolution of $CaCO_3$ microparticles by EDTA solution resulted in the formation of microcapsules containing PSMA nanoparticles. PSMA unloaded and loaded microcapsules were characterized by optical microscopy. Figure 6.6 shows the unloaded (a) and loaded (b) microcapsules. The presence of sub-micro-aggregates in the volume of the PSMA loaded-microcapsules was observed, indicating the successful encapsulation of the nanoparticles.

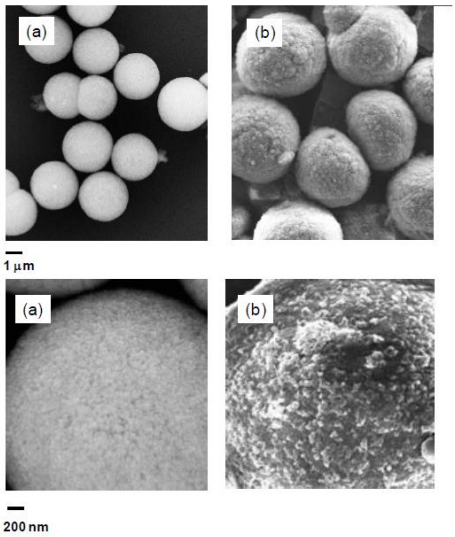

Figure 6.5. SEM images of $CaCO_3$ microparticles plain (a) and loaded (b) with PSMA nanoparticles.

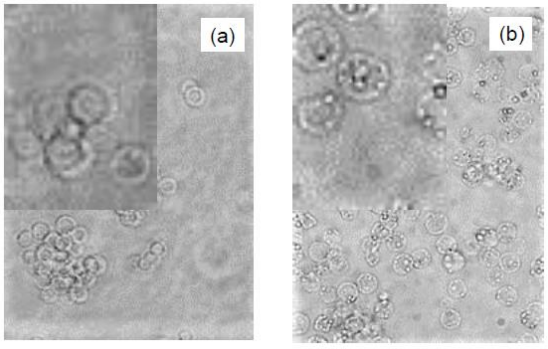

Figure 6.6. $(DEX/PAR)_4$ capsules plain (a) and loaded (b) with PSMA nanoparticles.

6.4 References

1. Liese A, Hilterhaus L. Evaluation of immobilized enzymes for industrial applications. *Chem Soc Rev*. 2013;42(15):6236. doi:10.1039/c3cs35511j.
2. Hwang ET, Gu MB. Enzyme stabilization by nano/microsized hybrid materials. *Eng Life Sci*. 2013;13(1):49-61. doi:10.1002/elsc.201100225.
3. Temporini C, Calleri E, Brusotti G, Massolini G. Protein-Labs on Separative Analytical Scale in Medicinal Chemistry: from the Proof of Concept to Applications. *Curr Org Chem*. 2016;20(11):1169-1185. doi:10.2174/1385272819666150810220825.
4. DiCosimo R, McAuliffe J, Poulose AJ, Bohlmann G. Industrial use of immobilized enzymes. *Chem Soc Rev*. 2013;42(15):6437. doi:10.1039/c3cs35506c.
5. Wilson CJ. Rational protein design: developing next-generation biological therapeutics and nanobiotechnological tools. *Wiley Interdiscip Rev Nanomedicine Nanobiotechnology*. 2015;7(3):330-341. doi:10.1002/wnan.1310.
6. Kintzing JR, Filsinger Interrante M V., Cochran JR. Emerging Strategies for Developing Next-Generation Protein Therapeutics for Cancer Treatment. *Trends Pharmacol Sci*. 2016;37(12):993-1008. doi:10.1016/j.tips.2016.10.005.
7. Leader B, Baca QJ, Golan DE. Protein therapeutics: a summary and pharmacological classification. *Nat Rev Drug Discov*. 2008;7(1):21-39. doi:10.1038/nrd2399.
8. Vaishya R, Khurana V, Patel S, Mitra AK. Long-term delivery of protein therapeutics. *Expert Opin Drug Deliv*. 2015;12(3):415-440. doi:10.1517/17425247.2015.961420.
9. Mitragotri S, Burke PA, Langer R. Overcoming the challenges in administering biopharmaceuticals: formulation and delivery strategies. *Nat Rev Drug Discov*. 2014;13(9):655-672. doi:10.1038/nrd4363.
10. Yu M, Wu J, Shi J, Farokhzad OC. Nanotechnology for protein delivery: Overview and perspectives. *J Control Release*. 2016;240:24-37. doi:10.1016/j.jconrel.2015.10.012.
11. Wu Y, Ng DYW, Kuan SL, Weil T. Protein–polymer therapeutics: a macromolecular perspective. *Biomater Sci*. 2015;3(2):214-230. doi:10.1039/C4BM00270A.
12. Kontos S, Hubbell JA. Drug development: longer-lived proteins. *Chem Soc Rev*. 2012;41(7):2686. doi:10.1039/c2cs15289d.
13. Zhao H, Lin ZY, Yildirimer L, Dhinakar A, Zhao X, Wu J. Polymer-based nanoparticles for protein delivery: design, strategies and applications. *J Mater Chem B*. 2016;4(23):4060-4071. doi:10.1039/C6TB00308G.
14. Cipolatti EP, Silva MJA, Klein M, et al. Current status and trends in enzymatic nanoimmobilization. *J Mol Catal B Enzym*. 2014;99:56-67. doi:10.1016/j.molcatb.2013.10.019.
15. Banerjee S, Sen K, Pal TK, Guha SK. Poly(styrene-co-maleic acid)-based pH-sensitive liposomes mediate cytosolic delivery of drugs for enhanced cancer chemotherapy. *Int J Pharm*. 2012;436(1-2):786-797. doi:10.1016/j.ijpharm.2012.07.059.
16. McGill SL, Smyth HDC. Disruption of the Mucus Barrier by Topically Applied Exogenous Particles. *Mol Pharm*. 2010;7(6):2280-2288. doi:10.1021/mp100242r.
17. Pereira de Sousa I, Cattoz B, Wilcox MD, et al. Nanoparticles decorated with proteolytic enzymes, a promising strategy to overcome the mucus barrier. *Eur J Pharm Biopharm*. 2015;97:257-264. doi:10.1016/j.ejpb.2015.01.008.
18. Müller C, Leithner K, Hauptstein S, Hintzen F, Salvenmoser W, Bernkop-Schnürch A. Preparation and characterization of mucus-penetrating papain/poly(acrylic acid) nanoparticles for oral drug delivery applications. *J Nanoparticle Res*. 2013;15(1):1353. doi:10.1007/s11051-012-1353-z.
19. Vicent MJ, Duncan R. Polymer conjugates: nanosized medicines for treating cancer. *Trends*

Biotechnol. 2006;24(1):39-47. doi:10.1016/j.tibtech.2005.11.006.
20. Maeda H, Konno T. Metamorphosis of Neocarzinostatin to SMANCS: Chemistry, Biology, Pharmacology, and Clinical Effect of the First Prototype Anticancer Polymer Therapeutic. In: *Neocarzinostatin*. Tokyo: Springer Japan; 1997:227-267. doi:10.1007/978-4-431-66914-2_12.
21. Feijoo-Siota L, Villa TG. Native and Biotechnologically Engineered Plant Proteases with Industrial Applications. *Food Bioprocess Technol*. 2011;4(6):1066-1088. doi:10.1007/s11947-010-0431-4.
22. Müller C, Perera G, König V, Bernkop-Schnürch A. Development and in vivo evaluation of papain-functionalized nanoparticles. *Eur J Pharm Biopharm*. 2014;87(1):125-131. doi:10.1016/j.ejpb.2013.12.012.
23. Dünnhaupt S, Kammona O, Waldner C, Kiparissides C, Bernkop-Schnürch A. Nano-carrier systems: Strategies to overcome the mucus gel barrier. *Eur J Pharm Biopharm*. 2015;96:447-453. doi:10.1016/j.ejpb.2015.01.022.
24. Köllner S, Dünnhaupt S, Waldner C, Hauptstein S, Pereira de Sousa I, Bernkop-Schnürch A. Mucus permeating thiomer nanoparticles. *Eur J Pharm Biopharm*. 2015;97:265-272. doi:10.1016/j.ejpb.2015.01.004.
25. Küchler A, Yoshimoto M, Luginbühl S, Mavelli F, Walde P. Enzymatic reactions in confined environments. *Nat Nanotechnol*. 2016;11(5):409-420. doi:10.1038/nnano.2016.54.
26. Li W, Liu D, Zhang H, et al. Microfluidic assembly of a nano-in-micro dual drug delivery platform composed of halloysite nanotubes and a pH-responsive polymer for colon cancer therapy. *Acta Biomater*. 2017;48:238-246. doi:10.1016/j.actbio.2016.10.042.
27. Zhang H, Liu D, Shahbazi M-A, et al. Fabrication of a Multifunctional Nano-in-micro Drug Delivery Platform by Microfluidic Templated Encapsulation of Porous Silicon in Polymer Matrix. *Adv Mater*. 2014;26(26):4497-4503. doi:10.1002/adma.201400953.
28. Imperiale JC, Sosnik A. Nanoparticle-in-Microparticle Delivery Systems (NiMDS): Production, Administration Routes and Clinical Potential. *J Biomater Tissue Eng*. 2013;3(1):22-38. doi:10.1166/jbt.2013.1064.
29. Restani RB, Silva AS, Pires RF, et al. Nano-in-Micro POxylated Polyurea Dendrimers and Chitosan Dry Powder Formulations for Pulmonary Delivery. *Part Part Syst Charact*. 2016;33(11):851-858. doi:10.1002/ppsc.201600123.
30. De Geest BG, De Koker S, Sukhorukov GB, et al. Polyelectrolyte microcapsules for biomedical applications. *Soft Matter*. 2009;5(2):282-291. doi:10.1039/B808262F.
31. Sukhorukov GB, Möhwald H. Multifunctional cargo systems for biotechnology. *Trends Biotechnol*. 2007;25(3):93-98. doi:10.1016/j.tibtech.2006.12.007.
32. Pastorino L, Erokhina S, Erokhin V. Smart Nanoengineered Polymeric Capsules as Ideal Pharmaceutical Carriers. *Curr Org Chem*. 2013;17(1):58-64. doi:10.2174/138527213805289088.
33. Sukhorukov GB, Donath E, Lichtenfeld H, et al. Layer-by-layer self assembly of polyelectrolytes on colloidal particles. *Colloids Surfaces A Physicochem Eng Asp*. 1998;137(1-3):253-266. doi:10.1016/S0927-7757(98)00213-1.
34. Donath E, Sukhorukov GB, Caruso F, Davis SA, Möhwald H. Novel Hollow Polymer Shells by Colloid-Templated Assembly of Polyelectrolytes. *Angew Chemie Int Ed*. 1998;37(16):2201-2205. doi:10.1002/(SICI)1521-3773(19980904)37:16<2201::AID-ANIE2201>3.0.CO;2-E.
35. Sukhorukov GB, Donath E, Davis S, et al. Stepwise polyelectrolyte assembly on particle surfaces: a novel approach to colloid design. *Polym Adv Technol*. 1998;9(10-11):759-767. doi:10.1002/(SICI)1099-1581(1998100)9:10/11<759::AID-PAT846>3.0.CO;2-Q.
36. De Koker S, De Geest BG, Cuvelier C, et al. In vivo Cellular Uptake, Degradation, and Biocompatibility of Polyelectrolyte Microcapsules. *Adv Funct Mater*. 2007;17(18):3754-3763. doi:10.1002/adfm.200700416.

37. Petrov AI, Volodkin D V., Sukhorukov GB. Protein-Calcium Carbonate Coprecipitation: A Tool for Protein Encapsulation. *Biotechnol Prog*. 2008;21(3):918-925. doi:10.1021/bp0495825.
38. Homaei AA, Sajedi RH, Sariri R, Seyfzadeh S, Stevanato R. Cysteine enhances activity and stability of immobilized papain. *Amino Acids*. 2010;38(3):937-942. doi:10.1007/s00726-009-0302-3.
39. Mateo C, Abian O, Fernandez–Lafuente R, Guisan JM. Increase in conformational stability of enzymes immobilized on epoxy-activated supports by favoring additional multipoint covalent attachment☆. *Enzyme Microb Technol*. 2000;26(7):509-515. doi:10.1016/S0141-0229(99)00188-X.
40. Talbert JN, Goddard JM. Enzymes on material surfaces. *Colloids Surfaces B Biointerfaces*. 2012;93:8-19. doi:10.1016/j.colsurfb.2012.01.003.
41. Lauth V, Maas M, Rezwan K. Coacervate-directed synthesis of CaCO 3 microcarriers for pH-responsive delivery of biomolecules. *J Mater Chem B*. 2014;2(44):7725-7731. doi:10.1039/C4TB01213E.
42. Sukhorukov GB, Volodkin D V., Günther AM, Petrov AI, Shenoy DB, Möhwald H. Porous calcium carbonate microparticles as templates for encapsulation of bioactive compounds. *J Mater Chem*. 2004;14(14):2073-2081. doi:10.1039/B402617A.
43. Lenggoro IW, Xia B, Okuyama K, de la Mora JF. Sizing of Colloidal Nanoparticles by Electrospray and Differential Mobility Analyzer Methods. *Langmuir*. 2002;18(12):4584-4591. doi:10.1021/la015667t.
44. Kumbar SG, Bhattacharyya S, Sethuraman S, Laurencin CT. A preliminary report on a novel electrospray technique for nanoparticle based biomedical implants coating: Precision electrospraying. *J Biomed Mater Res Part B Appl Biomater*. 2007;81B(1):91-103. doi:10.1002/jbm.b.30641.
45. Zweers MLT, Grijpma DW, Engbers GHM, Feijen J. The preparation of monodisperse biodegradable polyester nanoparticles with a controlled size. *J Biomed Mater Res*. 2003;66B(2):559-566. doi:10.1002/jbm.b.10046.
46. Vermeesch I, Groeninckx G. Chemical modification of poly(styrene- co -maleic anhydride) with primary N -alkylamines by reactive extrusion. *J Appl Polym Sci*. 1994;53(10):1365-1373. doi:10.1002/app.1994.070531011.
47. Tian Y, He Q, Tao C, Cui Y, Ai S, Li J. Fabrication of Polyethyleneimine and Poly(styrene-alt-maleic anhydride) Nanotubes Through Covalent Bond. *J Nanosci Nanotechnol*. 2006;6(7):2072-2076. doi:10.1166/jnn.2006.369.
48. Gauthier MA, Klok H-A. Polymer–protein conjugates: an enzymatic activity perspective. *Polym Chem*. 2010;1(9):1352. doi:10.1039/c0py90001j.
49. Cloete WJ, Adriaanse C, Swart P, Klumperman B. Facile immobilization of enzymes on electrospun poly(styrene-alt-maleic anhydride) nanofibres. *Polym Chem*. 2011;2(7):1479. doi:10.1039/c1py00069a.
50. Sahoo B, Sahu SK, Bhattacharya D, Dhara D, Pramanik P. A novel approach for efficient immobilization and stabilization of papain on magnetic gold nanocomposites. *Colloids Surfaces B Biointerfaces*. 2013;101:280-289. doi:10.1016/j.colsurfb.2012.07.003.

Conclusion

In this present thesis, different aspects concerning the formulation of novel materials, based on electrospun fibers and nanoparticles, potentially applicable in the biomedical and environmental fields were considered.

Indeed, as a fist effort, it was verified the feasibility of the modification of the thermal, decomposition and mechanical features as well of the affinity with drug molecules of electrospun fibers by the addition of ad-hoc synthesized dendritic molecules. In particular, in order to enhance the affinity of fibers based on poly(ε-caprolactone) (PCL) for a hydrophilic drug, that is doxorubicin, and tune its release a synthesized star polymer, made up of a poly(amido-amine) (PAMAM) core and PCL branches (PAMAM-PCL), was added into the electrospun fibers. Conversely to the inorganic nanofillers, commonly applied as drug carriers in the polymer fibers, our star system is characterized by a good affinity with PCL, it being characterized by arms whose chemical nature is identical to that of the polymer matrix. Moreover, the PAMAM core of the star polymer, which renders the fibers more hydrophylic, interacting with the chosen hydrophylic drug turned out to ameliorate its dispersion in the fibers and allowed its prolonged and controlled release.

Another studied system consisted of electrospun fibers based on poly(L-lactide) PLLA. In this case, it was demonstrated the enhancement of the fiber enzymatic degradation rate by the addition of a synthesized hyperbranched polymer made up of a high molecular mass hyperbranched polyglicerol (HBPG) core and PDLA arms (HBPG-PDLA), which behaviour was explained by considering the higher hydrophilicity of the composite fibers. Moreover, unlike the systems reported in the literature, whose addition of organic additive generally produces a decrease of the electrospun mat mechanical properties, our composite fibers were found to be characterized by a modulus similar to that of the neat polymer matrix. This phenomenon is probably related to the crystallinity of the fibers, which is not altered by the addition of the dendritic additive and to the stereocomplexation, which occurs through the arrangement of the PLLA chains of the polymer matrix with the PDLA-type arms of the dendritic additive.

The subsequent development, a novel bio-based nanostructured material, characterized by suitable features for water pollutant removal, was developed. Indeed, it was proved the possibility to anchor, on the surface of stereocomplex polylactide (sc-PLA) electrospun nanofibers, functionalized by the nanometric dispersion of an amino bearing polyhedral oligomeric silsesquioxane (POSS-NH_2), *ad hoc* modified cyclodextrine molecules. The decoration of the surface of the support, having a "bio" nature, a higher thermal/chemical resistance compared to PLLA or PDLA single polymers, as well as a high surface area, with cyclodextrin molecules, that is compounds capable of interacting with numerous organic molecules, allowed to obtain a system with a much higher absorption capacity than the active absorbent species in powder form, consisting of the CD linked to the silsesquioxane siliceous cage. These results, obtained by studying the absorpion of two model pollutant molecules, namely alizarin red and 2-chlorophenol, indicate an high accessibility of the absorption sites on the surface of the nanofibers.

In detail, the reaction between CD and POSS-NH_2 was proved both for the sc-PLA/POSS-NH_2 nanofibers and the POSS-NH_2 powder, applying the same reaction conditions. Indeed, in the case of the latter system, the development of the above reaction allowed to obtain a novel organic/inorganic hybrid molecule, which combining the features of the silsesquioxane with those of cyclodextrins, might find application not only as absorbent of contaminant molecules but also in other fields, such as that of nanocomposite materials and for biomedical applications.

The last part of the thesis work was devoted to the different aspects concerning the formulation of novel materials, based on nanoparticles, potentially applicable in the biomedical field. In the case of PSMA nanoparticles, the successful production of PSMA-nanoparticles and their conjugation with the proteolytic model enzyme papain were demonstrated. The PSMA nanoparticles were obtained by combining the nanoprecipitation method with the electrospray technique. The conjugation of the enzyme to the nanoparticle surface was carried out in water at room temperature by exploiting the reaction of the maleic group in the polymer chain and the primary amines on lysine residues of the enzyme molecules. The successful conjugation was demonstrated by zeta potential measurements and by infra-red spectroscopy. Moreover, the characterization of the residual catalytic activity of the conjugated papain was carried out and showed a value around 79 (±11)% respect to the free enzyme. Overall, the obtained results pointed out that PSMA-nanoparticles could act as ideal protein carriers do to their easy production and to the mild conditions for protein conjugation. Finally, preliminary results on microencapsulation indicated that NPCs could represent an efficient system for the microencapsulation of PSMA nanoparticles to be used in applications where the microencapsulation plays a pivotal role for the overall efficiency of the process.